

University of Windsor

Scholarship at UWindor

Electronic Theses and Dissertations

Theses, Dissertations, and Major Papers

1-1-1987

Raman structural studies of phthalocyanine thin solid films.

Carol Ann Jennings
University of Windsor

Follow this and additional works at: <https://scholar.uwindsor.ca/etd>

Recommended Citation

Jennings, Carol Ann, "Raman structural studies of phthalocyanine thin solid films." (1987). *Electronic Theses and Dissertations*. 6815.

<https://scholar.uwindsor.ca/etd/6815>

This online database contains the full-text of PhD dissertations and Masters' theses of University of Windsor students from 1954 forward. These documents are made available for personal study and research purposes only, in accordance with the Canadian Copyright Act and the Creative Commons license—CC BY-NC-ND (Attribution, Non-Commercial, No Derivative Works). Under this license, works must always be attributed to the copyright holder (original author), cannot be used for any commercial purposes, and may not be altered. Any other use would require the permission of the copyright holder. Students may inquire about withdrawing their dissertation and/or thesis from this database. For additional inquiries, please contact the repository administrator via email (scholarship@uwindsor.ca) or by telephone at 519-253-3000ext. 3208.

RAMAN STRUCTURAL STUDIES OF PHTHALOCYANINE
THIN SOLID FILMS

by
Carol Ann Jennings

A Thesis
submitted to the
Faculty of Graduate Studies and Research
through the Department of
Chemistry and Biochemistry in Partial
Fulfillment of the requirements for the
Degree of Master of Science at
the University of Windsor

Windsor, Ontario, Canada
1987

UMI Number: EC54804

INFORMATION TO USERS

The quality of this reproduction is dependent upon the quality of the copy submitted. Broken or indistinct print, colored or poor quality illustrations and photographs, print bleed-through, substandard margins, and improper alignment can adversely affect reproduction.

In the unlikely event that the author did not send a complete manuscript and there are missing pages, these will be noted. Also, if unauthorized copyright material had to be removed, a note will indicate the deletion.

UMI[®]

UMI Microform EC54804
Copyright 2010 by ProQuest LLC
All rights reserved. This microform edition is protected against
unauthorized copying under Title 17, United States Code.

ProQuest LLC
789 East Eisenhower Parkway
P.O. Box 1346
Ann Arbor, MI 48106-1346

© Carol Ann Jennings 1987
All Rights Reserved

866638

ABSTRACT
RAMAN STRUCTURAL STUDIES OF PHTHALOCYANINE
THIN SOLID FILMS

by Carol Ann Jennings

Raman spectra of evaporated thin solid films (200nm thickness) have been studied using excitation frequencies in resonance and near resonance with the red absorption band of chloroaluminum (AlPcCl), chlorogallium (GaPcCl) and chloroindium (InPcCl) phthalocyanine. Molecular orientation of these films have been probed by polarization techniques. Expressions have been developed for SS,SP,PS and PP polarizations of A,B and E symmetry types for C_{4v} molecules such as AlPcCl, GaPcCl and InPcCl. Experimentally the angle β (between the laser beam and the normal to the substrate) can be varied and values obtained for the angle θ which describes the stacking of molecular columns on a substrate. Correlation field splitting (Davydov) of non-degenerate vibrational fundamentals were observed using polarization techniques with these thin solid films. The Davydov splitting pattern permits assignment of the crystallites in the AlPcCl film to a monoclinic system as opposed to a triclinic system.

Surface-enhanced Raman scattering (SERS) has been observed for a Langmuir-Blodgett monolayer of tetratertiarybutyl metal-free phthalocyanine $(t\text{-bu})_4\text{H}_2\text{Pc}$ on silver and indium island films.

Langmuir-Blodgett films of arachidic acid have been used as spacer layers to control the separation distance between evaporated Ag or In metal island films and the LB monolayer of (t-bu)₄H₂Pc. The distance dependence of the SERS enhancement factor was established and results support an electromagnetic mechanism rather than a short-range chemical mechanism.

DEDICATION

To my family and friends

ACKNOWLEDGEMENTS

I would like to express my sincere thanks to Dr. R. Aroca for his constant encouragement and advice during this project.

I would like to thank the following people from Xerox Research Centre of Canada located in Mississauga: Dr. R.O. Loutfy, Dr. A. Hor and Dr. G. Kovacs. Their suggestions and the opportunity to work in the Xerox laboratory on several occasions was appreciated.

Finally, I would like to thank my friends in the department and others who have made my stay in Windsor an enjoyable one.

TABLE OF CONTENTS

ABSTRACT.....	iv
DEDICATION.....	vi
ACKNOWLEDGEMENTS.....	vii
LIST OF ABBREVIATIONS.....	viii
CHAPTER	
I. APPLICATIONS.....	1
II. STRUCTURE	
General.....	5
Metal-free phthalocyanine.....	6
Polymorphs.....	9
Tetratertiarybutyl metal-free phthalocyanine.....	12
Planar divalent.....	12
Non-planar divalent.....	16
Vanadyl phthalocyanine.....	17
Trivalent phthalocyanines.....	17
III. NORMAL RAMAN, RESONANCE RAMAN AND SURFACE ENHANCED RAMAN	
Normal Raman.....	21
Resonance Raman.....	25
Surface enhanced Raman.....	28
IV. POLARIZATION TECHNIQUES IN RAMAN SPECTROSCOPY	
Coordinate systems and notation.....	32
Random orientation versus ordered.....	37
Transformations from molecular to laboratory.....	39

V. LANGMUIR-BLODGETT FILMS	
. Introduction.....	60
Trough, material, subphase, solvent.....	61
Phthalocyanine LB films.....	65
VI. EXPERIMENTAL	
Vacuum evaporation.....	68
Chemicals and preparation of LB films.....	68
Raman systems.....	72
VII. RESULTS	
Uv-visible absorption.....	76
Davydov splitting.....	91
SERS of $(t\text{-bu})_4\text{H}_2\text{Pc}$	101
VIII. ASSIGNMENT OF PHTHALOCYANINE VIBRATIONAL BANDS USING MODEL COMPOUNDS	
IX. REFERENCES.....	127

LIST OF ABBREVIATIONS

Pc - phthalocyanine

LB - Langmuir-Blodgett

(t-bu)₄H₂Pc - tetratertiarybutyl metal-free phthalocyanine

CuTSPc - 4,4',4'',4''' tetrasulfonated copper phthalocyanine

MPc - metallated phthalocyanine

NR - normal Raman

RR - resonance Raman

SERS - surface enhanced Raman scattering

CHAPTER 1: APPLICATIONS

Phthalocyanines (Pcs) in general are very stable, resistant to heat and light, fairly insoluble in water and organic solvents. Pcs are widely used as colorants. The pigments have been dispersed in paints, inks and plastics. They have been used as indicators, parts of lasers, catalysts and lubricants. Phthalocyanines have medical applications as stains for electron microscopy. Thin films of Pcs and derivatives are used in photography, semiconductor applications and xerography.

The laser properties of some phthalocyanines have been reported¹. Chloroaluminum phthalocyanine (AlPcCl), chlorogallium phthalocyanine (GaPcCl), magnesium phthalocyanine (MgPc) and zinc phthalocyanine (ZnPc) were dissolved in a number of solvents and pumped with a nitrogen laser. Two wavelength lasing was observed for AlPcCl in solution with lines separated by 70nm. The other phthalocyanines GaPcCl, MgPc and ZnPc lased at only one wavelength which was below 700nm.

An electrophotographic camera film consisting of X-metal-free phthalocyanine (X-H₂Pc) or vanadyl phthalocyanine (VOPc) has been described². Special features of the film include: handling in light prior to charging, high sensitivity in the visible and near IR, inexpensive raw materials, ease of fabrication, dry development and high resolution. The film is selectively erasable when developed using heat. The X-H₂Pc film could be

used for digital recording and one suggested application of the film would be "photography in the dark" where the "flash" is imperceptible to the subject.

Vanadyl phthalocyanine has been studied as a high density optical storage material³. The VOPc films were prepared by vacuum vapor deposition onto polymethylmethacrylate substrates and then annealed. A laser of wavelength in the region of 800nm evaporates the organic material and forms a pit (writing). The optical defects are detected or "read" a later time. Double and triple layer structures containing VOPc have also been tested.

Metal-free phthalocyanine has been considered as a material for archival data storage using a krypton ion laser line of 647.1nm for pit formation⁴. Experimental conditions must be manipulated to obtain the smallest pit and thus increase the storage capacity.

Argon ion beams interact with organic materials such as nickel phthalocyanine (NiPc) and 3,4,9,10-perylene tetracarboxylic dianhydride⁵. The organic solids turn optically dense and conductivity is greatly increased. Nearly amorphous carbon is formed with high doses and this technique could have lithographic applications.

Gas sensors have been fabricated from Langmuir-Blodgett (LB) monolayers of phthalocyanines. A chemiresistor consisting of microelectrodes and a LB film of copper tetra cumylphenoxy Pc has

been tested⁶. The conductivity of the film changes with the amount of ammonia vapor or nitrogen dioxide in contact with the device. Desirable properties of the chemical sensor are high sensitivity, fast response, selectivity, reproducibility and stability.

Phthalocyanines have photovoltaic and photoelectrolytic applications⁷⁻³¹. Solar cells composed of thin films offer two advantages over other choices: (1) material costs can be reduced as the thickness of the active material is small and (2) thin films can be produced continuously on a large scale²⁹. The presence of metal phthalocyanine as dopants within metal-free phthalocyanine photovoltaic cells has been discussed⁷⁻¹⁰. Heterojunction solar cells have been prepared consisting of cadmium sulfide and a phthalocyanine such as H₂Pc, ZnPc, MgPc, CuPc, MnPc, PbPc, VOPc, chloroaluminum chlorophthalocyanine (ClAlClPc), ClAlPc and ClInPc¹²⁻¹⁴.

Photoelectrochemical properties of X-H₂Pc and VOPc coated tin oxide (SnO₂) electrodes coupled with Fe(CN)₆^{4-/3-} and I₂/I₃⁻ have been optimized and reported¹⁵. Tri- and tetravalent Pc electrodes have been studied³⁰⁻³¹. The crystallite size within the films influences the photoelectrochemical behavior. Hydrogen evolution was observed for GaPcCl/Au films coated with small amounts of platinum²³.

Electrochemical studies have been carried out on water-soluble tetrasulfonated phthalocyanines³²⁻³⁵. The previous examples are not a complete list of Pc applications but illustrate their widespread use.

CHAPTER 2: STRUCTURE

In this discussion of structure, Pcs are arbitrarily divided according to symmetry:

- (i) D_{2h} : H_2Pc
- (ii) 4,4',4'',4'''-tetratertiarybutyl metal-free phthalocyanine ($(t\text{-bu})_4H_2Pc$)
- (iii) D_{4h} : BePc, CoPc, CuPc, FePc, MgPc, MnPc, ZnPc, hexadecachloro-copper phthalocyanine ($Cl_{16}CuC_{32}N_8$)
- (iv) C_{4v} : PbPc, SnPc, VOPc, AlPcCl, GaPcCl, InPcCl
- (v) 4,4',4'',4'''-tetrasulfonated copper phthalocyanine (CuTSPc)

Data obtained from x-ray crystallography is used in structure determination. Phthalocyanines and metallated phthalocyanines occur in various polymorphic forms. A section is devoted to this topic. Molecular symmetry (point group) and crystal symmetry (space group) are mentioned.

There are two types of symbols used to represent the two-hundred and thirty space groups¹. Hermann-Maugin symbols are frequently encountered in crystallographic reports and the other system is Schönflies notation. The notation to be adopted here is the Schönflies symbol is followed by the Hermann-Maugin symbol, for example: $C_{2h}^5(P2_1/a)$.

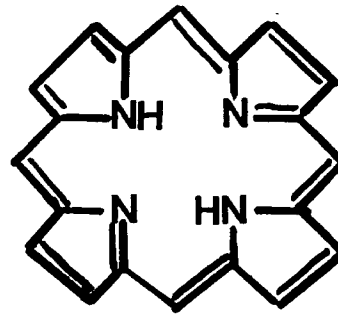
Phthalocyanines are structurally related to compounds of biological interest². Figure 1 gives the structures of porphyrin, chlorophyll a and hemin. All these compounds have four pyrrole units. Porphyrins can contain four bridging methine groups or from one to four aza groups. Chlorophyll a has a central magnesium atom and is a photosynthetic pigment. Hemin contains iron and combines with protein to give hemoglobin.

Metal-free phthalocyanine (H_2Pc) structure:

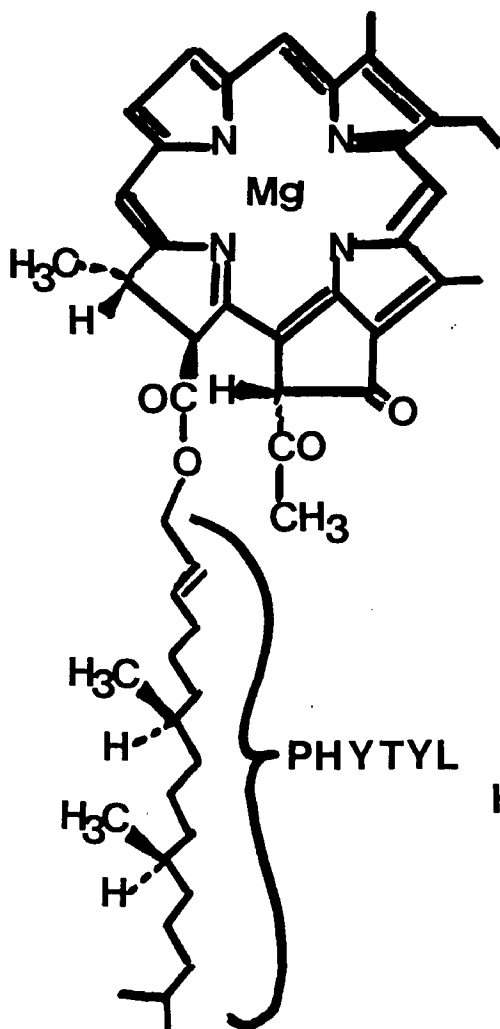
Robertson has determined the structure of H_2Pc and a number of MPCs by x-ray crystallography³⁻⁷. The skeleton of H_2Pc is given in figure 2. The first striking feature of this compound is its extensive conjugation which leads to a planar structure. It is convenient to discuss H_2Pc in terms of subunits. The core consists of a macrocycle of sixteen alternating carbon and nitrogen atoms. The interatomic C-N distance in the macrocycle has a constant value of 1.34\AA indicating a single-bond double-bond resonance^{3,4}. There are four isoindole groups in H_2Pc each consisting of a benzene and pyrrole ring. Four aza groups ($-N=$) bridge the isoindole moieties. The two imino hydrogens lie in the plane of the molecule and are shared by the nitrogens⁸. Peripheral hydrogens can be replaced by other atoms or groups. Metal-lated phthalocyanines (MPCs) are synthesized by substituting the two central hydrogens.

Figure 1. Structures of porphine, chlorophyll a and hemin².

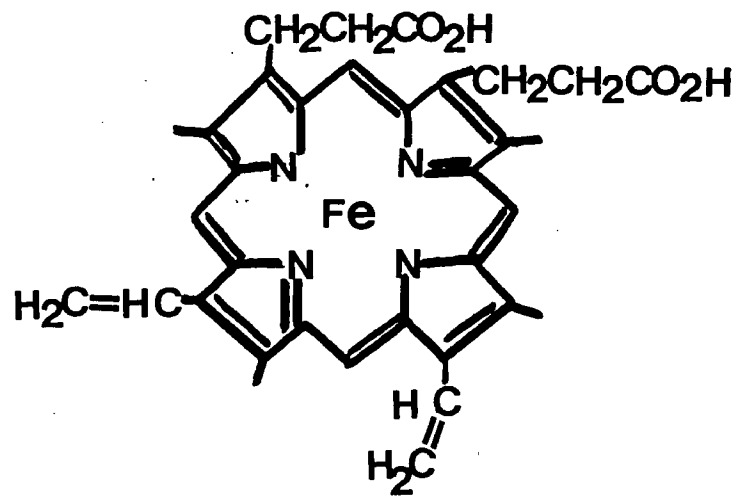
FIGURE 1



PORPHINE



CHLOROPHYLL A



HEMIN

Polymorphs:

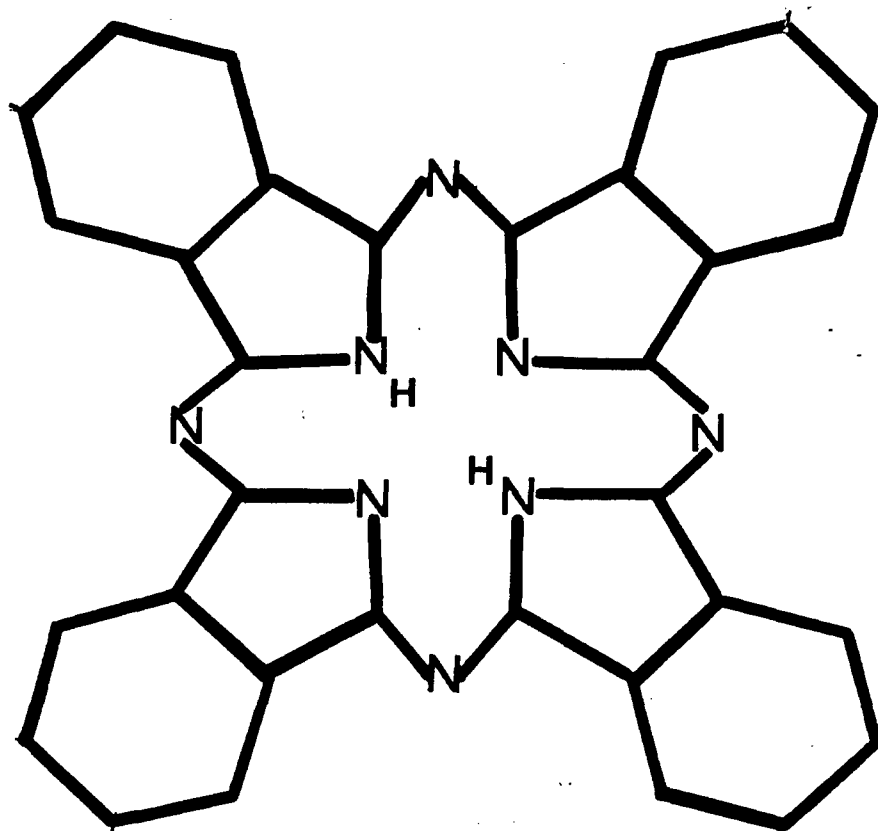
Metal-free Pc and metallated Pcs exist in various polymorphic forms⁹⁻¹². The polymorphic phase is determined by the orientation of adjacent molecules. A number of crystal packing arrangements are possible. Under a given set of conditions (pressure, temperature, solvent) there is only one stable phase which has the lowest free energy¹³. All other phases under the set of conditions are metastable. Metastable phases can exist for long periods of time.

Three polymorphic forms of H₂Pc (α, β, χ) have been qualitatively identified based on their IR and visible spectra^{9,14}. β and χ -H₂Pc polymorphic forms are more crystalline than the α form. All the crystals studied by Robertson³⁻⁷ were long needles that had been sublimed and corresponded to the β polymorph. The x-ray diffraction results for χ -H₂Pc have been reported¹⁵. α -H₂Pc is metastable and less ordered than β -H₂Pc⁹. The method of preparation determines which polymorphic form is present.

Intramolecular hydrogen bonding in β -H₂Pc is extensive due to the presence of parallel molecular stacks⁴. Each imino hydrogen is shared by nitrogen atoms of adjacent molecules⁹. One nitrogen of an isoindole group lies directly above the hydrogen, while the other isoindole nitrogen is directly below. The bands of

Figure 2. Skeleton of metal-free phthalocyanine (H_2Pc).

FIGURE 2



the IR spectra that are used to identify various polymorphs are mainly C-H deformations, N-H deformations and N-H stretching^{9,14}. The α -H₂Pc polymorph has a greater density and less hydrogen-bonding than β -H₂Pc¹⁴.

4,4',4'',4'''-tetratertiary butyl phthalocyanine, ((t-bu)₄H₂Pc) structure:

The structure of (t-bu)₄H₂Pc is given in figure 3. It is possible to prepare Langmuir-Blodgett films¹⁶ and this will be discussed in greater detail.

Planar divalent phthalocyanines, structure:

Early work on the structure of CuPc was done by Robertson³⁻⁵. Further studies of β -CuPc were carried out by Brown¹⁷. The β -CuPc is monoclinic with space group C_{2h}⁵(P2₁/a) and there are two molecules per unit cell^{3,5,17}. Within the molecule, the Cu-N distance is 1.934Å and there is square planar coordination¹⁷. The geometry of the copper can also be thought of as a distorted octahedral if one includes interaction with nitrogens of neighboring Pc molecules. Brown¹⁷ suggests that the difference between various polymorphs is due to the coordination of copper with different neighboring nitrogens and certain polymorphs could be selected by blocking specific nitrogen atoms with residues.

Figure 3. Skeleton of the most common type isomer of $(t\text{-bu})_4\text{H}_2\text{Pc}$.

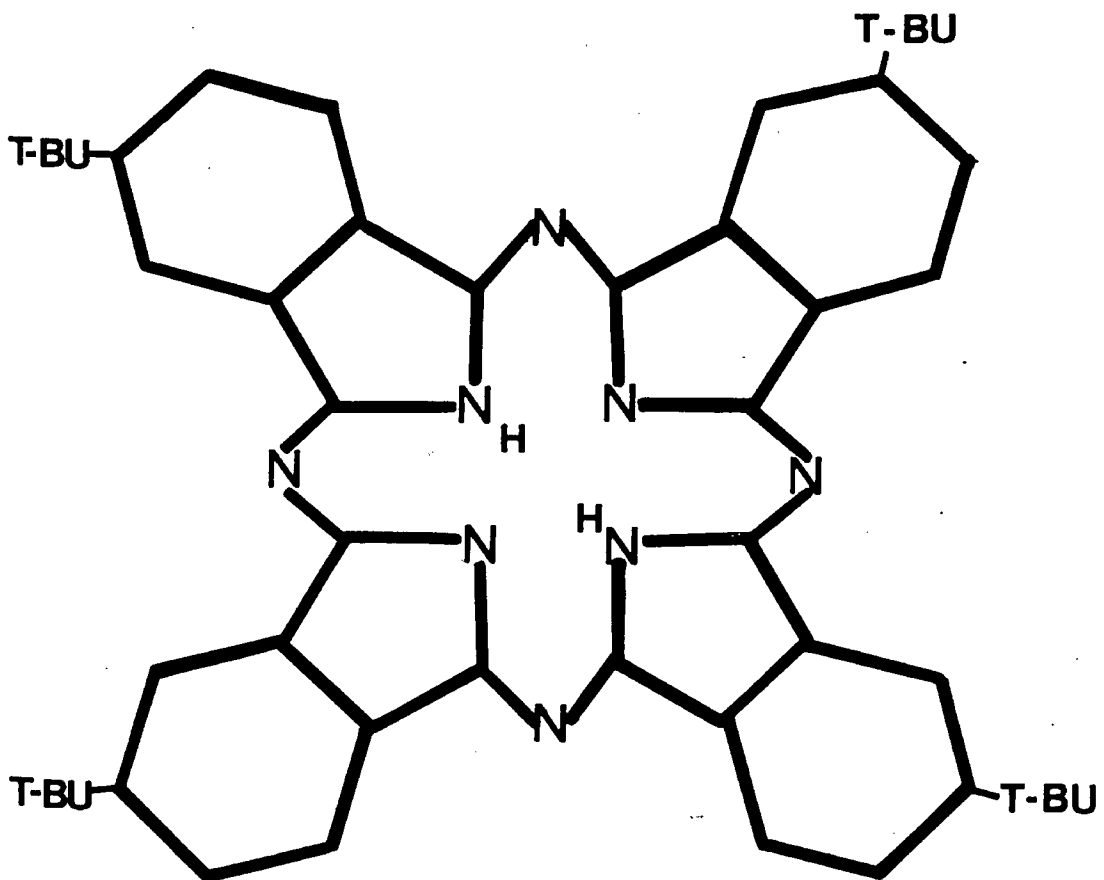


FIGURE 3

X-ray diffraction data for ZnPc reveals that the zinc is centrosymmetric and the molecule is essentially planar¹⁸. The mean Zn-N distance is 1.980\AA with a monoclinic structure and space group $C^5_{2h}(P2_1/a)$ ¹⁸. Additional planar compounds studied by Robertson were: NiPc, PtPc, BePc, CoPc, FePc, and MnPc^{3,5-7}. These compounds are all monoclinic, space group $C^5_{2h}(P2_1/a)$, and have two molecules per unit cell⁵. The PtPc is somewhat anomalous based on the fact that for nearest neighboring molecules there are no atoms vertically over each other and the distance between molecular planes is much smaller, 3.41\AA ⁷. Brown¹⁹ reinvestigated the structure of PtPc and found the original preparation by Linstead⁵ actually contained two polymorphs to be called α and γ . Both polymorphs were monoclinic and the space groups were $C^6_{2h}(C2/c)$ and $C^5_{2h}(P2_1/a)$ for α and γ forms respectively¹⁹. These planar divalent phthalocyanines belong to the point group D_{4h} .

Tetravalent phthalocyanines which have two equal axial ligands and distorted octahedral coordination about the central metal will also belong to the point group D_{2h} . Hexadecachlorocopper phthalocyanine ($Cl_{16}CuC_{32}N_8$) has all the peripheral hydrogens substituted with chlorine atoms. This compound also has D_{4h} symmetry.

Non-planar divalent phthalocyanines, structure:

Lead phthalocyanine is not a planar molecule²⁰. Its shape can be described as that of a "shuttlecock". The lead atom is displaced from the plane defined by the four nitrogen atoms of the isoindole units. The lead atom sits above a concave structure formed by the Pc ligand. The molecular symmetry is C_{4v} .

Monoclinic and triclinic crystal forms of lead phthalocyanine have been identified by x-ray diffraction^{20,21}. Iyechika²³ obtained monoclinic and triclinic crystals by heating PbPc powder to 723^oK and transporting the vapor by nitrogen to a tube with a controlled temperature gradient. The triclinic crystals grew at a region of the tube kept at 593^oK while the monoclinic crystals grew at 523^oK²¹. The space groups of the monoclinic form and triclinic forms were found to be $C_{2h}^5(P2_1/c)$ and $C_i^1(P\bar{1})$ respectively^{20,21}. In both cases there were four molecules in the unit cell. Monoclinic PbPc is a better electrical conductor than the triclinic form²³. The monoclinic form is a one-dimensional conductor due to a stacking of the PbPc molecules. It can be seen that if the crystal structure of a compound is modified, electrical and other properties change.

A triclinic form of tin phthalocyanine (SnPc) was studied by x-ray diffraction²². The space group was $C_i^1(P\bar{1})$ with two

molecules per unit cell. The tin atom is out of the plane of the four isoindole nitrogens, the inner macrocycle is puckered and the Pc ligand is "saucer" shaped²².

Vanadyl phthalocyanine (VOPc), structure:

Three polymorphic forms (phase I,II,III) have been observed for vanadyl phthalocyanine (VOPc)¹². These three phases are not isomorphous with α , β and χ polymorphs of other phthalocyanines. X-ray diffraction data has been reported for phase II and suggests the crystals are triclinic with $C^1_1(\overline{P1})$ symmetry¹². The oxovanadium cation lies above the plane defined by the four isoindole nitrogens. The preparation of the three phases is given¹². Phase I occurs if VOPc is vacuum deposited onto fused quartz at 10^{-5} torr. Phase II is obtained by crystal growth from solvents such as quinoline and 1-chloronaphthalene, by crystal growth from vapor or by heating phase I to 200°C and above. Phase III occurs if a melt at 610°C is quenched. The point group of VOPc is C_{4v} .

Trivalent phthalocyanines (AlPcCl, GaPcCl, InPcCl), structure:

Single crystal x-ray analysis has been reported for AlPcCl and ClGaPc²³. These trivalent phthalocyanines belong to the point group C_{4v} . Chloroaluminum phthalocyanine as a single crystal is triclinic and of space group $C^1_1(\overline{P1})$ with four molecules per unit cell²³. The coordination geometry of AlPcCl is square

pyramidal and the Al-Cl bond length is 2.179\AA with Al 0.410\AA above the plane defined by the four isoindole nitrogens²³. A crystal of chlorogallium phthalocyanine has the following properties: triclinic, space group $C_1^1(\bar{1})$, two molecules per unit cell, square pyramidal coordination, Ga-Cl= 2.217\AA and the gallium atom is 0.439\AA above the plane of the four isoindole nitrogens²³.

4,4',4'',4'''-tetrasulfonated copper phthalocyanine (CuTSPc), structure:

The presence of sulfate groups makes this compound water-soluble.

Lattice parameters for the various phthalocyanines are summarized in table 1.

TABLE 1.1: A COMPARISON OF LATTICE PARAMETERS FOR VARIOUS PHTHALOCYANINES

	a(Å)	b(Å)	c(Å)	$\alpha(^{\circ})$	$\beta(^{\circ})$	$\gamma(^{\circ})$	Z	space group
x-H ₂ Pc ^{3,4}								
monoclinic	19.85	4.72	14.8		122.25		2	C _{2h} ⁵ (P2 ₁ /a)
PbPc ^{20,21}								
monoclinic	24.48	25.48	3.73			90	4	C _{2h} ⁵ (P2 ₁ /b)
triclinic	13.123	16.131	12.889	94.22	96.20	114.19	4	Ci ¹ (P $\bar{1}$)
SnPc ²²								
triclinic	12.060	12.618	8.675	95.89	95.08	68.17	2	Ci ¹ (P $\bar{1}$)
VOPc(PhaseII) ¹²								
triclinic	12.032	12.579	8.712	96.15	94.88	68.16	2	Ci ¹ (P $\bar{1}$)
β -ZnPc ¹⁸								
monoclinic	19.274	4.8538	14.553		120.48		2	C _{2h} ⁵ (P2 ₁ /a)
β -CuPc ¹⁷								
monoclinic	19.407	4.790	14.628		120.56		2	C _{2h} ⁵ (P2 ₁ /a)
β -NiPc ^{3,5-6}								
monoclinic	19.9	4.71	14.9		121.9		2	C _{2h} ⁵ (P2 ₁ /a)
β -BePc ⁵								
monoclinic	21.2	4.84	14.7		121.0		2	C _{2h} ⁵ (P2 ₁ /a)
β -CoPc ⁵								
monoclinic	20.2	4.77	15.0		121.3		2	C _{2h} ⁵ (P2 ₁ /a)
β -FePc ⁵								
monoclinic	20.2	4.77	15.0		121.6		2	C _{2h} ⁵ (P2 ₁ /a)
β -MnPc ⁵								
monoclinic	20.2	4.75	15.1		121.7		2	C _{2h} ⁵ (P2 ₁ /a)
α -PtPc ¹⁹								
monoclinic	26.29	3.818	34.0		135.6		4	C _{2h} ⁶ (C2/c)
γ triclinic	23.16	3.969	16.62		129.4		2	C _{2h} ⁵ (P2 ₁ /a)

TABLE 1.1 CONTINUED: A COMPARISON OF LATTICE PARAMETERS FOR VARIOUS PHTHALOCYANINES

	$a(\text{\AA})$	$b(\text{\AA})$	$c(\text{\AA})$	$\alpha(^{\circ})$	$\beta(^{\circ})$	$\gamma(^{\circ})$	Z	Group
AlPcCl^{23}								
triclinic	13.776	13.775	14.059	98.36	108.60	90.16	4	$C_2^1(P\bar{1})$
GaPcCl^{23}								
triclinic	9.301	11.272	13.143	105.46	105.61	96.80	2	$C_2^1(PT)$

CHAPTER3: NORMAL RAMAN, RESONANCE RAMAN AND SURFACE-ENHANCED RAMAN SCATTERING

Normal Raman

A laser beam strikes a sample and light is scattered. If the scattered light has the same frequency as the incident light we have elastic or Rayleigh scattering. Inelastic or Raman scattering arises when scattered light has a different frequency from the laser beam and there are two possibilities, Stoke's and anti-Stoke's. For Stoke's scattering the frequency of scattered light is less than the frequency of the incident light. Molecules are excited from a ground vibrational state ($v=0$) to a higher energy level (virtual state). The molecules leave this virtual state and return to an excited vibrational state (eg. $v=1$). In the anti-Stoke's case, molecules start in an excited vibrational state (eg. $v=1$), are excited to a higher energy state and then return to the ground vibrational state ($v=0$). The frequency of anti-Stoke's scattering is greater than the frequency of the incident light. Stoke's scattering is much more intense than anti-Stoke's because few molecules start out in an excited vibrational energy level.

A laser source has an oscillating electric field which interacts with molecules to induce a dipole moment μ . The magnitude of μ depends on the amplitude of the light wave and the molecular polarizability α . The molecular polarizability describes the ease of electron deformation in the molecule.

$$\mu = \alpha E \quad (3.1)$$

The components of the induced dipole moment are given by a polarizability tensor where $\alpha_{xy} = \alpha_{yx}$, $\alpha_{zx} = \alpha_{zx}$ and $\alpha_{yz} = \alpha_{zy}$.

$$\begin{pmatrix} \mu_x \\ \mu_y \\ \mu_z \end{pmatrix} = \begin{pmatrix} \alpha_{xx} & \alpha_{xy} & \alpha_{xz} \\ \alpha_{yx} & \alpha_{yy} & \alpha_{yz} \\ \alpha_{zx} & \alpha_{zy} & \alpha_{zz} \end{pmatrix} \begin{pmatrix} E_x \\ E_y \\ E_z \end{pmatrix}$$

Any or all of the six polarizability components can be modulated by a molecular vibration. Components which have a polarizability change are Raman active. From this point on the symbol α represents the polarizability derivative.

In this case¹:

$$\alpha = \alpha_0 + (\delta\alpha/\delta Q_\nu)_0 Q_\nu$$

The equilibrium configuration is α_0 , Q_ν is the vibrational coordinate and $(\delta\alpha/\delta Q_\nu)_0$ is the rate of change of the polarization.

Number and types of IR and Raman active modes

The number of infrared and Raman active modes for any molecule can be calculated using the character table of the appropriate point group. For example, AlPcCl has C_{4v} molecular symmetry. This molecule possesses a fourfold axis of symmetry and vertical planes of symmetry. For a non-linear molecule, the total number of vibrations is $3N-6$. AlPcCl has 58 atoms giving a total of 171 vibrations.

The total number of fundamentals of each type is calculated using the following equation²:

$$N_i = \frac{1}{N_G} \sum N_e(R) \theta(R) \chi(R) \quad (3.2)$$

N_G is the number of elements in the group.

N_e is the number of elements in each class.

$$\theta(R) = (\mu-2)(1+2\cos\phi) \quad (3.3)$$

$$\text{or} = (\mu)(-1+2\cos\phi) \quad (3.4)$$

Equation (3.3) is used for PROPER ROTATIONS which include the identity E and rotations. Equation (3.4) applies to IMPROPER ROTATIONS which include reflections, inversion and rotation followed by reflection.

$\chi_i(R)$ is the character of the vibration species, μ_R is the number of atoms left unchanged by the operation and ϕ is the angle associated with the rotation.

Infrared-allowed fundamentals can be calculated using the formula²:

$$N_i = \frac{1}{N_G} \sum N_e \chi_M(R) \chi_i(R) \quad (3.5)$$

$$\chi_M(R) = +/-1+2\cos\phi \quad (3.6)$$

The positive sign is for proper rotations, the negative for improper rotations. Raman allowed fundamentals are given by²:

$$N_i = \frac{1}{N_G} \sum N_e \chi_\alpha(R) \chi_i(R) \quad (3.7)$$

$$\chi_\alpha(R) = 2 +/- 2\cos 2\phi \quad (3.8)$$

The total number of fundamentals of each type have been calculated for three examples H_2Pc , $CuPc$ and $AlPcCl$ and are given in table 3.1.

TABLE 3.1: TOTAL NUMBER OF FUNDAMENTALS OF EACH TYPE FOR REPRESENTATIVE PHTHALOCYANINES OF D_{2h} , D_{4h} AND C_{4v} MOLECULAR SYMMETRY

D_{2h} [H ₂ Pc]: $29A_g^* + 13A_u + 13B_{1g}^* + \underline{28B_{1u}} + 14B_{2g}^* + \underline{28B_{2u}} + 28B_{3g}^* + 15B_{3u}$
D_{4h} [CuPc]: $14A_{1g}^* + 6A_{1u} + 13A_{2g} + \underline{8A_{2u}} + 14B_{1g}^* + 7B_{1u} + 14B_{2g}^* + 7B_{2u} + 13E_g^* + \underline{28E_u}$
C_{4v} [AlPcCl]: $\underline{23A_1^*} + 19A_2 + 21B_1^* + 21B_2^* + \underline{42E}$

* indicates Raman active

— indicates IR active

Resonance Raman Scattering

Resonance Raman (RR) scattering is observed if the excitation frequency i.e. laser line coincides with the frequency of an electronic transition of the molecule. The intensity of RR scattering is much greater than that observed with normal Raman (NR) scattering. The total scattering I_S for a ground state G to final state F is given by^{3,4}:

$$I_S = \frac{8\pi\omega I_L}{9c^4} \sum_{p\sigma} |(\alpha_{p\sigma})_{GF}|^2 \quad (3.9)$$

ω is the frequency of scattered light, c is the speed of light and the intensity of the incident laser beam is I_L . $(\alpha_{p\sigma})_{GF}$ is the $p\sigma$ th component of the Raman scattering tensor and $p, \sigma = x, y$ or z .

The elements of the polarizability derivative tensor $(\alpha_{p\sigma})_{GF}$ are given by³⁻⁵:

$$(\alpha_{p\sigma})_{GF} = \frac{1}{\hbar} \sum_I \left(\frac{\langle F|r_p|I\rangle \langle I|r_\sigma|G\rangle}{\omega_{GI} - \omega_L - i\Gamma_I} + \frac{\langle I|r_p|G\rangle \langle F|r_\sigma|I\rangle}{\omega_{IF} + \omega_L - i\Gamma_I} \right) \quad (3.10)$$

I = rovibronic excited electronic states

r = electron position operator

Γ_I = damping term

The main reason for introducing equations 3.9 and 3.10 is to show why resonance Raman bands are intense. When ω_L approaches ω_{GI} the left hand term of the summation in equation 3.10 becomes very large for an allowed electronic transition. The term cannot reach infinity because of the damping Γ_I which is related to the bandwidth of the electronic transition.

In resonance Raman, the polarizability derivative tensor may become asymmetric, i.e. $\alpha_{xy} \neq \alpha_{yx}$, etc. This introduces a new term in intensity and the depolarization expression.

$(\alpha_{p\sigma})_{GF}$ is divided into two terms described by Albrecht^{3,4}. The first term in equation 3.10 is Albrecht's A term involves Franck-Condon factors. Only totally symmetric terms are enhanced in the RR spectrum. Albrecht's B term is important in RR by the Herzberg-Teller mechanism. Electronic states are mixed and asymmetric modes can be observed in the RR spectrum. Porphyrins and heme proteins which contain the porphyrin chromophore are molecules which produce RR scattering of the Herzberg-Teller type⁵.

Resonance Raman scattering can be compared with normal Raman scattering. NR follows a ω^4 dependence on excitation frequency whereas RR scattering varies greatly with the excitation frequency. The RR scattering time can be much slower than off-resonance or NR scattering. Overtones can be quite intense in RR spectra while they are weak in NR Raman spectra. The ratio of Anti-Stoke's to Stoke's

scattering for NR is given by the Boltzman distribution which considers the ground state population. This is not the case for RR and the intensities of Anti-Stoke's lines can exceed the intensity of Stoke's.

Surface-enhanced Raman scattering

Surface-enhanced Raman scattering (SERS) is a phenomenon which involves molecules on or close to metal surfaces. A number of reviews and books have appeared in the literature on SERS⁶⁻¹². The Raman cross section of a molecule can be increased by a factor as large as 10^6 by a "SERS-active surface"^{6,7}. A distinction is made between two types of adsorption processes. Chemisorbed molecules have strong interactions with the metal surface and Raman frequencies are shifted. Direct contact with the metal surface is necessary for chemisorption. Physisorbed molecules have Raman frequencies which coincide with those of the pure compound.

The type of metal surfaces that have been studied by SERS include electrode surfaces^{13,14}, island films¹⁵⁻²², cold-deposited films^{10,23}, lithographically produced assemblies such as gratings⁷, metal colloids²⁴, metal deposits on the top of CaF_2 ²⁵⁻²⁸, ion bombarded metals⁷, acid etched material⁷, particles supported on an oxide²⁹ and metal on latex spheres²⁹. Seki³¹ has compiled a list of metals which give SERS and the environment in which the measurements were taken. Silver is the most studied metal and is a very efficient "SERS" material^{7,31}. Work in our laboratory has been done on silver and indium island films¹⁵⁻¹⁸.

There are a number of reasons why the mechanism(s) for SERS must be found. We have a sensitive technique but interpretation of results is sometimes difficult. From an analytical point of view, one would like to optimize experimental conditions³² to get the highest sensitivity possible, identify adsorbates and allow geometries of adsorbates to be elucidated. Many theoretical models have been presented concerning the origin of SERS and no consensus regarding the mechanism has been achieved^{6-12,23-48}.

There are two electromagnetic models⁶, one for continuous surfaces (extended surface plasmons) and another for discontinuous metals (localized particle plasmons). A model which considers the increased formation of electron-hole pairs on roughened surfaces was proposed by Burstein et al⁴⁹. The adatom model of Otto¹⁰ requires the adsorption of molecules at active sites and surface roughness increases the number of these sites. A mechanism has been suggested which has the metal altering and broadening energy levels of adsorbed molecules⁵⁰⁻⁵². Large intensities would be observed when the frequency of the laser line was in resonance with one of the molecular transitions. This resonant Raman mechanism⁵⁰⁻⁵² requires direct contact of the adsorbate with the metal and surface roughness is not essential. One group⁵³ discusses the effect of the formation of surface complexes consisting of metal atoms, ions, adsorbate and solvent molecules. In specific geometries, the electronic transitions of the complex are altered and a resonant

Raman effect is observed⁵⁸. Another model of Otto⁵⁹ is modulated reflectance. A vibrating molecule has a charge density that fluctuates and is propagated to the metal surface either directly (chemisorption) or via Coulombic interactions (physisorption). One model for SERS is the image dipole mechanism⁶. A molecular dipole induces an image dipole on the metal and the molecular-metal distance is critical.

SERS mechanisms can be tested by posing the following experimental questions. Is surface roughness required? A particular adsorbate could be added to smooth and rough metals. Is direct contact between the molecule and metal necessary? Spacer-type experiments are useful in checking this point. What is the effect of changing the incident photon energy? Excitation profiles are constructed using an internal standard and observing how intensities change with different laser lines. For island films, what is the optimum size of islands and best aspect ratio? How are results affected by changing the identity of the adsorbate or the metal (dielectric constant)? Optical absorption spectra can be taken of colloids and metal island films. Is aggregation mandatory and must the laser line fall within the absorption of the metal to observe intense Raman signals? The experimenter should attempt to determine the magnitude of the enhancement. For example, in the case of colloids one could obtain a Raman spectrum of adsorbate molecules

only. The intensities and frequencies are compared with a spectrum of adsorbate with metal. Both solutions are run with identical conditions.

CHAPTER 4: POLARIZATION TECHNIQUES IN RAMAN SPECTROSCOPY

Nomenclature, Definition of Laboratory, Substrate and Molecular Coordinates

Three sets of cartesian coordinates must be considered in order to develop the theory for polarization ratios of phthalocyanines. The laboratory coordinates are given in figure 4 showing the laser and collection of scattered light. The incident laser line is always along the positive Z-axis, while scattered light is collected along the X-axis. The angle β is defined as the angle the laser beam makes with the normal to the substrate. Therefore, the ZX plane is the incident and scattering plane.

The electric field of the laser beam is perpendicular to the direction of propagation. The two possible polarizations of the incident laser beam are X and Y. An analyzer placed after the sample has two positions allowing either X or Y polarizations to pass. A scrambler depolarizes light before it enters the monochromator. Since the laser beam has two positions and the analyzer has two positions, there are four polarizations of scattered light that can be measured and these are shown in figure 5.

The notation used here for polarized spectra in terms of Porto's¹ nomenclature is:

$$Z(YY)X = SS$$

$$Z(YZ)X = SP$$

$$Z(XY)X = PS$$

$$Z(XZ)X = PP$$

Figure 4. a) Laboratory coordinates showing the incident laser beam along the Z-axis and collection of scattered light at 90° along the X-axis. The angle between the laser beam and the normal to the substrate (C-axis) is the β angle. The Y-axis goes into the plane of the paper. b) Substrate coordinates. Substrate and laboratory have a common Y-axis. The substrate can be experimentally rotated by β about the Y-axis. c) Molecular coordinates. Phthalocyanine skeleton shown. z-axis out of the plane of the paper.

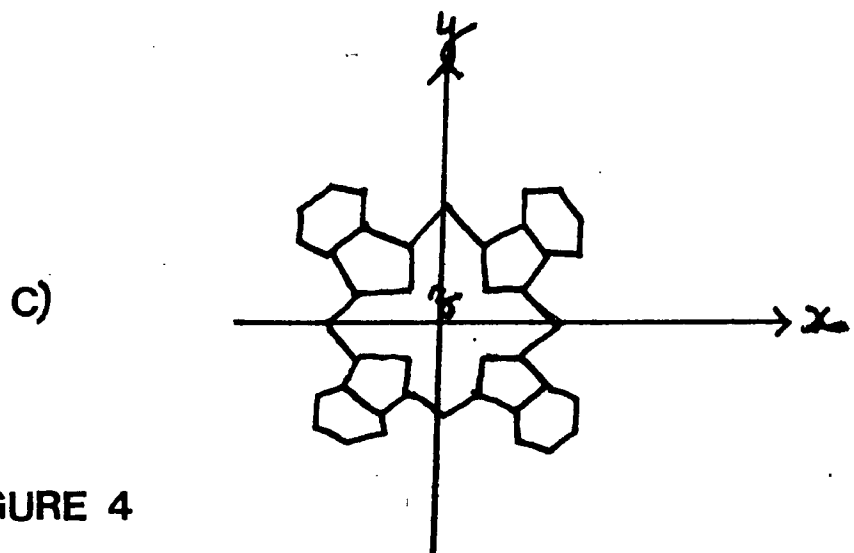
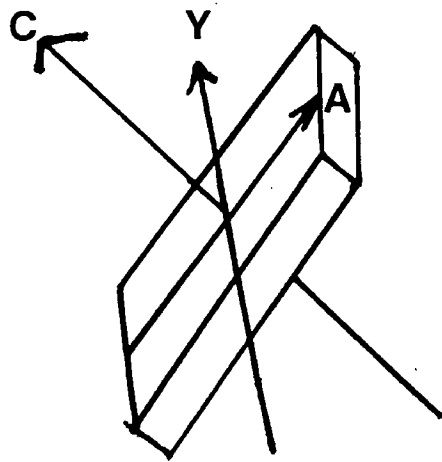
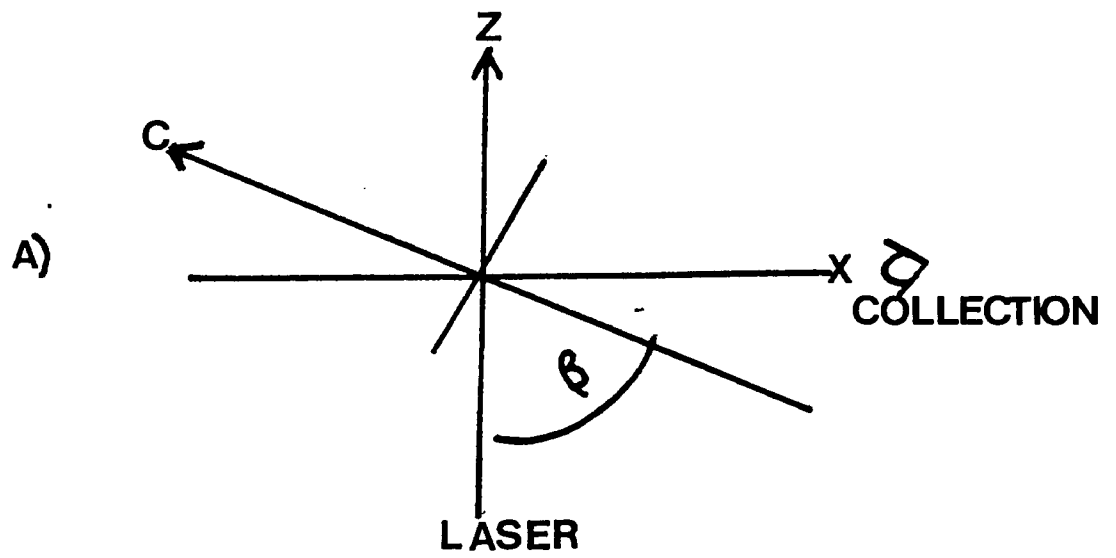


FIGURE 4

Figure 5. Four polarizations of laser light obtained by two positions of the rotator on the laser and an analyzer after the sample. Propagation of the laser beam along the Z-axis, collection along the X-axis.

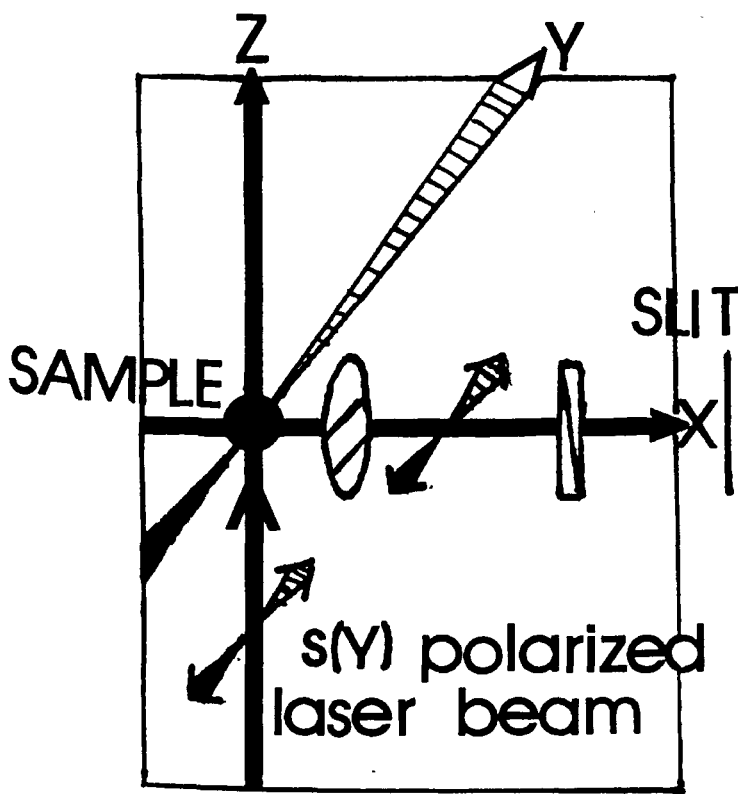
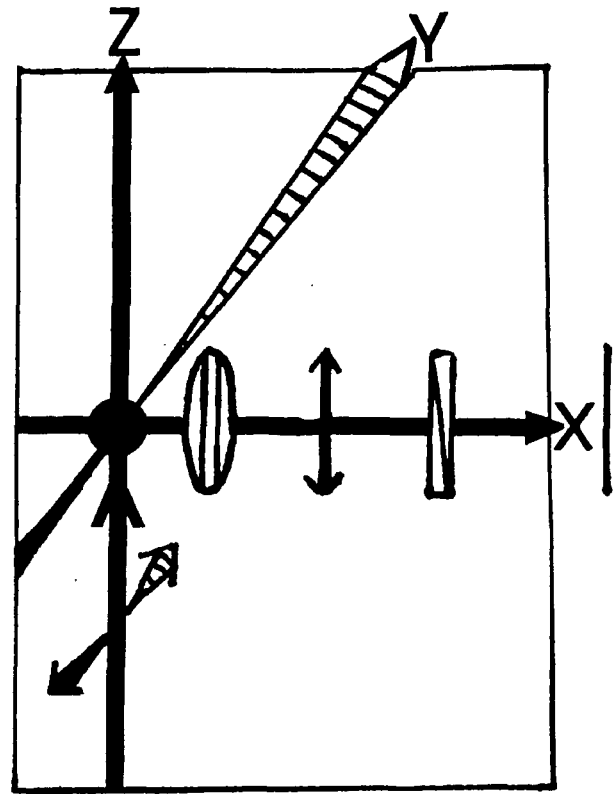
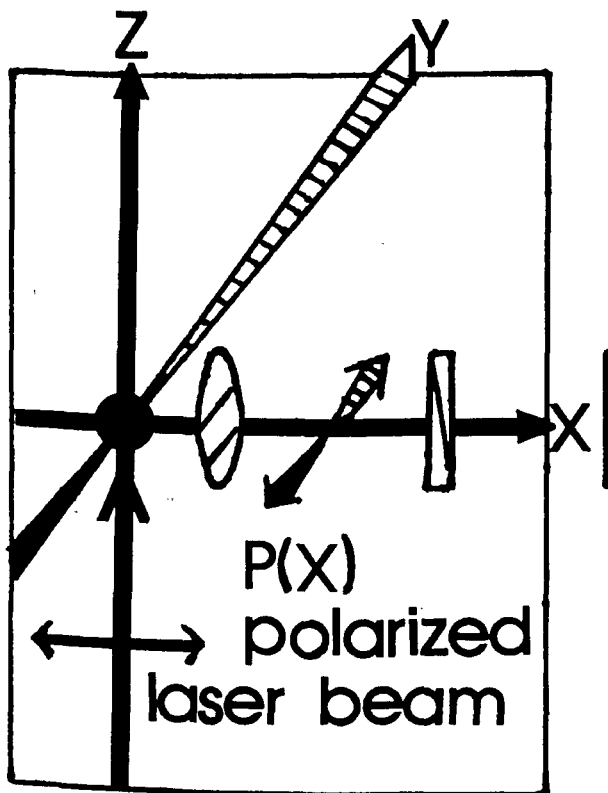
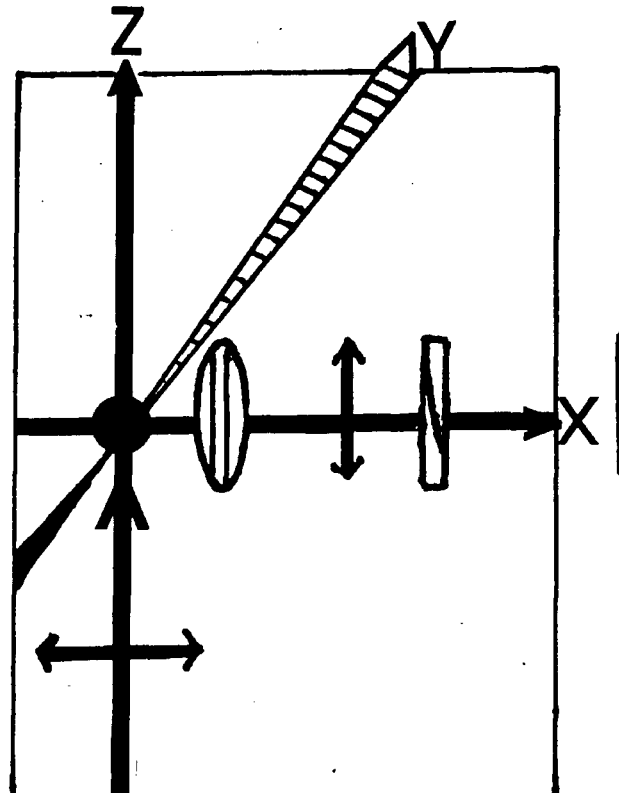
a) $Z(Y Y)X = SS$ b) $Z(Y Z)X = SP$ c) $Z(X Y)X = PS$ d) $Z(X Z)X = PP$

FIGURE 5

The first letter indicates the direction of propagation of the laser beam (Z) while the second letter is the polarization of the laser beam. The third letter gives the polarization of light passed by the analyzer. The last letter (X) describes the collection direction.

The symbols S and P are also used to describe polarized light. S represents an electric field perpendicular to the scattering plane and P is parallel. One letter gives the incident laser beam polarization, the other the analyzer.

The second set of coordinates (x',y',z') is related to the glass substrate and is shown in figure 4. The Y-axis is the same as in the case of lab coordinates. Figure 4 also gives the molecular coordinates which provide the third cartesian set. x and y axes are in the molecular plane and z is along the C_4 axis of metallated phthalocyanines.

Random-orientation versus oriented films and polarization values

Amorphous or randomly oriented films give polarization ratios similar to liquids. However, oriented "crystal-like" films behave quite differently. Specific components of the polarizability tensor can be probed with the appropriate polarized radiation. Let us first consider the case of random orientation. The molecular axes were described by x,y,z and the laboratory coordinates by X,Y,Z . The average of the squares of the polarizability derivative tensor components must be calculated for all possible molecular orien-

tations relative to the laboratory coordinate system. The Raman intensities depend only on two parameters, the mean polarizability α and the anisotropy γ^2 .

Expressions for the mean polarizability α and the anisotropy γ are:

$$\alpha = 1/3 (\alpha_{xx} + \alpha_{yy} + \alpha_{zz}) \quad (4.1)$$

$$\gamma = 1/2 [(\alpha_{xx} - \alpha_{yy})^2 + (\alpha_{yy} - \alpha_{zz})^2 + (\alpha_{zz} - \alpha_{xx})^2]^{1/2} \quad (4.2)$$

The depolarization ratio SP/SS or $\langle \alpha^2_{YY} \rangle / \langle \alpha^2_{YZ} \rangle$ is given by²:

$$\rho = \frac{3(\gamma)^2}{45(\alpha)^2 + 4(\gamma)^2} \quad (4.3)$$

An example of randomly oriented molecules would be carbon tetrachloride liquid. The minimum value of $\rho=0$ would occur for the totally symmetric vibration at 459 cm^{-1} and only polarized radiation is scattered with $\gamma=0$. A maximum of $\rho=3/4$ is expected for a depolarized band such as 218 cm^{-1} with $\alpha=0$.

Expression (4.3) does not hold for materials with preferred molecular orientations. The most ordered system would be a single crystal. Raman depolarization ratios have supplied information concerning the short-range order in liquid crystals³⁻⁶. Silver tetracyanoquino-dimethane (AgTCNQ) films have been prepared by vapor deposition of alternating layers of metal and TCNQ followed by heating to 100°C ⁷. Raman polarization results indicated the

TCNQ units were oriented at approximately 45° to the substrate but domains were not oriented with respect to each other⁷.

Electron micrographs have shown block-like crystallites in AlPcCl, GaPcCl and InPcCl films⁸. These trivalent phthalocyanines have a preferred orientation that can be probed using Raman polarization techniques. The next section derives polarization expressions for compounds of C_{4v} molecular symmetry. Information can be obtained about the angle the Pc stacks make with the substrate. Experimentally one can vary the angle the laser beam makes with the substrate and the polarizations of light.

Transformations from molecular coordinates to laboratory coordinates

The purpose of considering the transformation of cartesian coordinates is to convert from molecular coordinates to substrate coordinates. Once the substrate system is established, a transformation to laboratory coordinates is required. Theoretical expressions for polarization ratios SP/SS , PS/SS and PP/SS can be obtained.

Transformation from one set of coordinates to another is obtained by three successive rotations involving three Euler angles illustrated in figure 6. Right-handed coordinate systems are used which is also the convention adopted by Goldstein⁹.

The first step in the calculations is to transform from molecular to substrate coordinates. A counterclockwise rotation

Figure 6. Transformation from cartesian coordinates x,y,z to x',y',z' by three successive rotations involving Euler angles ϕ, θ, ψ . a) rotation by ϕ about z -axis. b) rotation by θ about ξ -axis. c) rotation by ψ about ξ' axis.

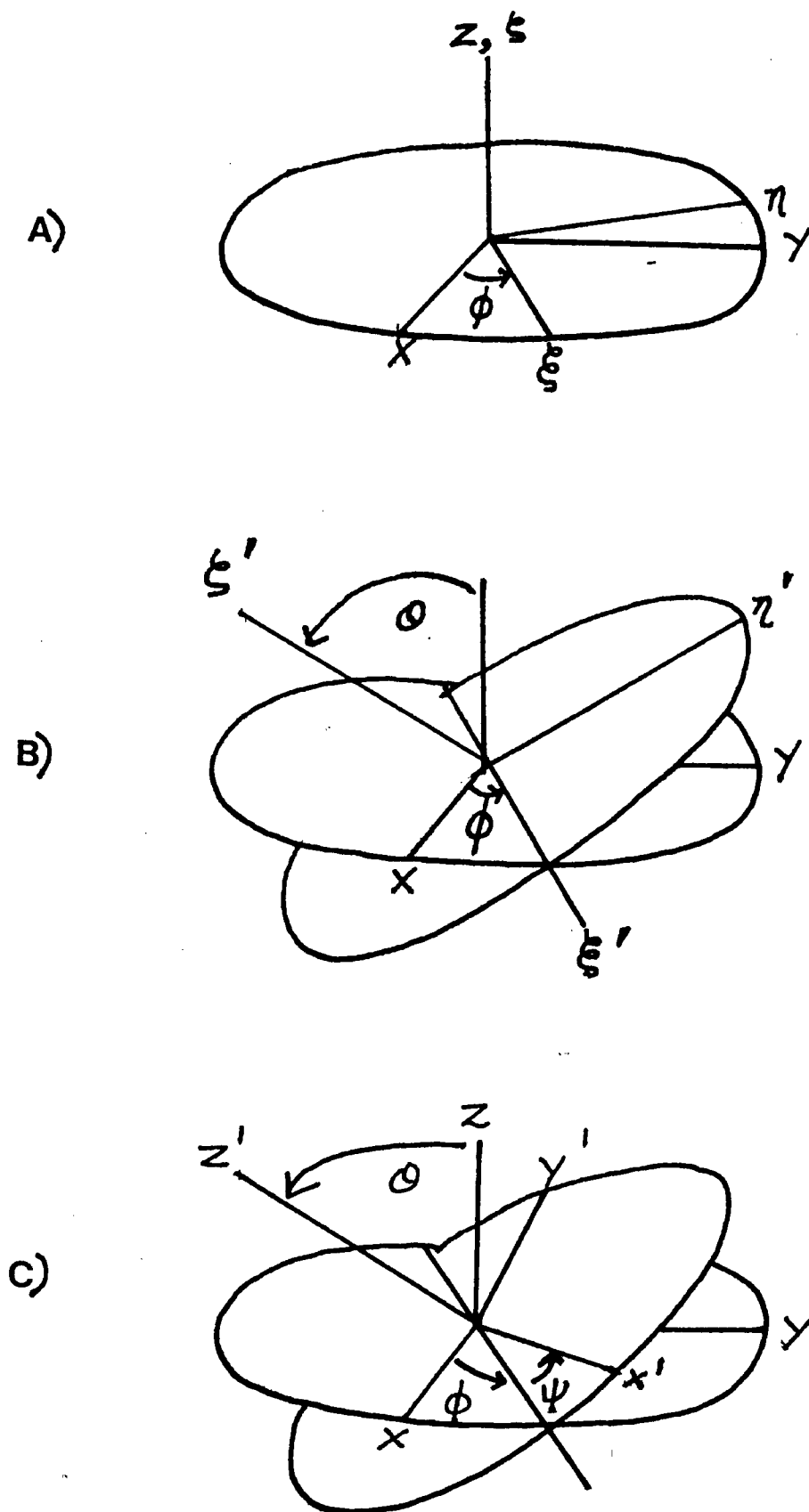


FIGURE 6

about the z-axis by the angle ϕ transforms from x,y,z to ξ,η,ζ and is described as:

$$\xi = Dx \quad (4.4)$$

ξ and x are column matrices while D is a 3 x 3 matrix.

The next rotation is about the ξ axis by the angle θ to go from axes ξ,η,ζ to ξ',η',ζ' :

$$\xi' = C\xi \quad (4.5)$$

The final rotation about ζ' by ψ converts ξ',η',ζ' to x',y',z' :

$$x' = B\zeta' \quad (4.6)$$

The three successive rotations can be described by:

$$A = BCD \quad (4.7)$$

The column matrix x_S describes substrate coordinates and the molecular coordinates are given by x_m . The transformation from molecular to substrate coordinates is:

$$x'_S = Ax_m \quad (4.8)$$

According to Goldstein⁹, the product matrix A is:

$$\begin{vmatrix} \cos\psi\cos\phi & \cos\psi\sin\phi & \sin\psi\sin\theta \\ -\cos\theta\sin\phi\sin\psi & +\cos\theta\cos\phi\sin\psi & \\ -\sin\psi\cos\phi & -\sin\psi\sin\phi & \cos\phi\sin\theta \\ -\cos\theta\sin\phi\cos\psi & +\cos\theta\cos\phi\cos\psi & \\ \sin\theta\sin\phi & -\sin\theta\cos\phi & \cos\theta \end{vmatrix} = A$$

The polarizability component will be transformed according to:

$$\alpha_S = A\alpha_m A^{-1} \quad (4.9)$$

A^{-1} is the symbol for the transpose matrix. The angle ϕ represents a rotation about the z molecular axis and is set equal to zero in this particular problem. The molecular-substrate

angle is given by θ , representing the angle between z_S and z_m axes. If $\theta=0^\circ$, the molecule is flat on the substrate. $\theta=90^\circ$ indicates a perpendicular stacking to the substrate. Finally the ψ angle should be averaged between 0 and 2π . The transformation A is reduced to:

$$\begin{vmatrix} \cos\psi & \cos\theta\sin\psi & \sin\psi\sin\theta \\ -\sin\psi & \cos\theta\cos\psi & \cos\psi\sin\theta \\ 0 & -\sin\theta & \cos\theta \end{vmatrix} = A$$

The second transformation is from substrate to experimental coordinates:

$$x_L = Tx_S \quad (4.10)$$

The glass slide containing the thin film is located on the yz plane, with the laser beam along the z direction and observation is along the x axis. Therefore, the transformation is reduced to a counterclockwise rotation about the y axis. In this case:

$$\begin{vmatrix} \cos\beta & 0 & \sin\beta \\ 0 & 0 & 0 \\ -\sin\beta & 0 & \cos\beta \end{vmatrix} = T$$

The polarizability components are finally obtained from the relation:

$$\alpha_L = T\alpha_S T^{-1} \quad (4.11)$$

Experimentally, spectra can be recorded for different values of the angle β . Specific expressions are obtained for the average of the squared polarizability derivatives of each symmetry type as a function of the angle β (laser beam-normal to the surface of slide) and θ (molecular-substrate angle). In particular equa-

tions were derived for $\langle \alpha_{YY}^2 \rangle$, $\langle \alpha_{YZ}^2 \rangle$, $\langle \alpha_{XZ}^2 \rangle$ and $\langle \alpha_{XY}^2 \rangle$ which correspond to polarized spectra SS, SP, PP and PS respectively.

For all symmetry type vibrations the $\langle \alpha_{YY}^2 \rangle$ expression is only a function of the θ angle. This indicates that the SS spectrum should remain unaffected by changes in the experimental geometry (β angle).

$A_1(A_{1g})$ type vibrations:

According to Loudon¹⁰ the diagonal tensor of A_1 type vibrations has $\alpha_{XX} = \alpha_{YY} = a$ and $\alpha_{ZZ} = b$.

Conventionally the z axis is chosen along the C_4 symmetry element. It is reasonable to assume that $a > b$ for this nearly planar molecule, and for practical considerations we take $b = 0$.

Results for $A_1(A_{1g})$ type vibrations going from molecular to laboratory coordinates follow. Expressions are obtained for SS, SP, PP and PS polarizations.

For $A_1(A_{1g})$ type vibrations¹⁰:

$$\begin{vmatrix} a & 0 & 0 \\ 0 & a & 0 \\ 0 & 0 & 0 \end{vmatrix} = \alpha_m$$

$$A\alpha_m A^{-1} =$$

$$\begin{array}{ccc|c} \begin{array}{l} a\cos^2\psi \\ +a\cos^2\theta + \sin^2\psi \end{array} & \begin{array}{l} -a\sin\psi\cos\psi \\ +a\cos^2\theta\sin\psi\cos\psi \end{array} & \begin{array}{l} -a\sin\theta\cos\theta\sin\psi \\ -a\sin\theta\cos\theta\cos\psi \end{array} & \\ \begin{array}{l} -a\sin\psi\cos\psi \\ +a\cos^2\theta\sin\psi\cos\psi \end{array} & \begin{array}{l} a\sin^2\psi \\ +a\cos^2\theta\cos^2\psi \end{array} & \begin{array}{l} -a\sin\theta\cos\theta\cos\psi \\ a^2\sin^2\theta \end{array} & \\ \begin{array}{l} -a\sin\theta\cos\theta\sin\psi \\ -\sin\theta\cos\theta\cos\psi \end{array} & & & = \alpha_S \end{array}$$

Using equation 4.11, one determines the laboratory values for α_{XY} , α_{YY} , α_{XZ} and α_{YZ} . The calculated average of the squared polarizability derivatives are given:

$$PS = \langle \alpha_{XY}^2 \rangle = 1/4 a^2 \cos^2 \beta (1 + \cos^4 \theta - 2 \cos^2 \theta) + 1/2 a^2 \sin^2 \beta \sin^2 \theta \cos^2 \theta \quad (4.12)$$

$$SS = \langle \alpha_{YY}^2 \rangle = 3/8 a^2 + 1/2 a^2 \cos^2 \theta + 3/8 a^2 \cos^4 \theta \quad (4.13)$$

$$PP = \langle \alpha_{XZ}^2 \rangle = 1/2 a^2 \sin^2 \theta \cos^2 \theta (\sin^4 \beta + \cos^4 \beta) + a^2 \sin^2 \beta \cos^2 \beta (3/8 + \sin^4 \theta + 3/8 \cos^4 \theta + 1/2 \cos^2 \theta - \sin^2 \theta - 2 \sin^2 \theta \cos^2 \theta) \quad (4.14)$$

$$SP = \langle \alpha_{YZ}^2 \rangle = \sin^2 \beta (1/4 a^2 + 1/4 a^2 \cos^4 \theta - 1/2 a^2 \cos^2 \theta) + 1/2 a^2 \cos^2 \beta \sin^2 \theta \cos^2 \theta \quad (4.15)$$

The $SS = \langle \alpha^2_{YY} \rangle$ expression is only a function of θ angle therefore, the SS spectrum should be unaffected by changes in experimental geometry (β angle). The SS spectrum for A_1 would have a maximum intensity when $\theta = 0^\circ$ and a minimum for $\theta = 90^\circ$.

$B_1(B_{1g})$ type vibrations:

The molecular polarizability tensor for B_1 type vibrations is¹⁰

$$\begin{vmatrix} c & 0 & 0 \\ 0 & -c & 0 \\ 0 & 0 & 0 \end{vmatrix} = \alpha_m$$

$$PS = \langle \alpha^2_{XY} \rangle = c^2 \cos^2 \beta (1/4 + 1/2 \cos^2 \theta + 1/4 \cos^4 \theta) + 1/2 c^2 \cos^2 \theta \sin^2 \theta \sin^2 \beta \quad (4.16)$$

$$SS = \langle \alpha^2_{YY} \rangle = c^2 (3/8 - 1/2 \cos^2 \theta + 3/8 \cos^4 \theta) \quad (4.17)$$

$$PP = \langle \alpha^2_{XZ} \rangle = c^2 \cos^2 \beta \sin^2 \beta (3/8 + 3/8 \cos^4 \theta + \sin^4 \theta - 1/2 \cos^2 \theta + \sin^2 \theta - 2 \sin^2 \theta \cos^2 \theta) + 1/2 c^2 \sin^2 \theta \cos^2 \theta (\sin^4 \beta + \cos^4 \beta) \quad (4.18)$$

$$SP = \langle \alpha^2_{YZ} \rangle = c^2 \sin^2 \beta \quad (4.19)$$

B₂ type vibrations:

The molecular polarizability tensor¹⁰ and equations for the average of the squared polarizability derivatives for B₂ vibrations are:

$$\begin{vmatrix} 0 & d & 0 \\ d & 0 & 0 \\ 0 & 0 & 0 \end{vmatrix} = \alpha_m$$

$$PS = \langle \alpha^2_{XY} \rangle = d^2 (1/4 \cos^2 \theta \cos^2 \beta + 1/2 \sin^2 \beta \sin^2 \theta) \quad (4.20)$$

$$SS = \langle \alpha^2_{YY} \rangle = d^2 \cos^2 \theta \quad (4.21)$$

$$PP = \langle \alpha^2_{XZ} \rangle = 1/2 d^2 \sin^2 \theta (\sin^4 \beta + \cos^4 \beta) + d^2 \sin^2 \beta \cos^2 \beta (\cos^2 \theta - \sin^2 \theta) \quad (4.22)$$

$$SP = \langle \alpha^2_{YZ} \rangle = d^2 (1/4 \sin^2 \beta \cos^2 \theta + 1/2 \sin^2 \theta \cos^2 \beta) \quad (4.23)$$

E_x type vibrations:

The molecular polarizability tensor α and equations for the average of the squared polarizability derivatives:

$$\begin{vmatrix} 0 & 0 & e \\ 0 & 0 & 0 \\ e & 0 & 0 \end{vmatrix} = \alpha_m$$

$$PS = \langle \alpha_{XY}^2 \rangle = e^2 (1/4 \sin^2 \theta \cos^2 \beta + 1/2 \sin^2 \beta \cos^2 \theta) \quad (4.24)$$

$$SS = \langle \alpha_{YY}^2 \rangle = e^2 \sin^2 \theta \quad (4.25)$$

$$PP = \langle \alpha_{XZ}^2 \rangle = e^2 \sin^2 \beta \cos^2 \beta + 1/2 e^2 \cos^2 \theta (\sin^4 \beta + \cos^4 \beta) \quad (4.26)$$

$$SP = \langle \alpha_{YZ}^2 \rangle = e^2 (1/2 \cos^2 \beta \cos^2 \theta - 1/4 \sin^2 \theta \sin^2 \beta) \quad (4.27)$$

E_y type vibrations:

The molecular polarizability tensor¹⁰ and the equations for the average of the squared polarizability derivatives follow:

$$\begin{vmatrix} 0 & 0 & 0 \\ 0 & 0 & e \\ 0 & e & 0 \end{vmatrix} = \alpha_m$$

$$PS = \langle \alpha^2_{XY} \rangle = 1/2 e^2 \sin^2 \beta (\cos^4 \theta + \sin^4 \theta) + e^2 \sin^2 \theta \cos^2 \theta (\cos^2 \beta - \sin^2 \beta) \quad (4.28)$$

$$SS = \langle \alpha^2_{YY} \rangle = 3/2 \sin^2 \theta \cos^2 \theta \quad (4.29)$$

$$PP = \langle \alpha^2_{XZ} \rangle = 3/2 e^2 \sin^2 \beta \sin^2 \theta \cos^2 \theta + 1/2 e^2 \sin^4 \beta (\cos^4 \theta \sin^4 \theta + \cos^2 \theta \sin^2 \theta) \quad (4.30)$$

$$SP = \langle \alpha^2_{YZ} \rangle = e^2 \sin^2 \theta \cos^2 \theta (\sin^2 \beta - \cos^2 \beta) + 1/2 e^2 \cos^2 \beta (\sin^4 \theta + \cos^4 \theta) \quad (4.31)$$

Expressions have been derived for various symmetry types of a C_{4v} molecule; $A_1(A_{1g})$, $B_1(B_{1g})$, B_2 , E_x and E_y . For each symmetry type, the four laboratory expressions were given; SS, SP, PP and PS. For all symmetry type vibrations, the SS expression is only a function of the θ angle. The SS spectrum should remain unaffected by changes in the experimental geometry (β angle). Experimentally relative intensities are remarkably constant for different values of the β angle (45° , 60° and 75°).

$A_1(A_{1g})$ type vibrations. The SS spectrum of A_1 would have a maximum intensity when the molecular-substrate angle equals zero and a minimum intensity for $\theta = 90^\circ$. If the molecules were flat on the

surface ($\theta=0$), there would be zero intensity for A_1 types in the SP and PS spectra. The depolarization ratios SP/SS and PS/SS have maximum values (0.66) for $\theta=90^\circ$. Measurements of all depolarization ratios with three different experimental geometries for typical A_1 type vibrations (macrocycle breathing at 671cm^{-1} , pyrrole stretching at 1338 and 1503cm^{-1}) agree well with these findings. Experimental measurements for the 1338cm^{-1} vibration of InPcCl (200nm film on corning glass) indicate molecular stacks with $\theta=75^\circ$.

B₁, B₂ and E type vibrations. Calculations show all three depolarization ratios can be found with values greater than 0.7. For instance, for SP/SS and PS/SS ratios of B_1 species a maximum of four could be observed in the case of a perfectly oriented film. The PP/SS ratio should reach a maximum value of 1.58. Figure 7 gives the calculated depolarization ratio PP/SS versus experimental angle for B_1 type and three stacking angles ($\theta=30,55,80^\circ$). Figure 8 presents the PP/SS depolarization ratio versus stacking angle θ for three experimental β angles.

Some examples of how polarization ratios can be used to assign vibrations follow. For a 200nm film of AlPcCl on NaCl, the resonance Raman spectrum has bands at 1525cm^{-1} and 1541cm^{-1} . Recall, totally and non-totally symmetric bands can appear in resonance Raman spectra.

The NR spectra show 1541cm^{-1} as the predominant signal. The polarization ratio SP/SS is about 0.1 for the 1541cm^{-1} band but 0.7 for the 1525cm^{-1} band. Polarization ratio calculations for a C_{4v} molecule indicate the polarization ratio for an A_1 type vibration should not exceed 0.66. All polarization ratio measurements for the 1541cm^{-1} band support its assignment as A_1 . The 1525cm^{-1} band would be B_1 , B_2 or E. Polarization ratios of Raman bands measured for a film grown on quartz are given in table 4.1.

Differences in relative intensities between the two bands 1525cm^{-1} and 1541cm^{-1} can now be explained. The intensity of an A_1 vibration in the SS spectrum is independent of the experimental angle β but a function of the molecular-substrate angle θ , with a maximum intensity at $\theta=0^\circ$ and a minimum value at $\theta=90^\circ$. Therefore, the low intensity of the 1541cm^{-1} band in the NaCl sample could be correlated with an angle θ close to a right angle. According to the data for polarization ratios the 1525cm^{-1} band can be assigned to a B_1 symmetry type.

The assignment of other observed fundamentals can be advanced by comparing results from RS, RRs and the infrared spectra of the film on NaCl substrate. For instance, the Raman band at 752cm^{-1} is seen in the SP,PS and PP spectra only, indicating that it could be a B_1 , B_2 or E type vibration. Since this frequency is also seen the i.r. it can be assigned to an E representation (A_1 and E only are

i.r. active). Similarly, the 785cm^{-1} band with PR higher than 1, and also active in the i.r. spectra, could be assigned to an E symmetry type. Molecular vibrations that were assigned to the A_1 representation (see table 1) can be active in both RS and i.r.. - However, they are not seen in the i.r. spectra, indicating that the change in dipole moment with these modes is negligible, instead these vibrations produce a significant change of the molecular polarizability.

Figure 7 Calculated PP/SS polarization ratio curves for experimental angle $\beta=0$ to 90° and molecular-substrate stacking angle $\theta=30^\circ, 55^\circ$ and 80° for B_1 symmetry type of a C_{4v} molecule.

Figure 7

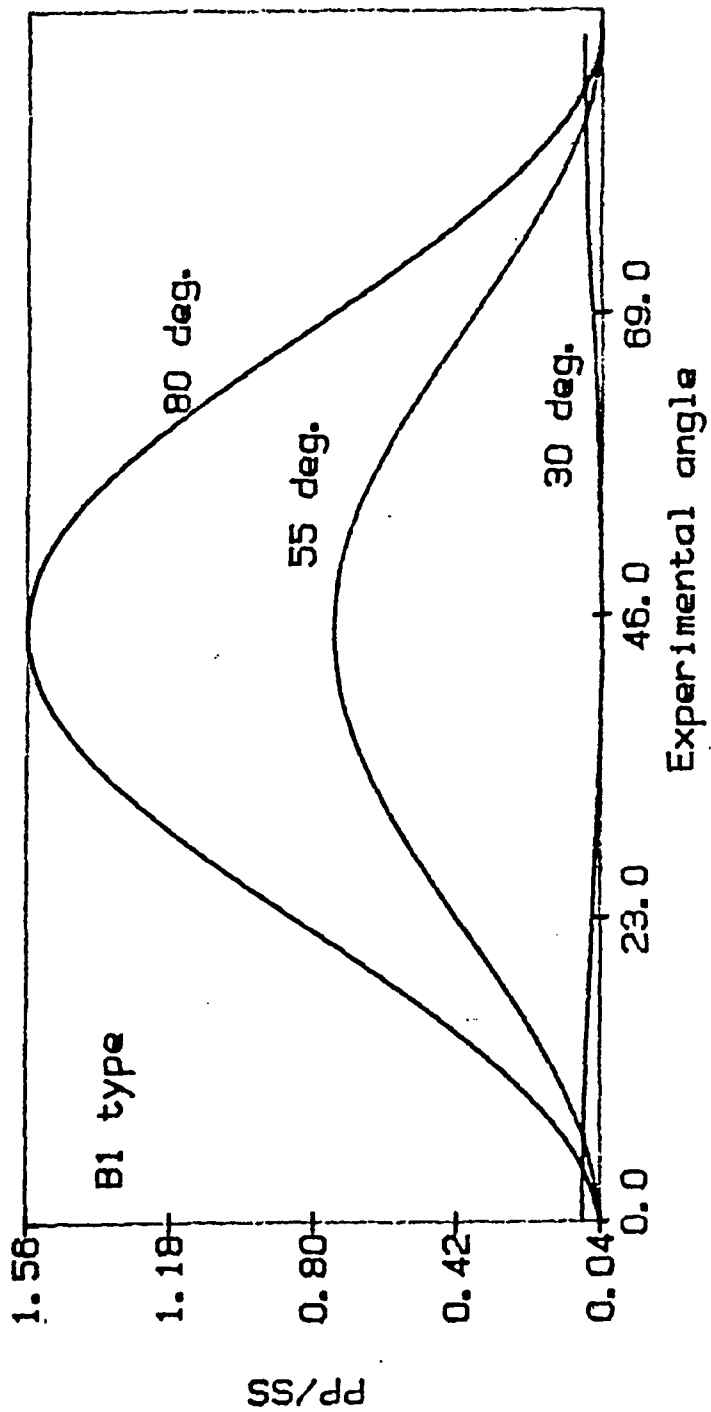


Figure 8 PP/SS polarization ratio curves for molecular-substrate angle $\theta=0$ to 90° and experimental angle $\beta=45^\circ, 60^\circ$ and 75° for B_1 symmetry.

Figure 8

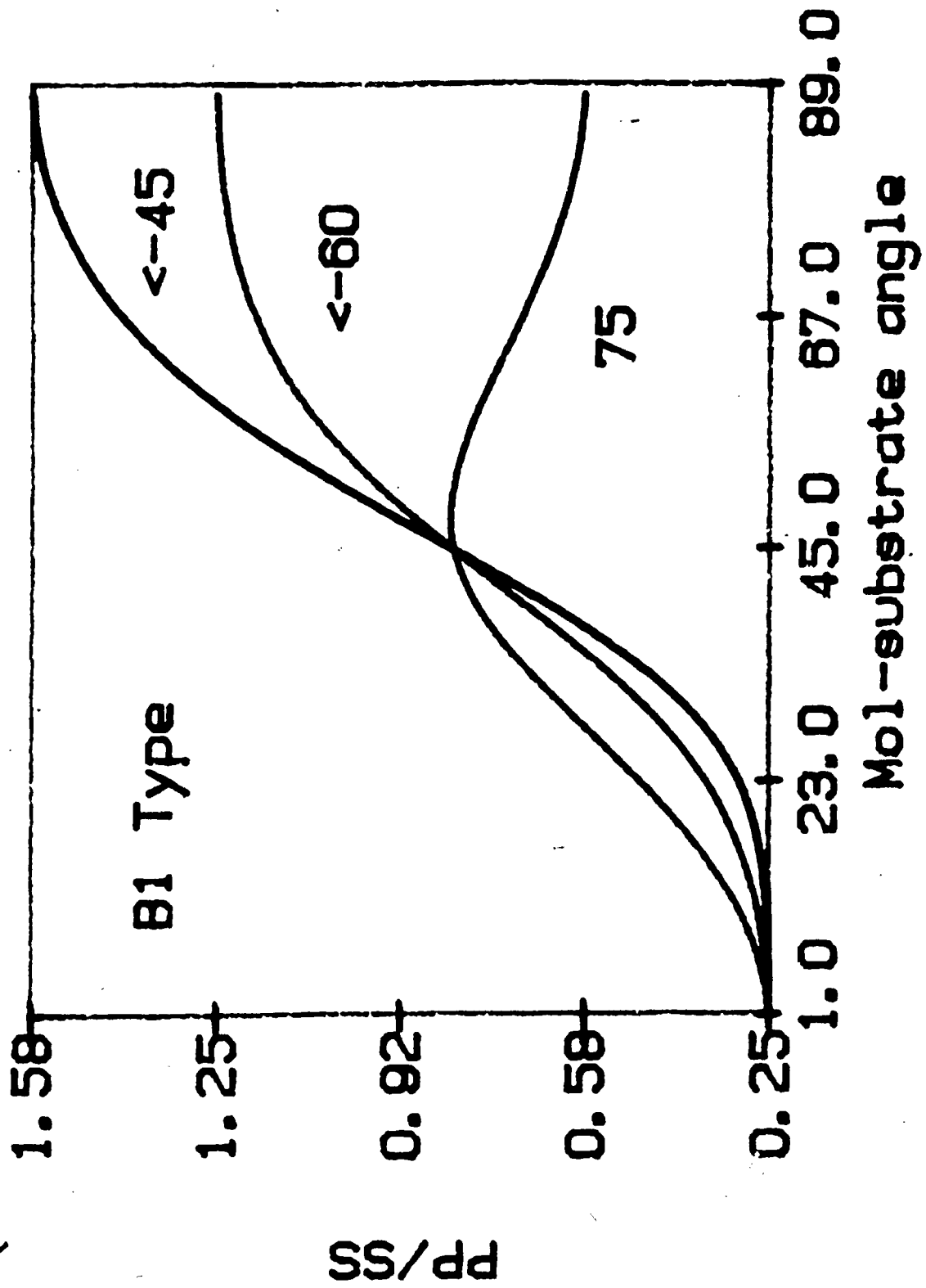


Figure 9 Normal Raman PS and SS spectra for a 200nm film of AlPcCl on quartz.

Figure 9

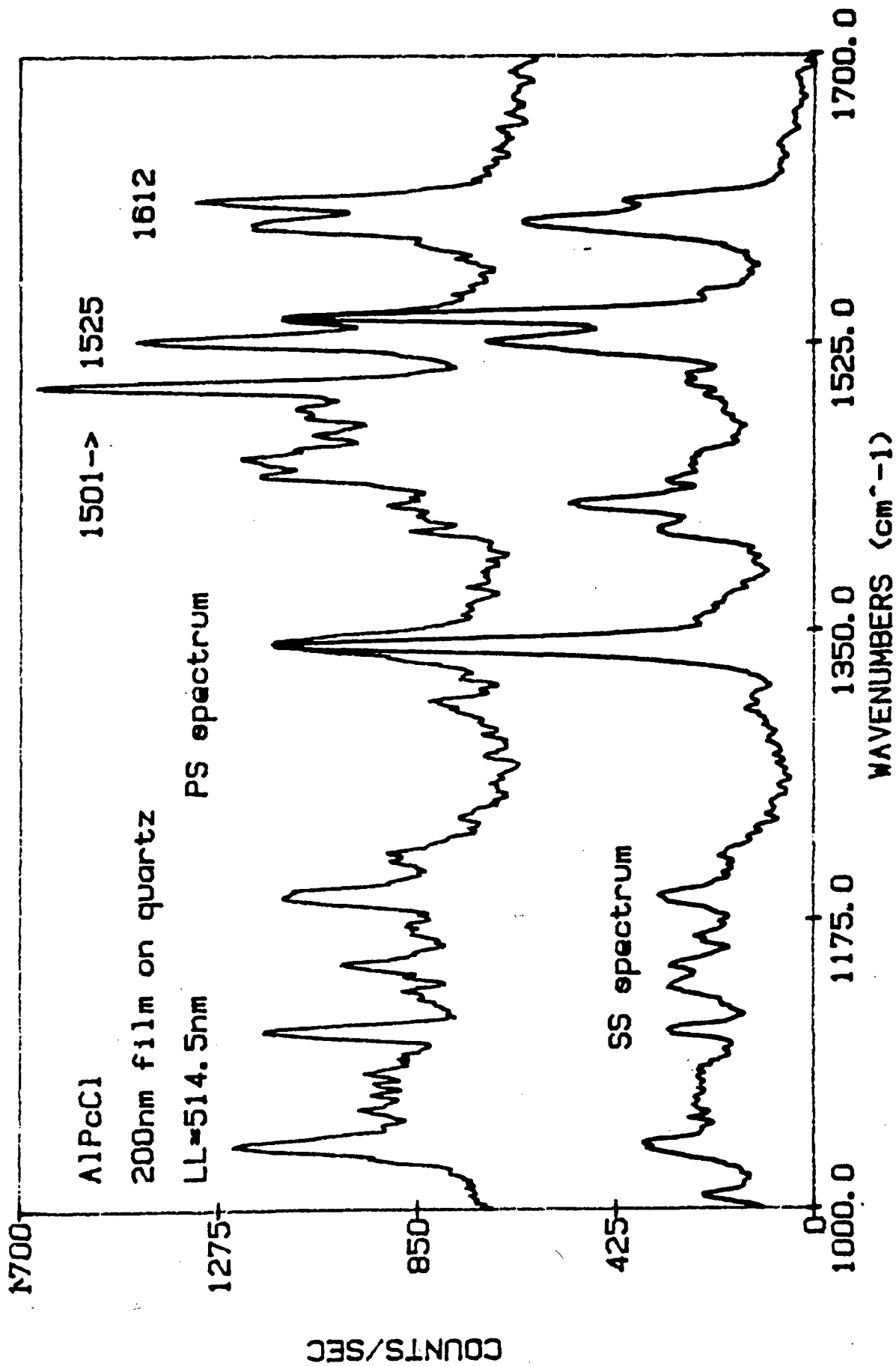


Table 4-1

Polarization ratios measured on a 200nm film of AlPcCl

Wavenumbers	514.5nm		488nm		Interpretation-
	PS/SS	PP/SS	PS/SS	PP/SS	
559 (16)	0.5	0.5	-	-	
591 (70)	0.1	0.5	0.1	0.6	A ₁
681 (93)	0.1	0.6	0.1	0.6	A ₁ macro-breathing
752 -	∞	∞	∞	∞	E ir active
785 (30)	0.6	3.7	1.4	1.2	E ir active
831 (55)	0.2	0.5	-	0.5	A ₁
1009 (14)	-	0.4	-	0.4	A ₁ CH bend
1038 (11)	0.8	0.4	1.2	0.8	CH bend
1063 -	∞	∞	∞	∞	E ir active
1107 (14)	0.9	0.9	1.2	0.8	CH bend
1131 (11)	0.2	0.5	-	0.5	CH bend
1147 (7)	1.0	0.8	-	-	
1169 (8)	-	0.7	-	-	E ir active
1191 (14)	0.7	0.5	0.7	1.7	E ir active
1212 (9)	0.5	0.6	0.8	-	CH bend
1303 (9)	0.6	0.5	0.9	1.0	CH bend
1339 (100)	0.2	0.6	0.1	0.6	A ₁ pyrole st.
1407 (17)	-	0.4	-	0.7	isoindole st.
1425 (28)	0.2	0.4	0.1	0.5	A ₁ isoindole st.
1450 (14)	-	0.5	-	-	isoindole st.
1501 (10)	2.5	0.7	1.6	0.9	isoindole st.
1525 (27)	0.7	0.9	0.7	0.7	B ₁ aza-group st.
1543 (71)	0.1	0.6	0.1	0.6	A ₁ pyrole st.
1598 (34)	0.3	0.5	0.3	0.5	A ₁ benzene st.
1612 (19)	0.9	0.6	-	-	benzene st.

CHAPTER 5: LANGMUIR-BLODGETT FILMS

Introduction

Early work (1930's) concerning the preparation of monolayer films on solid substrates was carried out by Irving Langmuir and Kathleen Blodgett of General Electric¹⁻⁴. Presently, there is renewed interest in Langmuir-Blodgett (LB) films⁵⁻²³ with possible applications as solar cells, gas sensors, superconductors, magnetic storage media, biological sensors and as microelectronic components.

The LB technique in many cases, allows one to assemble monolayers in a well-defined geometry. Kuhn⁷ has used the phrase "synthetic molecular organization" to describe the preparation of molecules to form a functional unit. Rather than attempting the task of finding systems which self-assemble in solution, the LB approach is favored where layers of different composition can be deposited on one another⁷.

Our interest in the LB technique has been to prepare a monolayer of $(t\text{-bu})_4\text{H}_2\text{Pc}$ which has been described by Kovacs¹¹ and obtain Raman spectra. The main objective was to deposit a monolayer of $(t\text{-bu})_4\text{H}_2\text{Pc}$ on silver and indium island films. Would surface enhanced Raman scattering (SERS) be observed and would frequencies be shifted due to an interaction with the metal? Further, what would happen to the Raman spectra if monolayer spacers were placed between the metal island and the $(t\text{-bu})_4\text{H}_2\text{Pc}$ monolayer?

LB trough, material, solvent and subphase

A schematic diagram of a Langmuir-Blodgett trough is given in figure 10. Usually the molecules to be deposited as LB films have a hydrophilic group and a hydrophobic part but this is not a mandatory prerequisite. Fatty acids have been the subject of numerous LB experiments. Other types of materials such as porphyrins, anthracenes, and phthalocyanines¹⁰⁻¹⁹ have been prepared as LB films. The molecules are dissolved in an appropriate solvent with a typical concentration being $5 \times 10^{-4} \text{M}$ for $(t\text{-bu})_4\text{H}_2\text{Pc}^{11}$.

A number of properties of the solvent must be considered. The solvent must dissolve the molecules of interest and be sufficiently volatile to evaporate after drops are placed on the subphase. The solvent should be very pure as any remaining impurities could be incorporated in the LB film. One problem in preparing phthalocyanine LB films has been their lack of solubility in organic solvents. Derivatives have been prepared with various peripheral groups¹⁰⁻¹⁹.

Drops of the LB material are placed on the subphase which is usually purified water. The solvent evaporates and the molecules remain on the surface of the water. It can be seen that the LB material must not dissolve in the subphase. The hydrophilic end of the molecule orients so that it is adjacent to the water surface. The hydrophobic or aliphatic region is positioned away from the water. One barrier of the LB trough is fixed while the other

Figure 10. A schematic of a Langmuir-Blodgett trough.

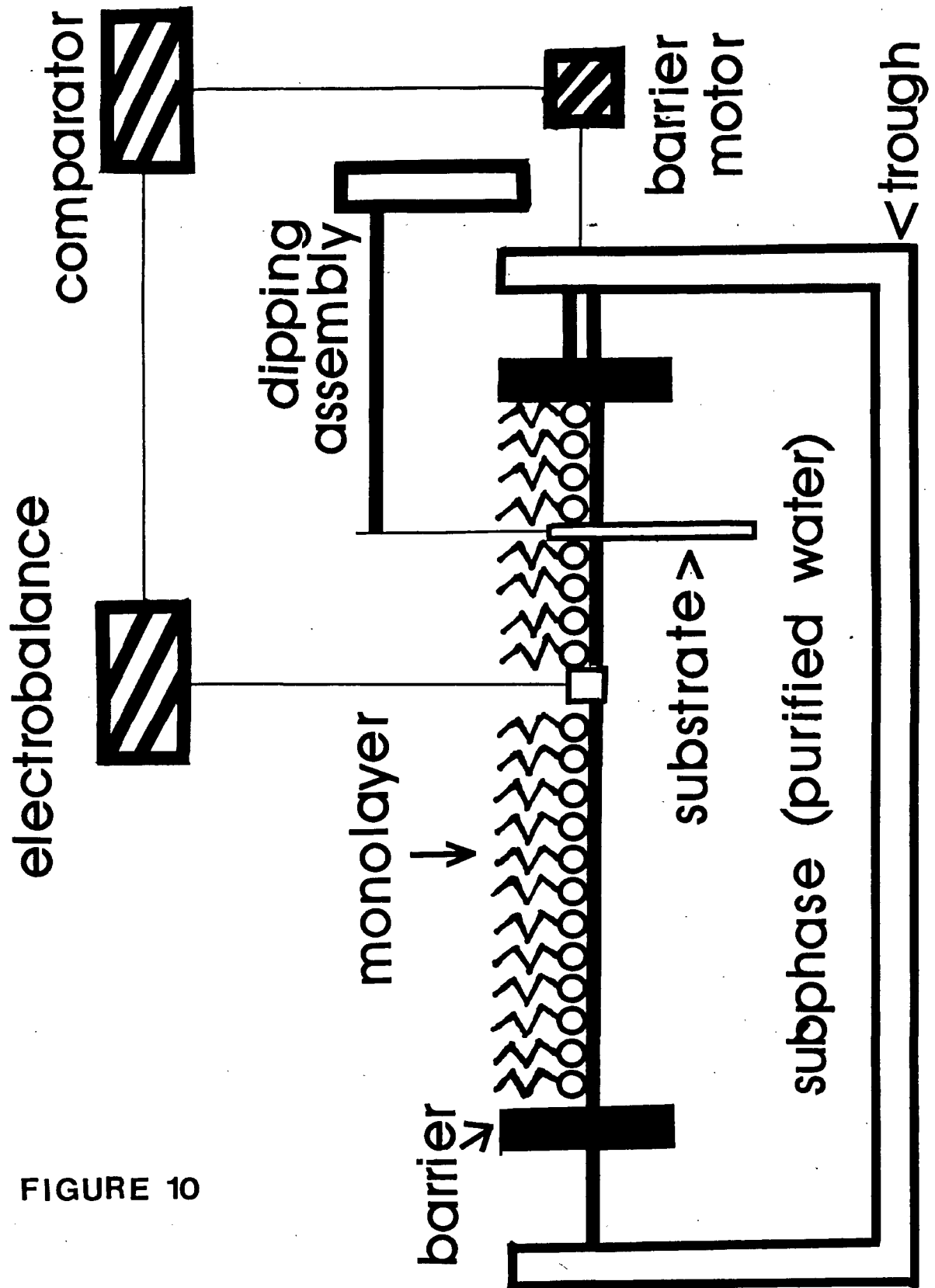


FIGURE 10

barrier can be motor driven. The barrier is moved until the desired surface pressure is reached. The surface pressure is monitored by the Wilhelmy or Langmuir method. The Wilhelmy method determines the surface tension on a partially immersed plate and the Langmuir method compares the surface tension of a clean part of the substrate and a coated portion of the substrate⁵. It is common to plot the surface pressure against the area occupied by the monolayer on the trough. These plots are called "pressure-area isotherms". A feedback system is required to maintain constant pressure as the LB film is deposited on a substrate.

The dipping assembly can raise or lower a substrate. Its motion must be smooth and different speeds can be selected. Many materials are used as substrates for LB deposition. Clean glass slides are hydrophilic and can be made hydrophobic by depositing a monolayer of arachidic acid. For metal layers vacuum deposited on clean glass slides, Au, Cu and Ag result in a hydrophobic surface, whereas Al and Pb produce hydrophilic surfaces due to formation of oxides⁵. Subsequent deposition of other monolayers on the metal is possible. LB material can be transferred to a solid substrate at constant pressure in a few ways. X-deposition takes place if the substrate is immersed only. Y-deposition involves immersion followed by withdrawal. Z-deposition requires withdrawal only. Two other less common methods are "touching" and "lifting" of the substrate⁵. The orientation of adjacent monolayers depends on the deposition technique selected.

Phthalocyanine LB films prepared by others

Specific phthalocyanine LB studies can now be discussed.

Yamamoto¹² prepared LB films of H_2Pc and observed color changes in aqueous KCl solutions. A comparison of absorption spectra leads one to conclude the film goes from a monomeric structure to a dimeric structure after thermal annealing at $300^{\circ}C$ for a few hours. No information was available on the stacking of the H_2Pc molecules in this film. Yamamoto¹² concluded that the electrochromic color changes correlate with the degree of molecular association.

Snow and Jarvis¹⁰ prepared LB films of the type $MPcX_4$ where $M = H_2, Co, Cu, Ni, Pd, Pt$ and X represents the cumylphenoxy group $(-O-C(CH_3)_2-C_6H_5)$. The presence of cumylphenoxy peripheral groups improves the solubilities of Pcs in organic solvents. The association of $MPcX_4$ compounds was studied in solution. Most compounds were dimeric, $PbPcX_4$ was monomeric and $PtPcX_4$ displayed the highest degree of association. The packing efficiency of LB monolayers correlated with the size of the Pc aggregate in solution¹⁰. The area/molecule at a constant film pressure for dimeric $CuPcX_4$ was less than the area/molecule for $PtPcX_4$.

Barger¹⁴ also examined LB films of metal-substituted tetracumylphenoxy phthalocyanines $MPcX_4$ with $M = Fe, Co, Ni, Cu, Zn, Pd, Pt$ and Pb . Other metallated derivatives prepared had pendant groups: phenoxy $(-O-C_6H_5)$, octadecoxy $(-O-(CH_2)_{17}-CH_3)$

and neopentoxy ($-O-CH_2-C(CH_3)_2-CH_3$). Pressure-area isotherms gave small areas compared to the known size of the Pc molecule¹⁴.

Two conclusions drawn from the data by Barger¹⁴ was that classical monomolecular films were not observed and stacking was likely but the stack axis was not parallel to the plane of the film. In the experiments by Snow¹⁰ more highly associated Pcs gave larger areas/monomer. This observation cannot be explained by simple vertical stacking and Barger¹⁴ suggests a tilting of stacks and variation of tilt angles with different metals.

DiLella¹⁶ prepared tetracumylphenoxy Pc derivatives in 1:1 mixtures with stearyl alcohol. LB monolayers were deposited on Au, Ag and Pd vacuum evaporated films. A high degree of aggregation for LB films was inferred from the electronic spectra¹⁶. The Raman results of this study will not be discussed in this section but for tetracumylphenoxy cobalt phthalocyanine [CoPc(Cp)₄] on gold, an adsorbate-substrate interaction was apparent¹⁶. Results are consistent with a stacking of CoPc(Cp)₄ molecules with the bottom member of the stack in contact with the surface¹⁶.

Roberts¹³ worked with LB films of (t-bu)₄ZnPc, (t-bu)₄CuPc, and an asymmetric compound CuPc tris(CH₂NHC₃H₇-iso). With an appropriate solvent cross-sectional areas were obtained which corresponded to molecules sitting vertically edge-on in the liquid¹³.

Hann¹⁵ performed experiments on (t-bu)₄ZnPc and (t-bu)₄CuPc. A sample

was prepared for electron microscopy (EM) by horizontally lifting a $(t\text{-bu})_4\text{CuPc}$ monolayer onto an amorphous-carbon coated grid. EM on $(t\text{-bu})_4\text{CuPc}$ indicated short range order but most of the film was amorphous¹⁵. Closest packing of tetra-tert-butyl phthalocyanine molecules is possible if the tert-butyl groups are interleaved^{11,15}.

CHAPTER 6 EXPERIMENTAL

Vacuum Evaporation

Thin solid films were prepared either by vacuum evaporation or as Langmuir-Blodgett films. A schematic diagram is given in figure 11 of a typical vacuum evaporation system. Three different types of vacuum systems were used: a Varian NRC3115, Balzers and Vacuum Generators DPUHV. The rate of evaporation was 0.5nm for trivalent phthalocyanines (AlPcCl, GaPcCl, InPcCl) monitored with an Inficon XTM quartz crystal oscillator. Total thicknesses were 100nm or 200nm. A typical pressure before evaporation was 1.0×10^{-6} torr or lower. A tantalum boat was used to contain the phthalocyanine material.

A number of different substrates have been used for vacuum evaporation. Quartz was preferable for red laser lines as it gave a low background. Other substrate materials were Corning 7059 glass, a cleavage face of NaCl and conductive tin-oxide (NESA) plates from the Pittsburg Glass Company.

Chemicals

The AlPcCl was purchased from Eastman Chemicals. The InPcCl and GaPcCl were provided by C.K. Hsiao and P. Kazmaier respectively of Xerox Research Centre of Canada. The InPcCl and GaPcCl were synthesized by reacting the metal chloride with phthalonitrile in quinoline. The Pcs were purified by the train sublimation procedure¹.

Figure 11. A schematic of a typical vacuum evaporation system.

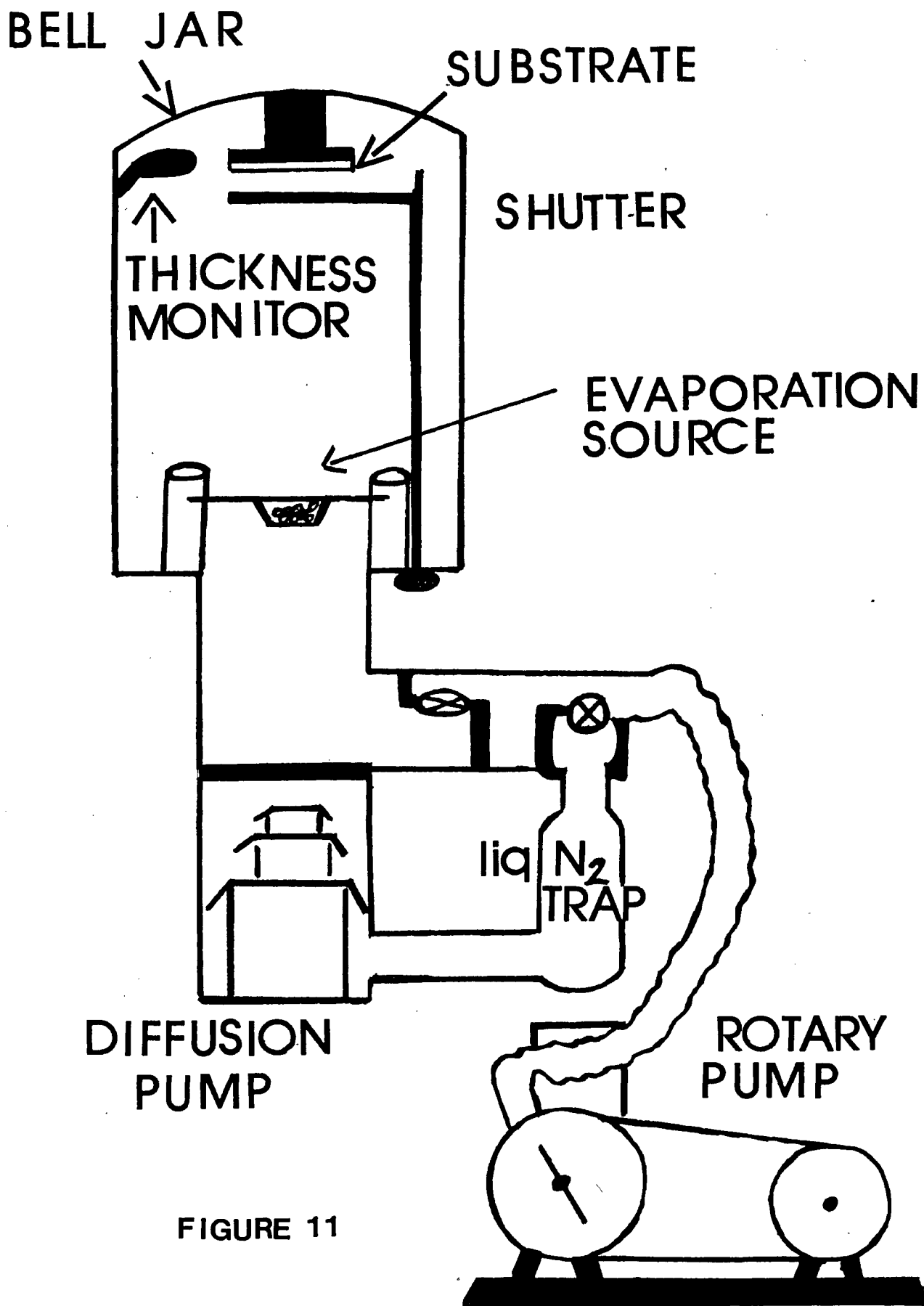


FIGURE 11

Synthesis of $(t\text{-bu})_4\text{H}_2\text{Pc}$, preparation of monolayers and their characterization have been reported previously². The purified $(t\text{-bu})_4\text{H}_2\text{Pc}$ was supplied by Xerox and was synthesized by refluxing 4-t-butyl phthalonitrile in amyl alcohol with sodium amylate present³ and purification was by acid pasting⁴. The solution of $(t\text{-bu})_4\text{H}_2\text{Pc}$ for spreading on the Langmuir Blodgett trough was $5 \times 10^{-4}\text{M}$ in Eastman Kodak Reagent ACS Spectro Grade toluene. The water used in the trough was milli-Q followed by another distillation and kept at room temperature. A Fromherz⁵ trough was used for preparation of the LB films. The trough was enclosed in a cabinet to exclude dust and was on a Terrazzo vibration-free table. The compression speed was 0.06 to 0.15 $\text{Å}^2/\text{molecule}/\text{second}$ and the lifting of the substrate was done at 3.8mm/min with pressures of 8-10 dynes/cm. The substrate was immersed before spreading the $(t\text{-bu})_4\text{H}_2\text{Pc}$ and the film was transferred to the glass on withdrawal. In the case of multilayers, the surface of the water was cleaned and this process repeated.

Mono and multilayer films of $(t\text{-bu})_4\text{H}_2\text{Pc}$ were deposited on the corning slides. Metal island films of silver and indium were deposited on corning to a thickness of 15nm measured by the quartz crystal thickness monitor at a rate of 0.1nm/sec. Subsequently a LB film of $(t\text{-bu})_4\text{H}_2\text{Pc}$ was deposited on the metal slides. One region of the slide had metal plus Pc while another region had Pc only. Absorption spectra were recorded on a HP8450 photodiode array spectrophotometer.

Samples were prepared for spacer studies by first depositing a region of 15nm silver or indium on Corning 7059 glass. The metal island films were then coated with close packed arachidic acid monolayers(s) (0,1,3...) on different regions of the slide. The (t-bu)₄H₂Pc monolayer was then deposited on top of the arachidic acid. Figure 12 shows the metal islands with a spacer layer of arachidic acid and a phthalocyanine monolayer.

Raman system

The microcomputer controlled Raman system used to study the thin films has been described elsewhere⁶. An IBM PC microcomputer was used to drive the stepper motor connected to the two 1800 grooves/mm holographic gratings. The microcomputer also acquired the signals from a Hamatsu R955 multialkali photomultiplier tube followed by conventional photon counting. Two software programs were used, one for data acquisition, another for data manipulation. Polarization measurements were carried out using a polarization rotator (Spectra Physics model 310-21) mounted on the 164 argon and krypton ion lasers. Scattered light was analyzed using a linear polarizer and scrambled before entering the Spex 1403 spectrophotometer. A RG375 dye laser has been used and was pumped by the model 164 argon ion laser. Backscattering Raman spectra were recorded in a Ramanor U-1000 instrument with microscope attachment.

The laser beam propagated along the Z-axis and the angle the laser beam made with the normal to the film was adjusted using the




Figure 12 Cross-sectional schematic view of metal island (modelled as a hemispheroid) coated with one spacer layer of arachidic acid and a phthalocyanine monolayer.

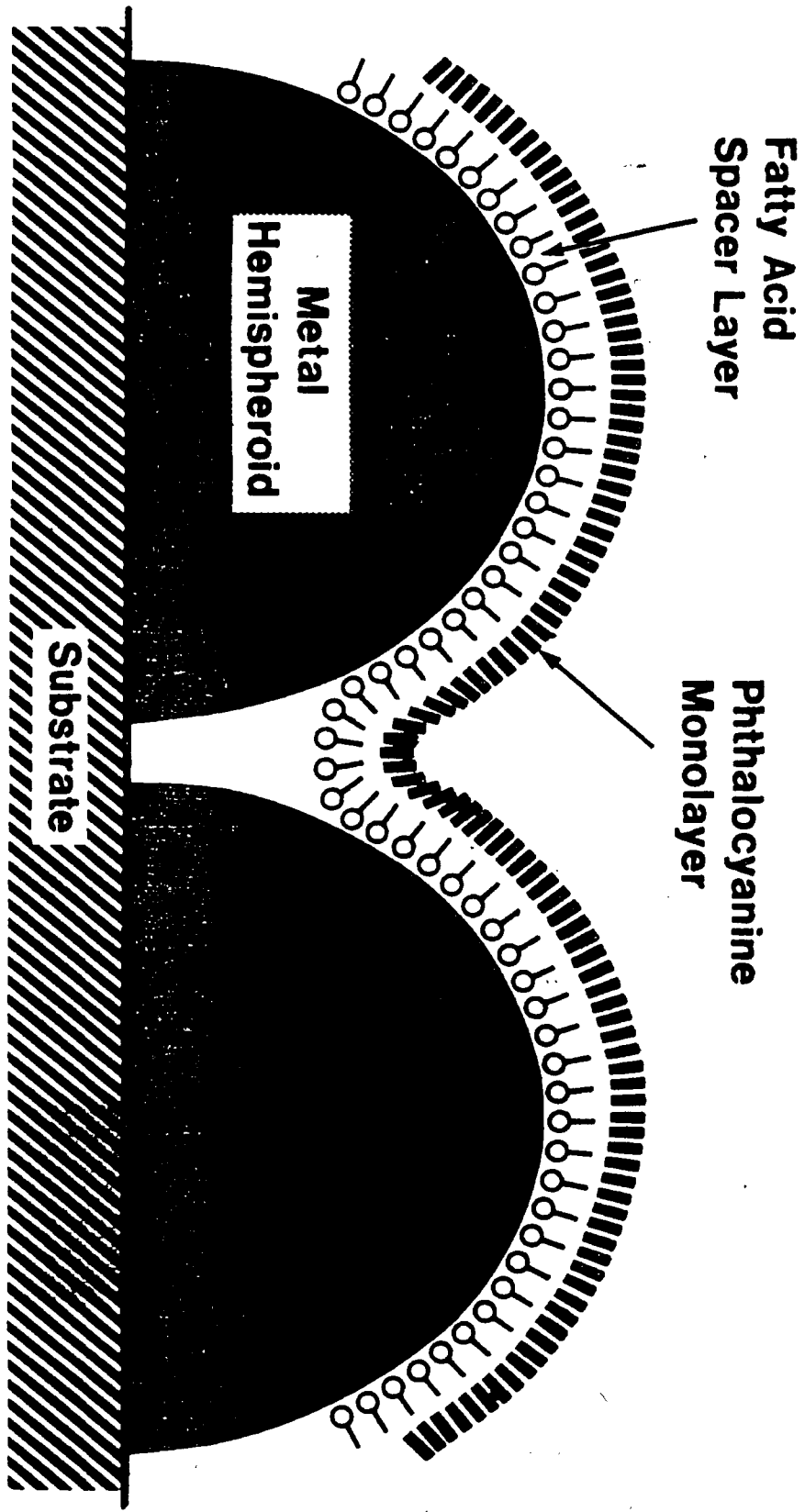


FIGURE 12

sample holder. The four polarizations (SS,SP,PP,PS) of light were obtained by moving the rotator on the laser and the analyzer. A quartz cell containing BDH spectroscopic grade carbon tetrachloride was used periodically to check the accuracy of Raman frequencies and polarization ratios. A more extensive calibration of the system was occasionally done with a capillary of distilled indene.

There are four slits present in the 1403 monochromator and settings are reported with the spectra. Other details given with the spectra are time delay and laser power. The laser lines used from the argon ion laser had wavelengths of 488.0nm (blue) and 514.5nm(green). A number of laser lines were available from the krypton ion laser and the most commonly used were 568.2nm (yellow), 647.1nm (red) and 676.1nm (red). A solution of rhodamine 6G pumped through the dye laser gave lines tunable over the region 580nm to 620nm.

Infrared spectra of 200nm films of AlPcCl, GaPcCl and InPcCl on NaCl were run using a Nicolet 5DX FTIR spectrophotometer. Other substrates were not suitable for IR study. Uv-visible spectra were run on a HP 8450 spectrophotometer.

CHAPTER 7: SPECTRA AND RESULTS

Figures 13 to 15 are a few of the many spectra obtained for the trivalent Pc films. The laser line was 647.1nm so these are resonance Raman spectra. The assignment of the various bands follows in Chapter 8. Figures 16 to 18 are the uv-visible spectra for 100nm films of AlPcCl, GaPcCl and InPcCl

Uv-visible absorption spectra

There are two main bands in the uv-visible region of phthalocyanines. A Soret band is present in the region 300 to 400nm and is associated with a π to π^* transition of the Pc ring¹.

The Q-band observed in the region 600 to 800nm is also a π to π^* transition, can have features from metal to ligand or ligand to metal charge transfer and is sensitive to the molecular environment^{1,2}.

All of the trivalent phthalocyanines (AlPcCl, GaPcCl, InPcCl) are blue in colour and the uv-visible spectra are red-shifted when compared with films of planar divalent Pcs such as CuPc, MgPc and ZnPc. The uv-visible absorption maxima for 100nm evaporated films were 344nm, 751nm (AlPcCl); 375nm, 750nm (GaPcCl) and 369nm, 732nm (InPcCl). Shoulders were also present in these spectra.

A compound which has its absorption bands into the IR is VOPc. Klofta² concluded that the Q-band red shift in VOPc, AlPcCl and GaPcCl was due to a slip-stack orientation in the films. As mentioned earlier in the section on structure, the oxyvanadium

Figure 13. Resonance Raman spectrum of 200nm AlPcCl on quartz. Total S polarization. slits 800 μ m and laser line 647.1nm.

Figure 13

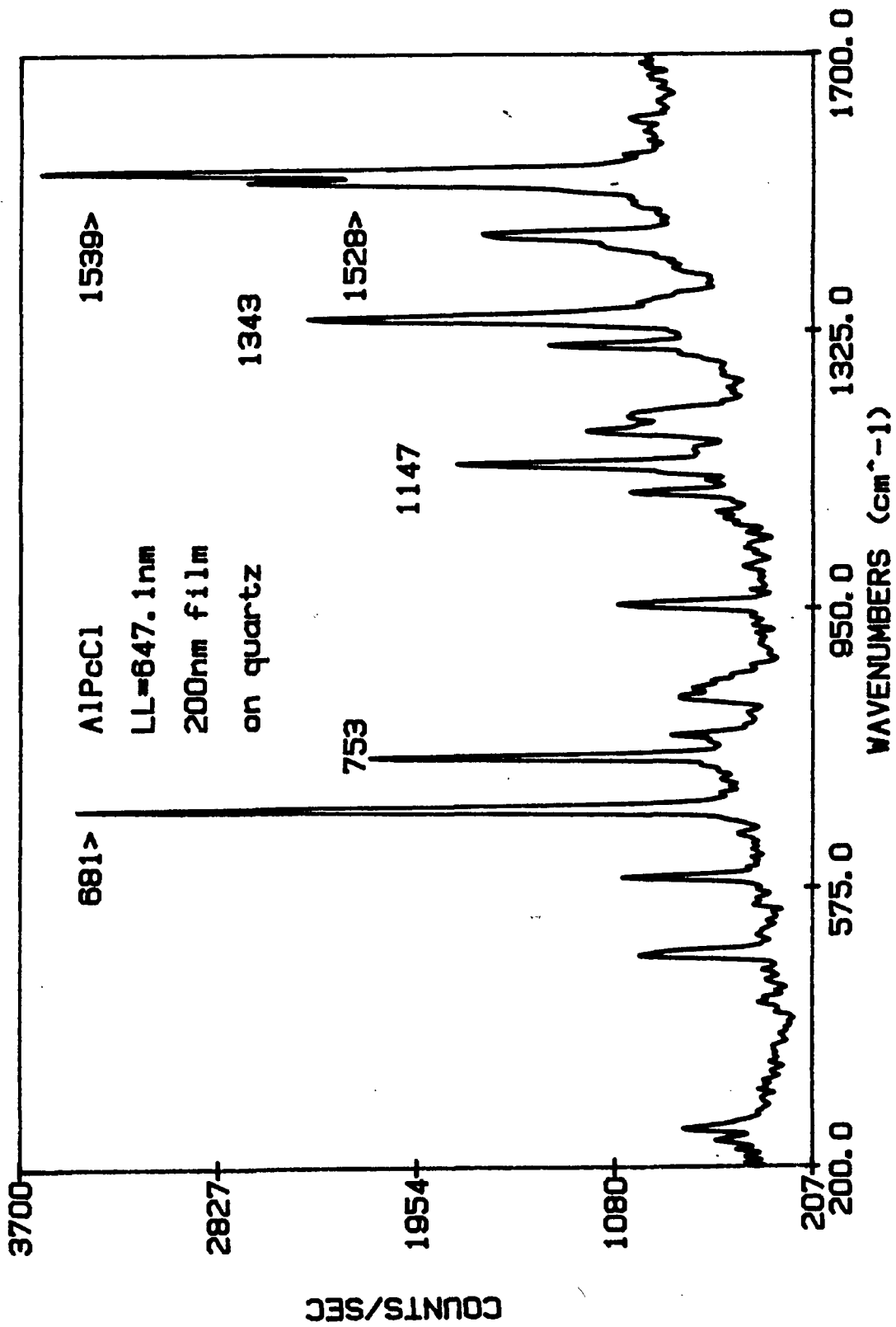


Figure 14. Resonance Raman spectrum of 200nm GaPcCl on quartz.
Total S polarization. slits 800 μ m and laser line 647.1nm

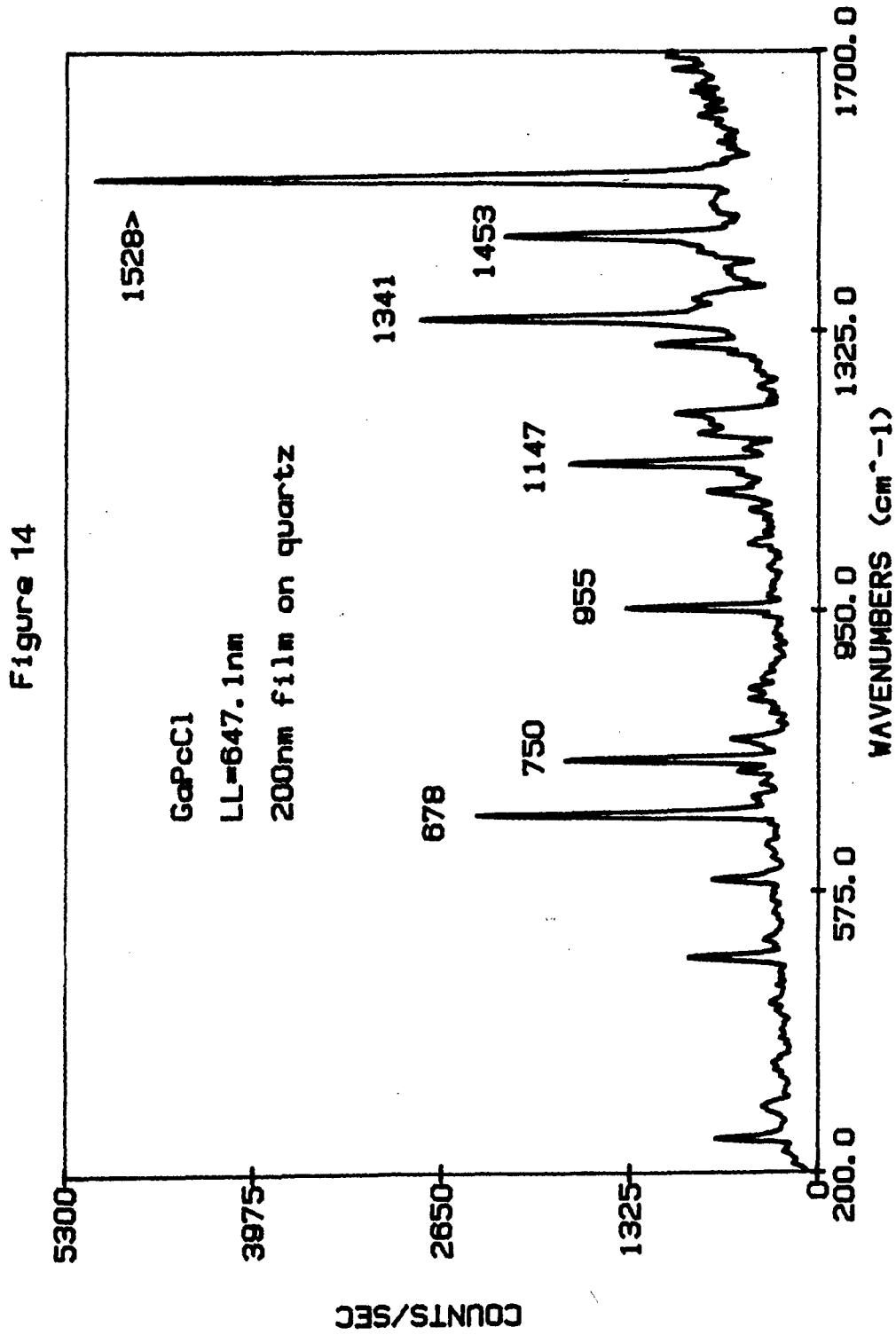
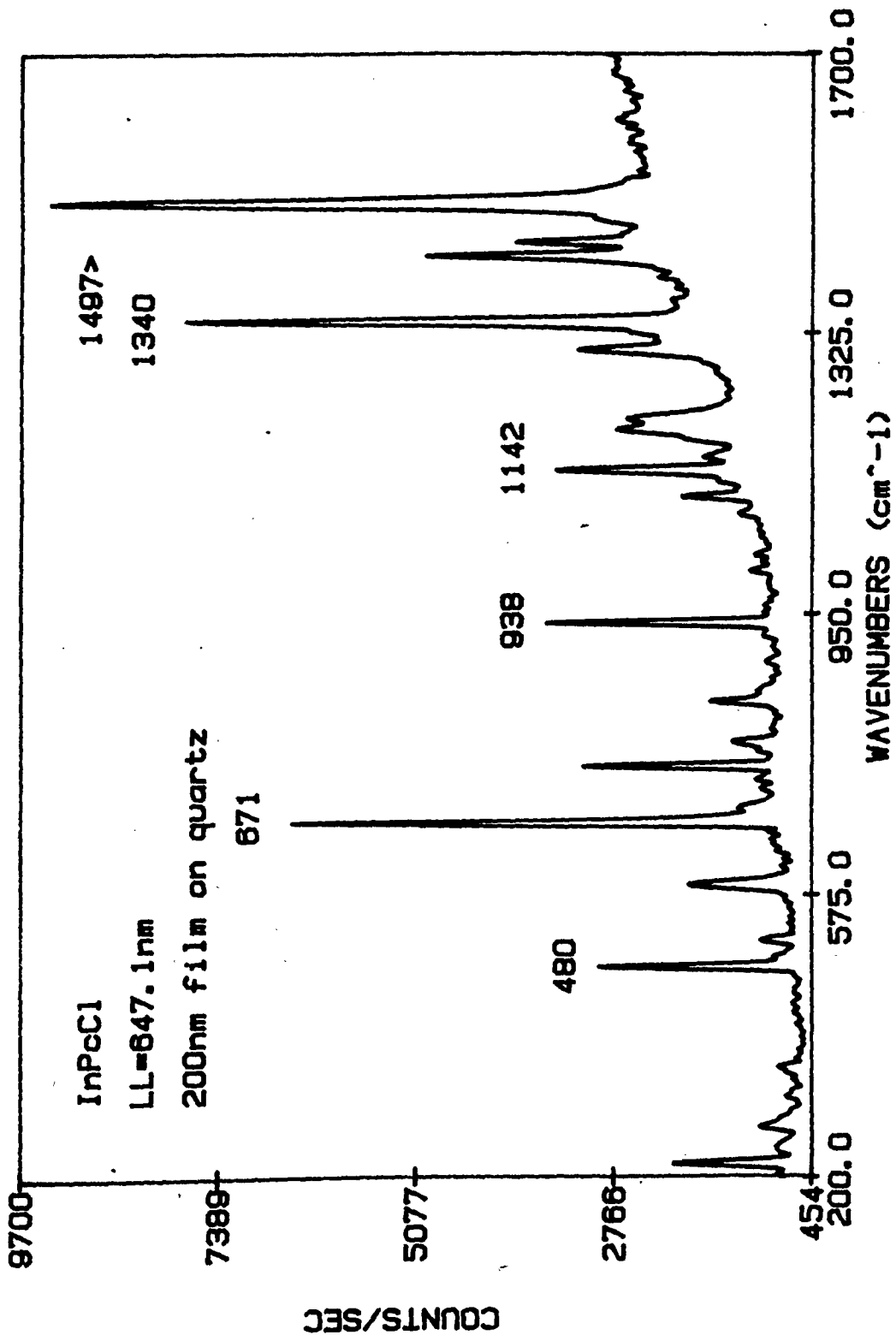


Figure 15. Resonance Raman spectrum of 200nm InPcCl on quartz. Total s polarization. slits 800 μ m and laser line 647.1nm.

Figure 15



cation lies above the plane of the four isoindole nitrogens³. Likewise the metal is displaced from the Pc plane in AlPcCl and GaPcCl⁴. The axial chlorine and oxyvanadium cation make cofacial stacking difficult. The bands of a film of AlPcF are not red-shifted like AlPcCl, GaPcCl and InPcCl films compared to planar divalent Pcs. AlPcF absorption bands occur at 328nm and 624nm in a 100nm film. The AlPcF molecules are cofacially aligned with a somewhat ionic structure⁵.

A number of Pc films (MgPc, ZnPc, VOPc, AlPcCl, ClAlPcCl and InPcCl) undergo a solvent-induced structural change^{6,7}. The films have been either dipped in a solvent such as CH₂Cl₂ or exposed to the vapor in a covered beaker. The solvent-induced changes in the absorption spectra of MPcs are due to molecular stacking changes which occur on dissolution and reorganization. Another way of inducing structural changes in Pc films is by annealing.

Uv-visible absorption spectra provide information concerning the angle Pc molecular stacks make with the substrates. As Pc molecules are stacked like pancakes with the plane of the molecule perpendicular to the substrate, the intensity of the Soret band decreases.

The argon ion laser lines 488.0nm and 514.5nm gave rise to normal Raman (NR) because of the valley in the trivalent Pc absorption spectra. The rhodamine 6G laser lines and the red laser lines of the krypton ion laser excited into the Q-bands of the Pcs.

Figure 16. Uv-visible absorption spectrum of 100nm film of AlPcCl on quartz.

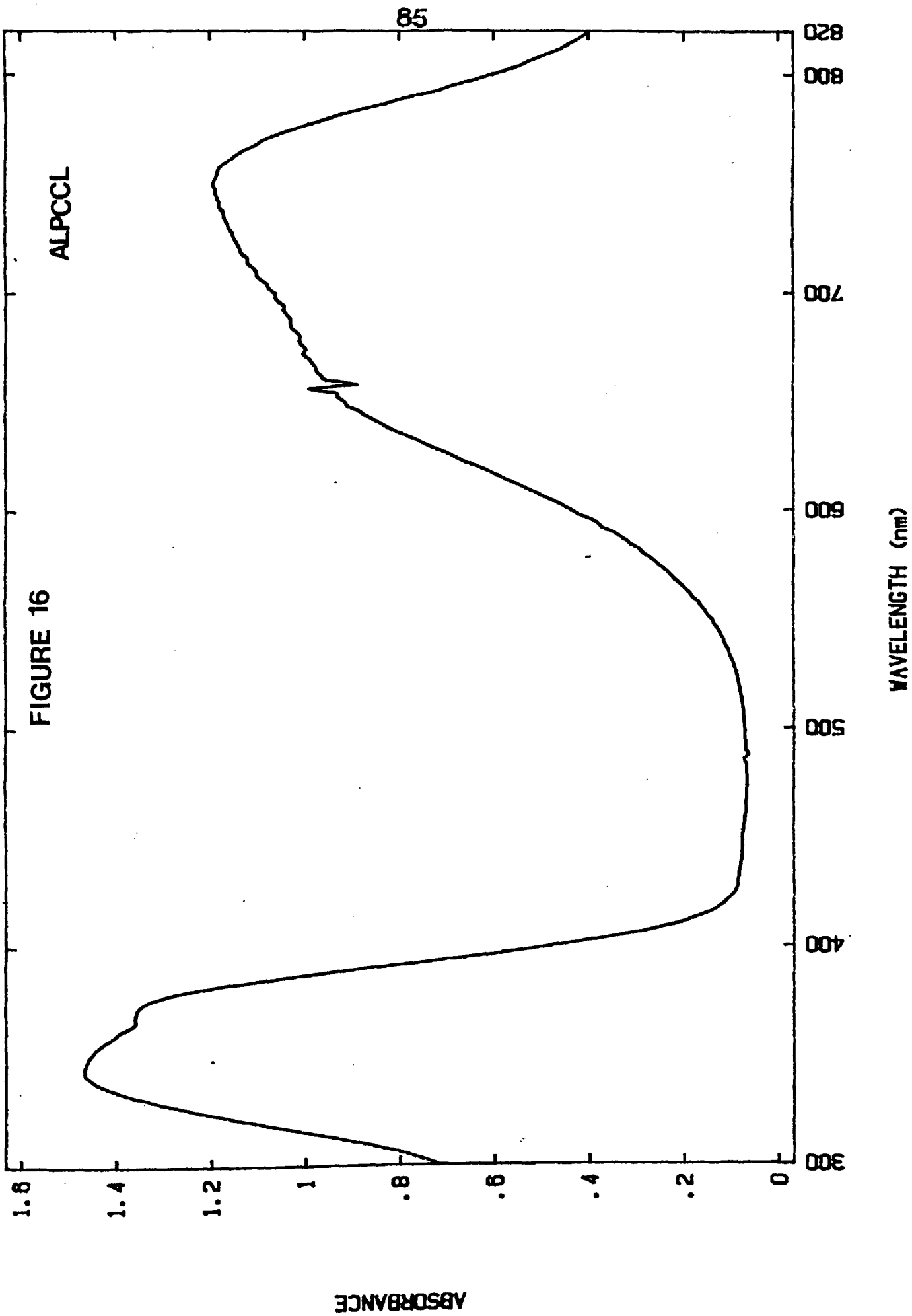


Figure 17. Uv-visible absorption spectrum of 100nm GaPcCl film on quartz.

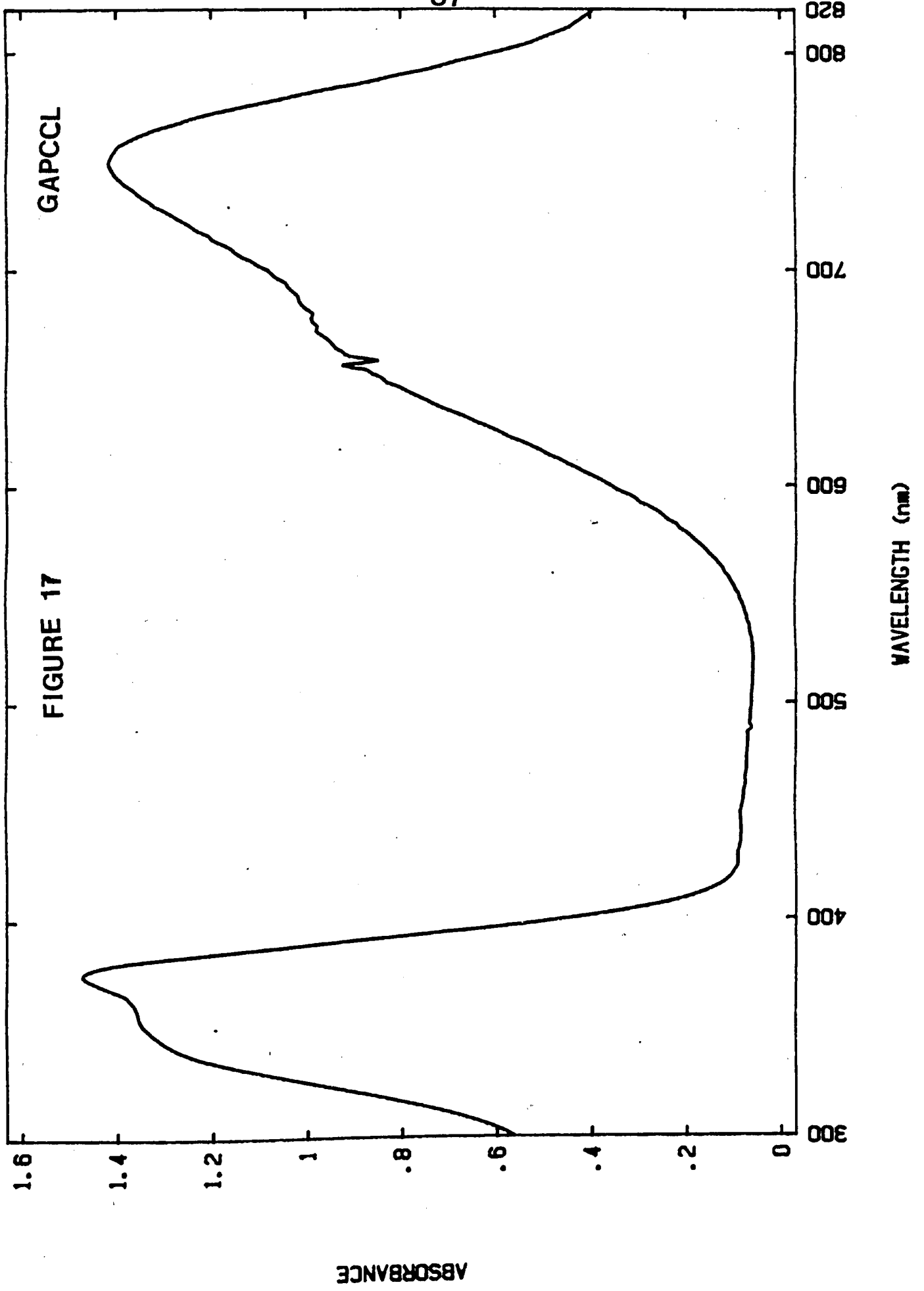


FIGURE 17

GAPCCL

ABSORBANCE

WAVELENGTH (nm)

Figure 18. Uv-visible absorption spectrum of 100nm InPcCl film on quartz.

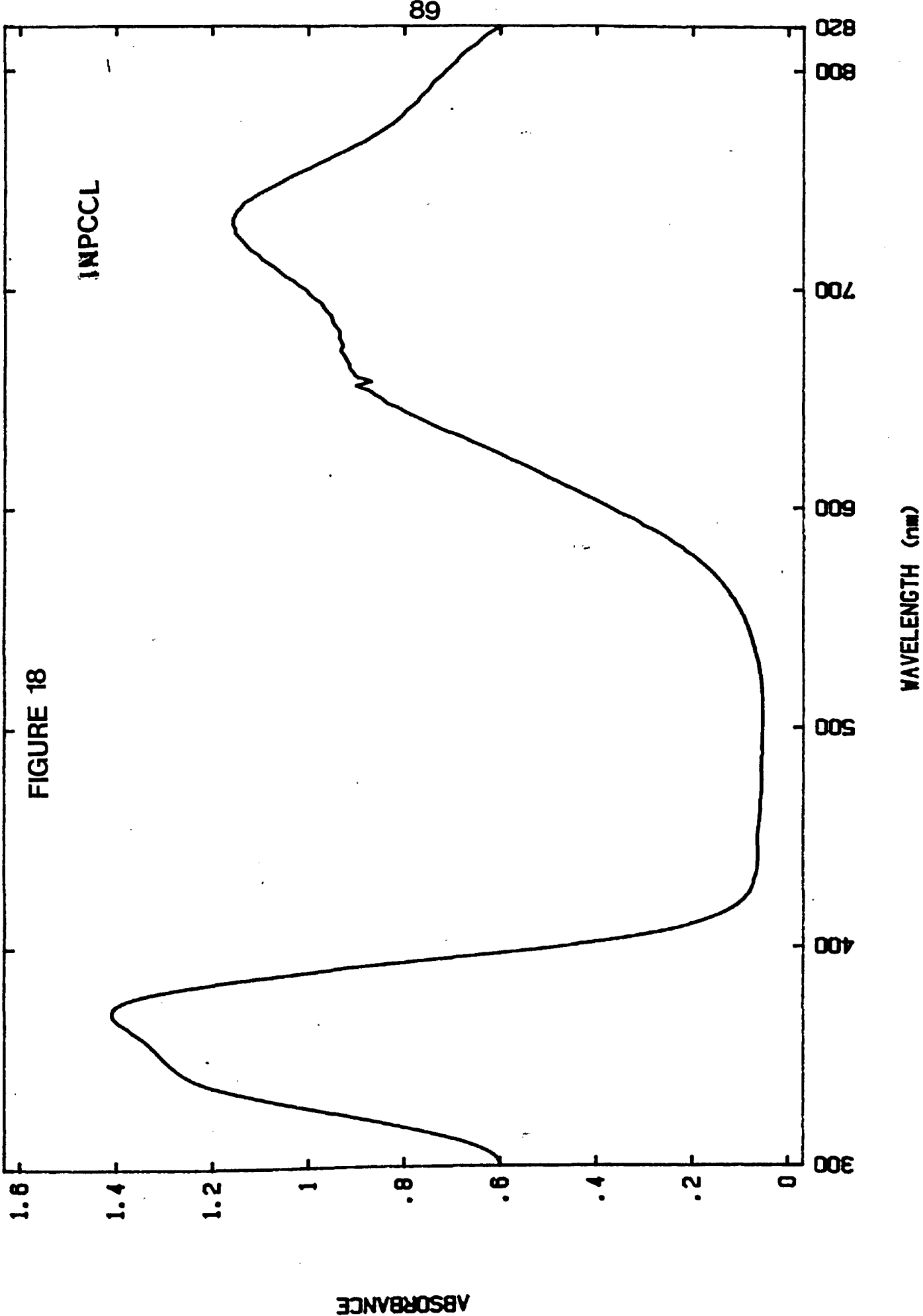


FIGURE 18

INPCCL

89

A single Langmuir-Blodgett monolayer of $(t\text{-bu})_4\text{H}_2\text{Pc}$ is visible to the naked eye and is blue in colour. The absorption spectra have been reported for two LB monolayers of $(t\text{-bu})_4\text{H}_2\text{Pc}$ and an evaporated film⁸. The evaporated $(t\text{-bu})_4\text{H}_2\text{Pc}$ film can be transformed by annealing to give a similar absorption spectrum to the LB film⁸. The sharpness of the long-wavelength band of the LB film compared to an evaporated film indicated a well-defined ordered structure⁸. There is a Soret band and a red band in the uv-visible absorption spectrum of the LB $(t\text{-bu})_4\text{H}_2\text{Pc}$ film. Thus, laser excitation at 488.0nm and 514.5nm was in the region of normal Raman while red laser excitation was in the region of resonance Raman.

DAVYDOV splitting

Figure 19 gives Raman spectra for a 200nm film of GaPcCl. Laser excitations of 488nm and 514.5nm would be in the preresonance region while the 609nm line is in the resonance region. Totally symmetric vibration modes dominate the preresonance region and are also seen in the RR spectrum. Non-totally symmetric vibrations also appear in the RR spectrum by the Herzberg-Teller mechanism. More detail on assignment follows in Chapter 8.

Figures 20 and 21 illustrate how different vibrational bands of InPcCl are observed depending on the polarization of light used. It was noted for trivalent Pcs that a number of Raman bands displayed splitting. For instance, the Raman band of AlPcCl that was observed at 1339cm^{-1} in the SS spectrum using preresonance laser lines (488 and 514.5nm) appeared at 1344cm^{-1} for PS or SP and in resonance Raman spectra. Polarization studies of components with different symmetry properties allow experimental observation of splitting when frequency differences are equal or less than the bandwidth of the Raman band. Nedungadi⁹ probed intramolecular vibrations of a naphthalene crystal using Raman polarization techniques and observed splitting differences of 4 to 5cm^{-1} for four bands.

The AlPcCl film behaves like a molecular crystal with Davydov (correlation field) splitting of non-degenerate vibrational energy levels of the free molecule. Molecular crystals have weak forces

Figure 19. Preresonance Raman (488 and 514.5nm) and resonance Raman spectra of a 200nm film of GaPcCl.

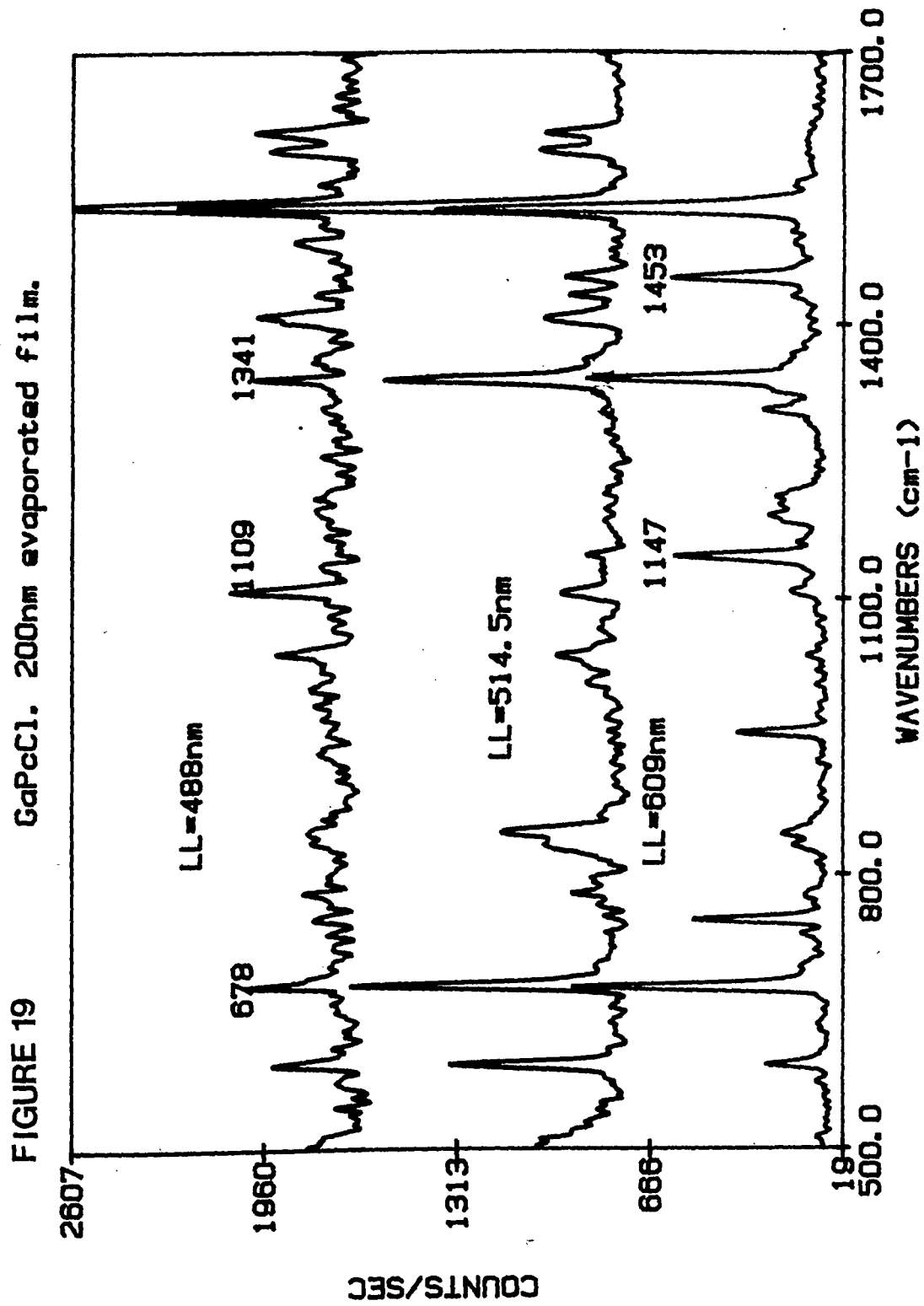


Figure 20. SP and SS polarized spectra for 200nm InPcCl using 514.5nm laser excitation.

Figure 20

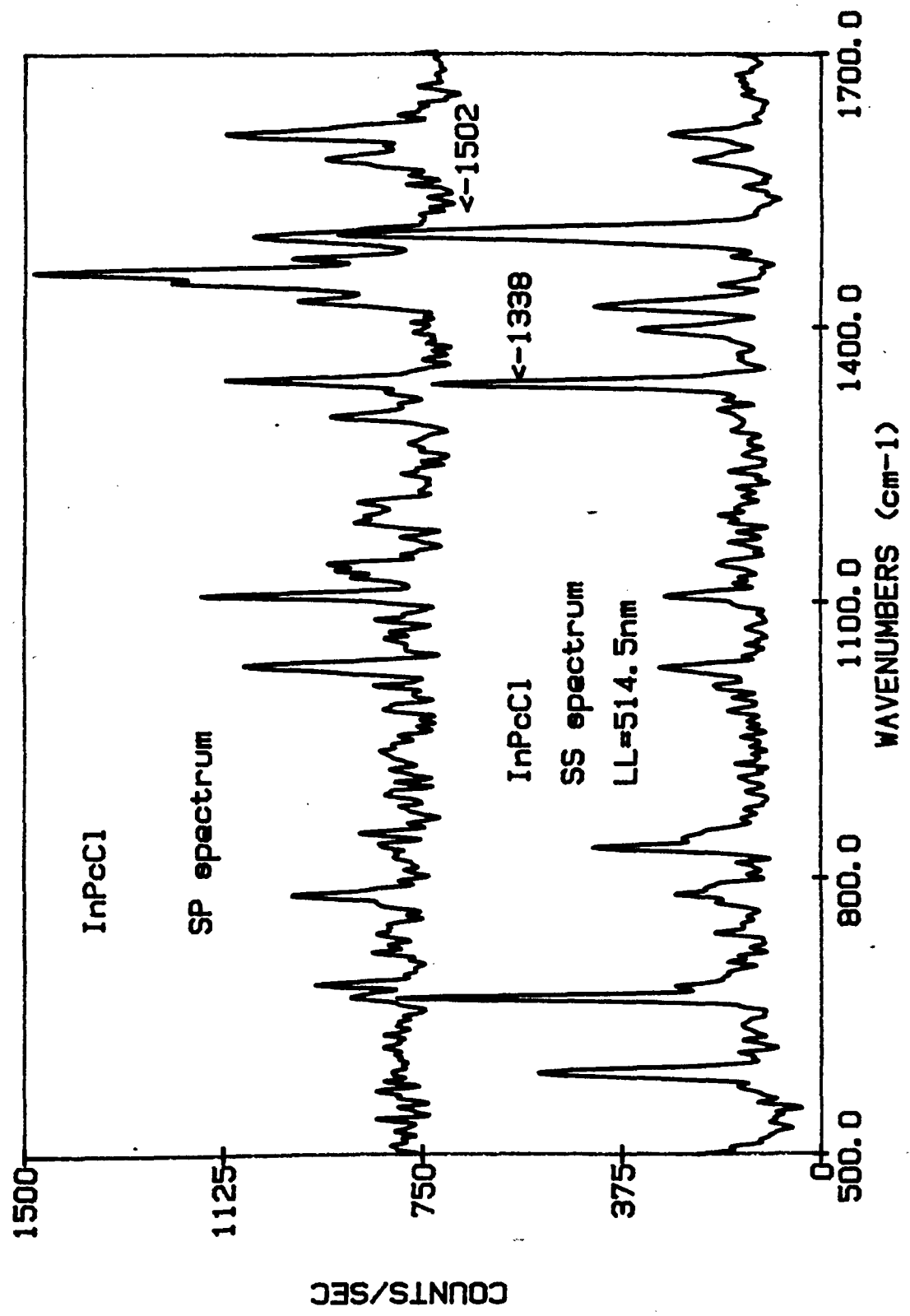
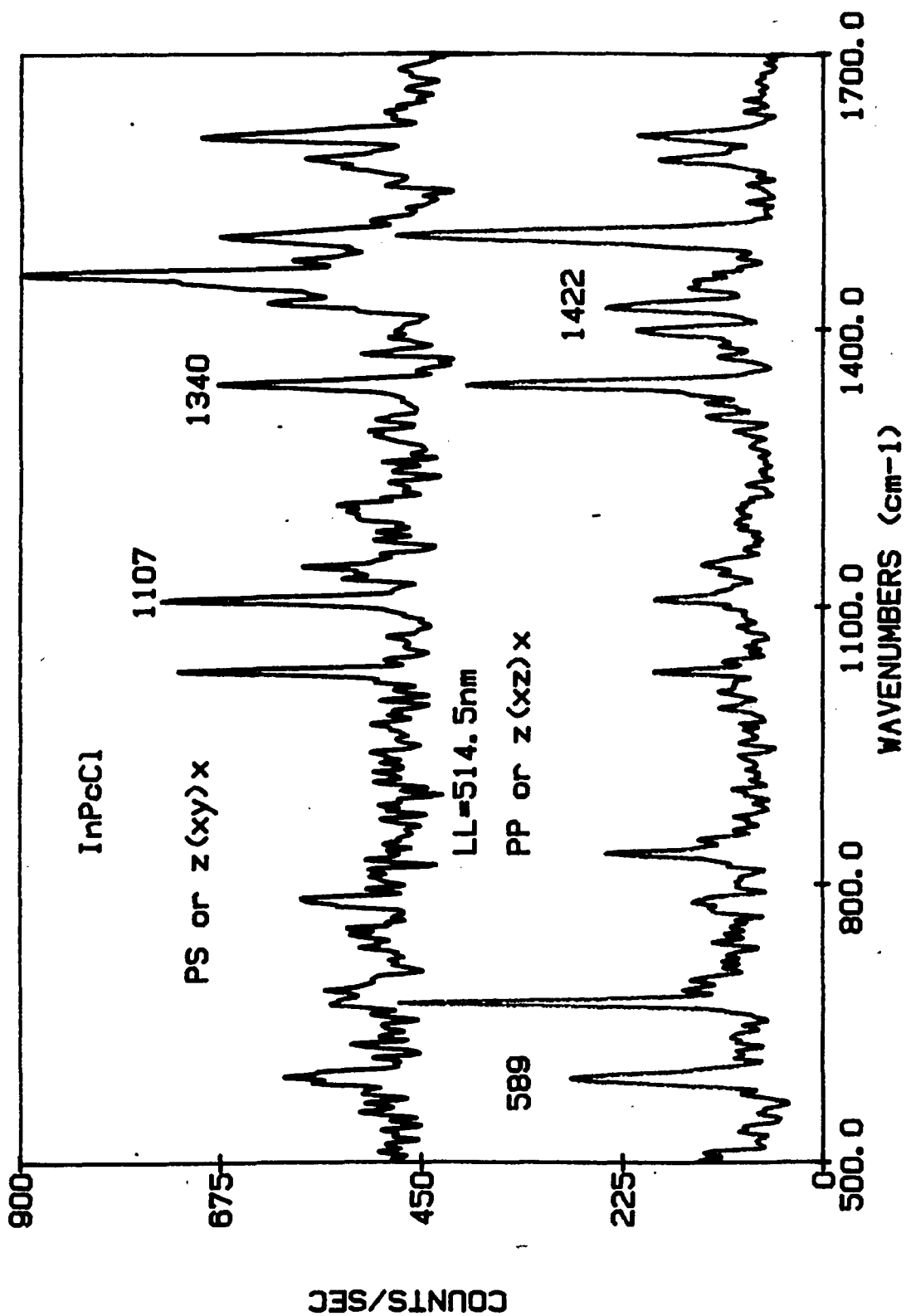


Figure 21. PS and PP polarized spectra for 200nm InPcCl using 514.5nm laser excitation.

Figure 21



between molecules of the van der Waals type. Davydov¹⁰ has pointed out that the magnitude and width of splittings is greatest for vibrations which have large changes in the molecular dipole moment. These vibrational frequencies appear in the infrared spectrum. This fact would suggest future work on Pc films or any oriented film could be done using a NaCl substrate with a polarizer inside a high resolution IR spectrophotometer.

Vibrations in molecular crystals are of two types, internal vibrations and external or lattice vibrations. The internal vibrations generally occur in the region 100cm^{-1} to 3600cm^{-1} while lattice vibrations appear at low frequencies usually below 200cm^{-1} . We previously observed low frequency vibrations for solid 2,4-dithiobiuret (DTB) and the deuterated derivative DTB-d₅¹¹. Translational and rotational frequencies of molecular crystals of DTB are sensitive to changes in temperature and when cooled by liquid nitrogen all frequencies below 200cm^{-1} shifted to higher values due to a compression of the crystal structure. In some cases, the crystalline lattice influences the internal vibrations, changes selection rules for polarization and splits internal vibrational frequencies¹⁰.

Crystal symmetry and group theory are invoked to calculate the symmetry types which are active in Raman spectra. The symmetry of an individual molecule is described by its point group and the

symmetry of an array of molecules (molecular crystal) is given by the space group. The symmetry of a molecule can be changed by placing it in a crystal environment. Site groups contain operations that simultaneously leave the molecule and the crystal unchanged. It is helpful to consult correlation tables¹² for irreducible representations of molecular point groups and crystal site groups.

Molecular crystals of Pc complexes have been found to be monoclinic of factor group $C_{2h}^5(P2_1/c)$ or triclinic; factor group $C_i(P\bar{1})$ ¹³. For PbPc both monoclinic and triclinic forms were identified¹⁴.

The number of Davydov components $N(\mu, \nu)$ for a molecular crystal with m molecules per unit cell, factor group symmetry μ and site group symmetry ν is given by¹³:

$$N(\mu, \nu) = \frac{m}{h} \sum \chi_{\mu}(R) \chi_{\nu}(R) \quad (7.1)$$

h is the order of the factor group, $\chi_{\mu}(R)$ and $\chi_{\nu}(R)$ are the characters of the irreducible representations μ and ν under an operation of the R class of the factor and site group respectively.

Assuming a C_{4v} point group for AlPcCl, a triclinic crystalline system and factor group C_i , the possible site symmetry is C_i . Davydov components for two molecules per unit cell are $1A_g$ and $1A_u$. The A_u vibrations are not Raman active so

singlets would be observed. If there were four molecules per unit cell, $2A_g$ Raman active vibrations are suggested. Experimentally doublets of different symmetries were observed for AlPcCl films. This observation can be best explained by a monoclinic system of factor group $C_{2h}^5(P2_1/c)$ with four molecules per unit cell. The calculated Raman active Davydov components for a C_1 site symmetry are $1A_g$ and $1B_g$. Table 7.1 correlates molecular symmetry and factor group with site symmetry. We have published more details concerning Davydov splitting¹³ and the reader is referred to this article for further information.

TABLE 7.1: GROUP THEORY OF A 200NM ALPCCL FILM WITH FOUR MOLECULES PER UNIT CELL

Molecule C_{4v}	Site C_1	Factor Group C_{2h}
$23A_1$	A	$1A_g$
$19A_2$		$1B_g$
$21B_1$		$1A_u$
$21B_2$		$1B_u$
$42E$		

SERS of tetratertiarybutyl phthalocyanine [(t-bu)₄H₂Pc]

We have published results for SERS observed from LB monolayers of (t-bu)₄H₂Pc on metal island films¹⁵ and reported results for the distance dependence of the SERS enhancement factor¹⁶. The molecules of (t-bu)₄H₂Pc as LB films are oriented with their molecular planes perpendicular to the metal surface¹⁷. The type of interaction of the Pc with the metal was physisorption since Raman frequencies were not shifted from (t-bu)₄H₂Pc alone. Figure 22 is the Raman spectrum of four LB monolayers of (t-bu)₄H₂Pc. Figures 23 and 24 show SERS enhancement against the distance of the (t-bu)₄H₂Pc from the surface of the metal for silver and indium. The intensity of the 686cm⁻¹ line of (t-bu)₄H₂Pc was used to generate these plots. The enhancement factor was calculated by comparing the intensity of the 686cm⁻¹ line of a (t-bu)₄H₂Pc LB monolayer in the presence of metal to the intensity of the 686cm⁻¹ line for a single LB monolayer of (t-bu)₄H₂Pc on glass. The results suggest that an electromagnetic mechanism is operating since long range enhancement of signals was observed. Higher enhancements were obtained for Ag than In and greater enhancement in the green (514.5nm) than the red (647.1nm). These results are attributed to differences in the dielectric constant at appropriate frequencies.

Figure 22. Resonance Raman spectrum of four LB monolayers of (t-bu)₄H₂Pc on corning with laser line 647.1nm.

Figure 22

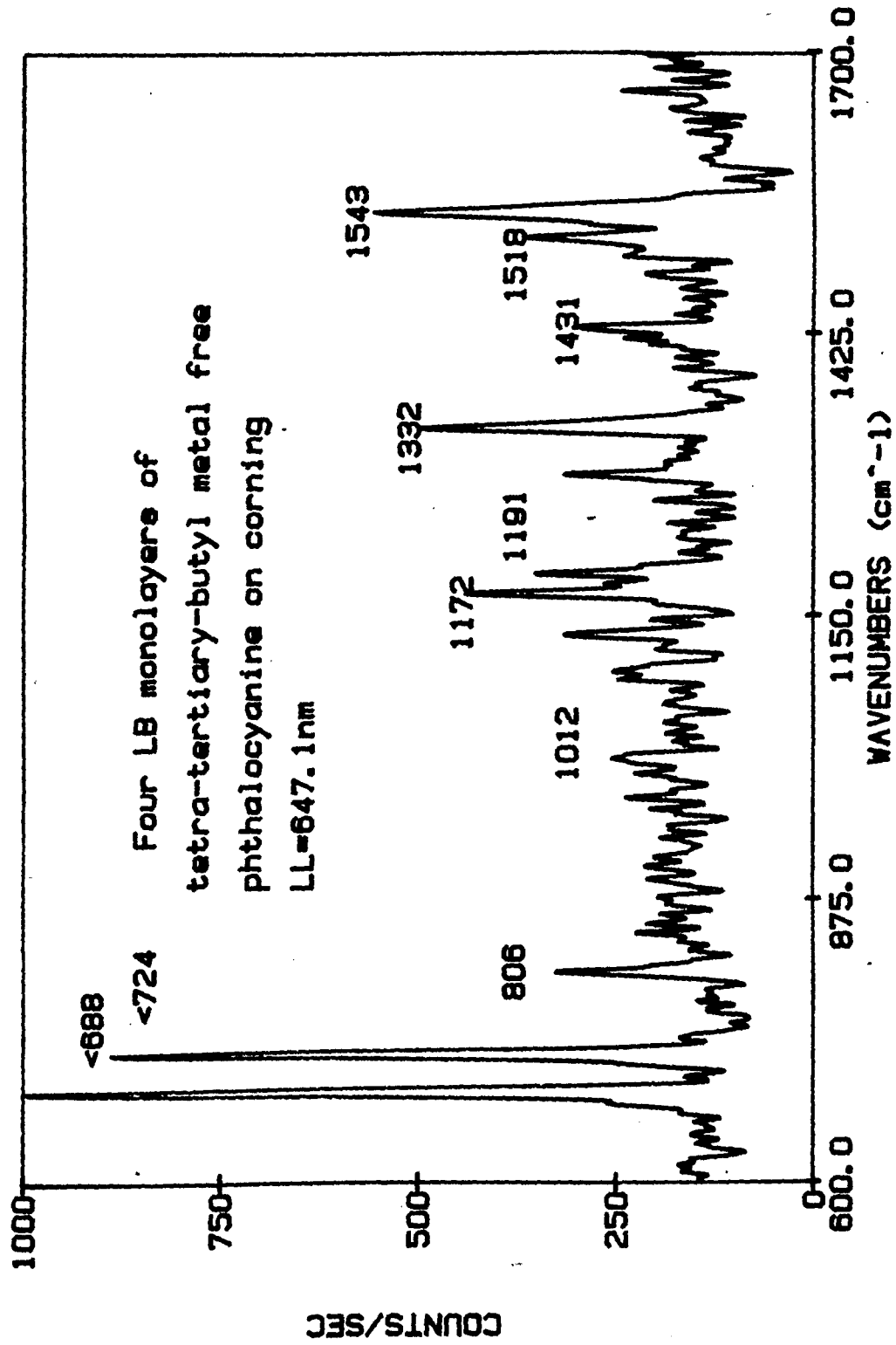


Figure 23. Enhancement factor versus distance from a Ag surface for a LB monolayer of $(t\text{-bu})_4\text{H}_2\text{Pc}$.

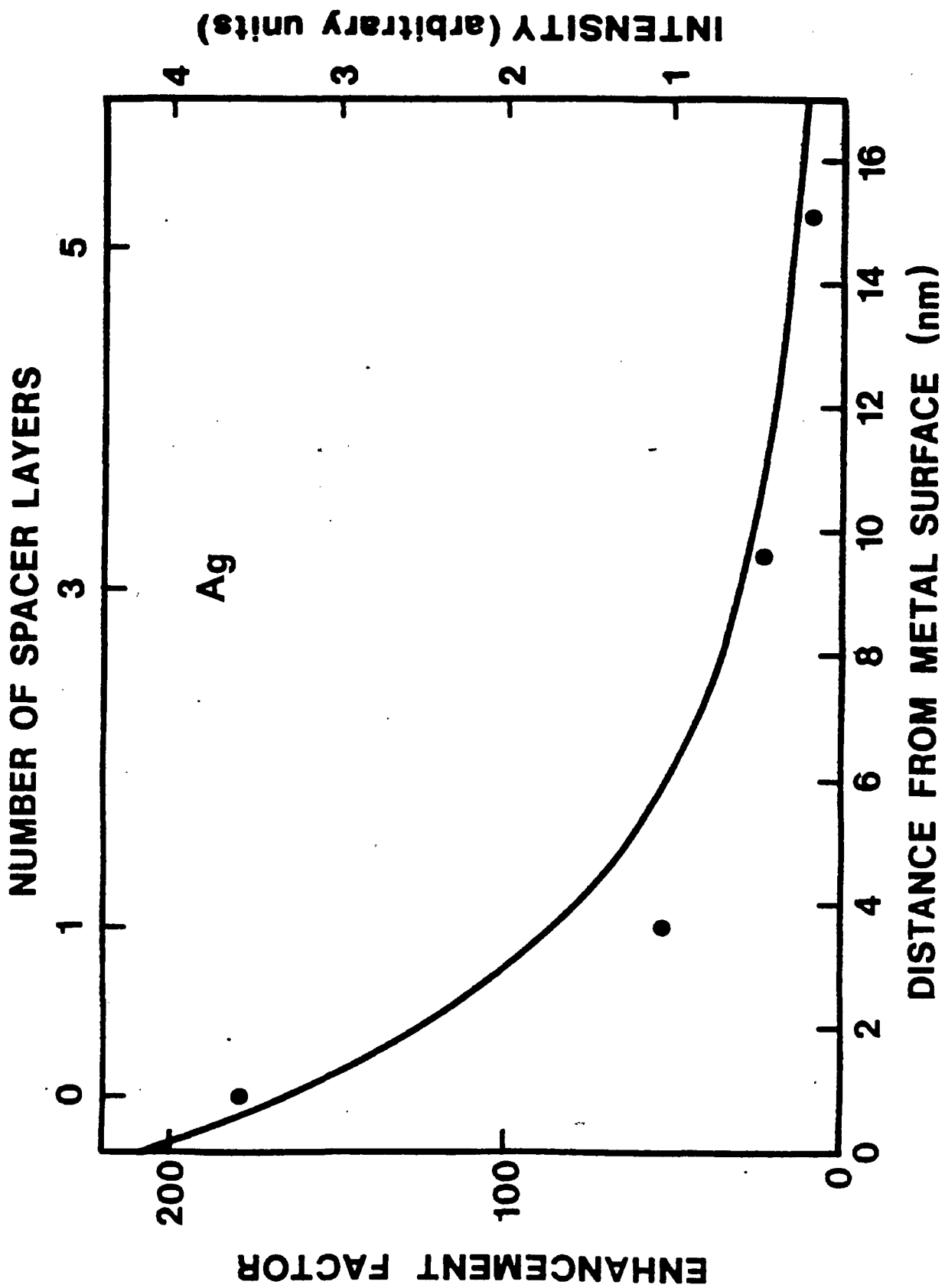


FIGURE 23

Figure 24. Enhancement factor versus distance from an In surface for a LB monolayer of $(t\text{-bu})_4\text{H}_2\text{Pc}$.

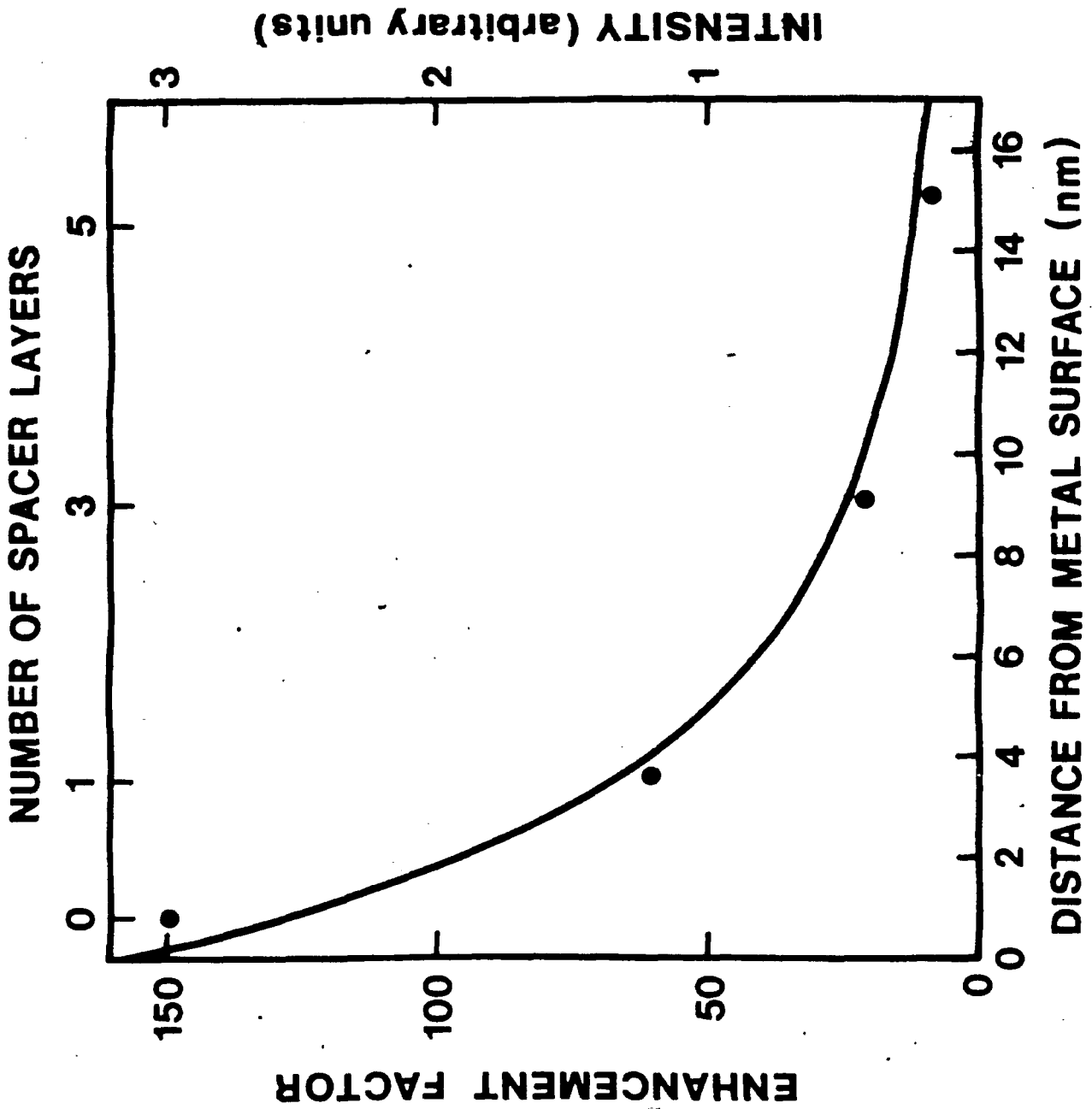


FIGURE 24

CHAPTER 8: ASSIGNMENT OF PHTHALOCYANINE VIBRATIONAL BANDS USING MODEL COMPOUNDS

There are a number of small molecules which are similar in structure to the subunits of phthalocyanine. These model compounds are useful in identifying vibrational bands of Pcs. The list of model compounds includes benzene, 1,3-diiminoisoindoline, imidazole, indole(isoindole), pyrrole and porphyrins.

The Raman spectrum has been reported for benzene¹. The most intense band occurs at 992 cm^{-1} and is a ring breathing mode. This band is polarized, totally symmetric and is due to the in-phase motion of the six carbon atoms. The high Raman intensity arises because of the large deformation of the electron cloud (polarizability). Carbon-hydrogen bending vibrations were observed at 849 cm^{-1} and 1178 cm^{-1} . Bands at 1326 cm^{-1} , 1585 cm^{-1} and 1606 cm^{-1} were attributed to ring stretching. The band at 606 cm^{-1} is caused by a ring deformation.

The Raman spectrum of solid 1,3-diiminoisoindoline run in our lab is shown in figures 25 and 26. 1,3-diiminoisoindoline can be used as a starting material when synthesizing phthalocyanines^{2,3}. An interesting feature of 1,3-diiminoisoindoline is the presence of intense bands in the low frequency region where lattice vibrations occur.

Figure 25. Raman spectrum of solid 1,3-diminoisoindoline using a 568.2nm laser line.

Figure 25

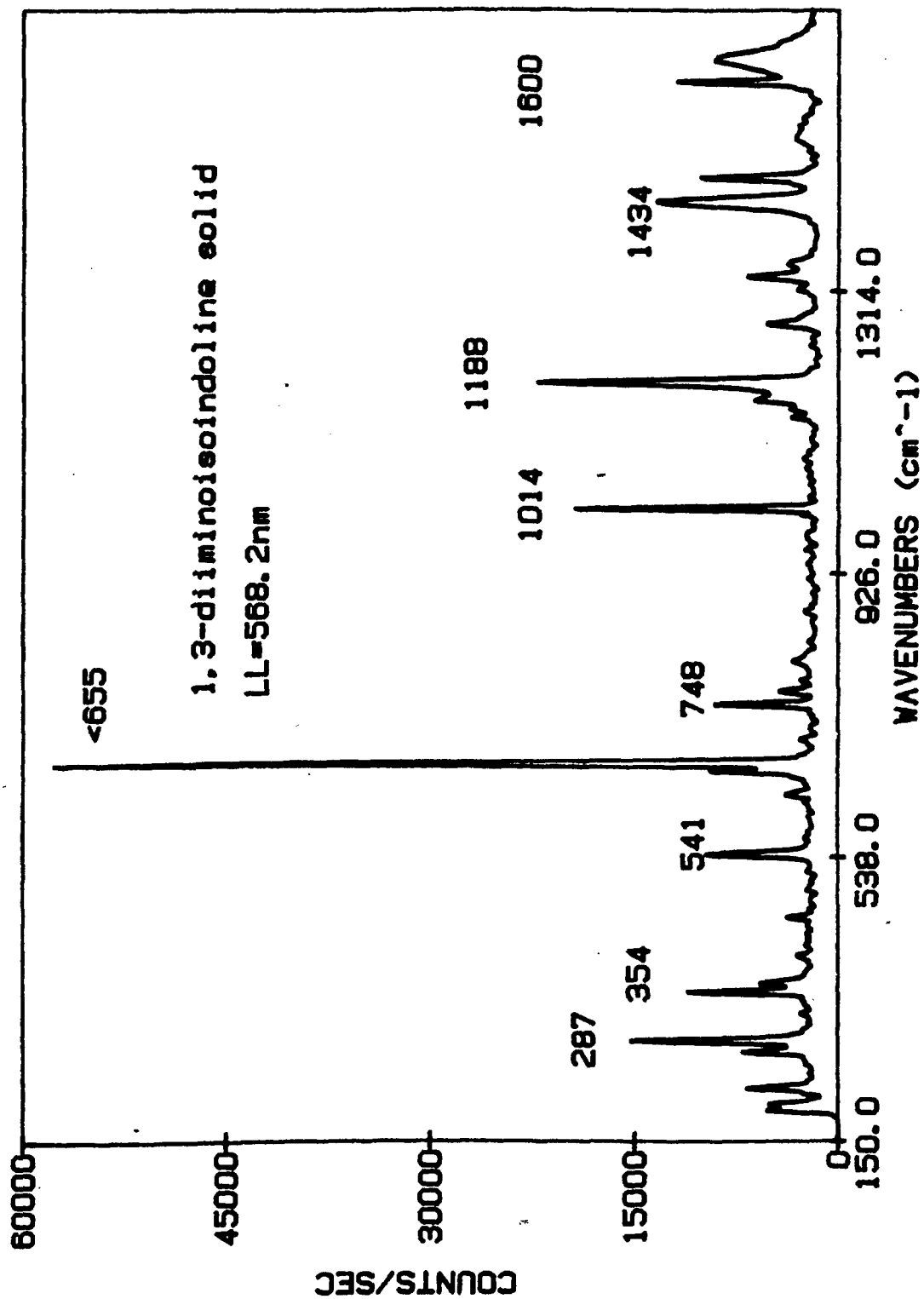
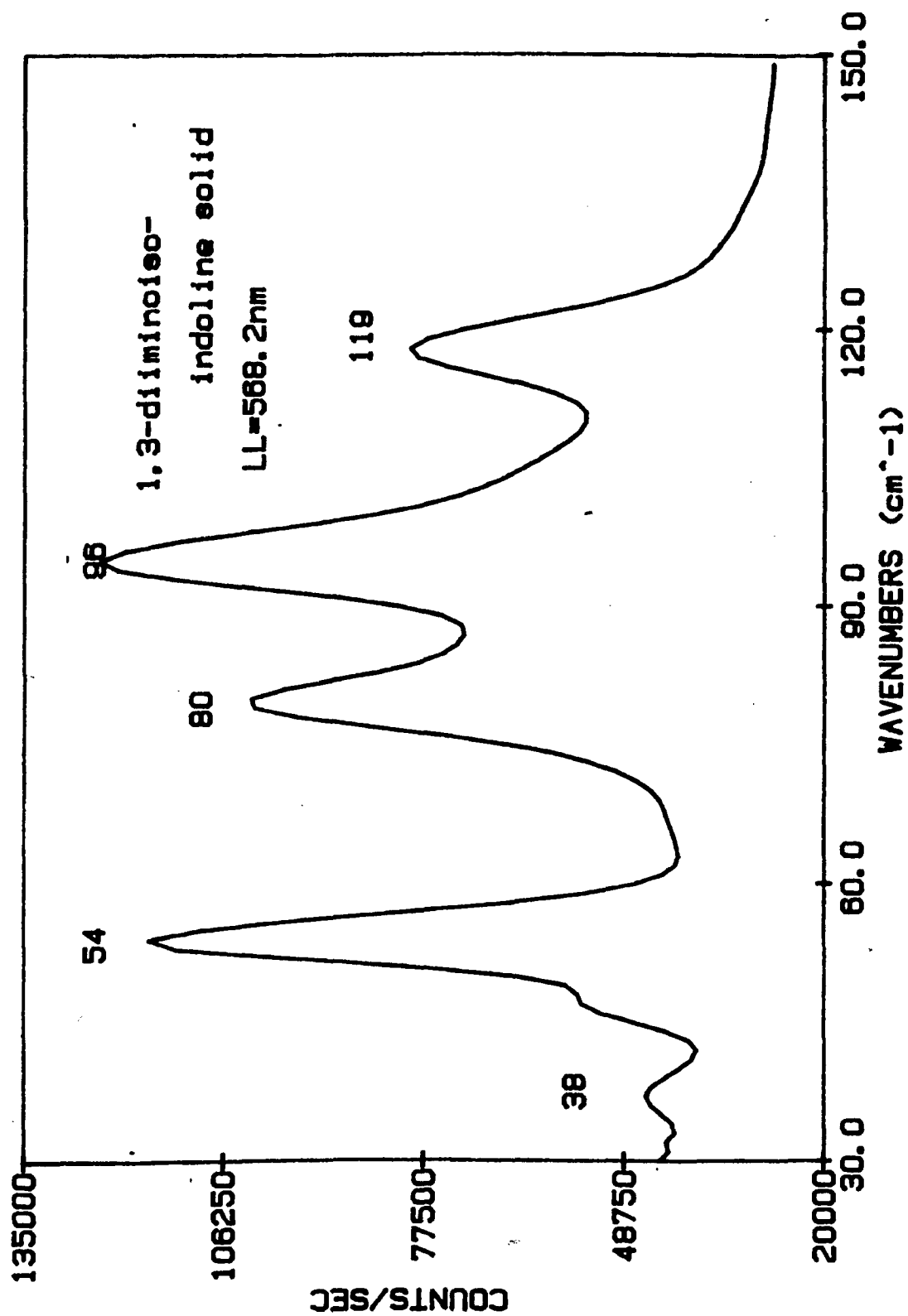


Figure 26. Low frequency lattice vibrations of solid 1,3-diiminoisoindoline using 568.2nm laser line.

Figure 26



Many studies have been carried out yielding IR and Raman results for imidazole⁴⁻⁹. The Raman spectrum from our lab is given in figure 24. According to Cordes⁸ imidazole has C_{2v} symmetry with equivalent nitrogens and the carbons at 4- and 5-positions. Intermolecular hydrogen bonding in solid imidazole is strong. Imidazole with C_{2v} symmetry should have a total of $9A_1$, $8B_1$, $3A_2$ and $4B_2$ IR and Raman active modes. Imidazole has a number of bands due to lattice vibrations below 150 cm^{-1} .

The Raman spectrum of indole has been run in our lab and was reported in the literature¹⁰. A large number of bands are present due to the low symmetry of the molecule. No Raman data has been found for isoindole which is unstable.

Raman data has been reported in the literature for pyrrole. Figure 27 is the spectrum of liquid pyrrole obtained in our lab showing SP and SS polarizations. Carbon-hydrogen and nitrogen-hydrogen stretching vibrations are in the region above 3100 cm^{-1} . The ring breathing vibration occurs at 1148 cm^{-1} and is very intense. Other ring type vibrations have been assigned¹¹ to 1472 cm^{-1} , 1416 cm^{-1} , 1384 cm^{-1} , 883 cm^{-1} , 870 cm^{-1} ,

Figure 27. Raman spectrum of imidazole solid obtained using 608.9nm laser line.

Figure 27

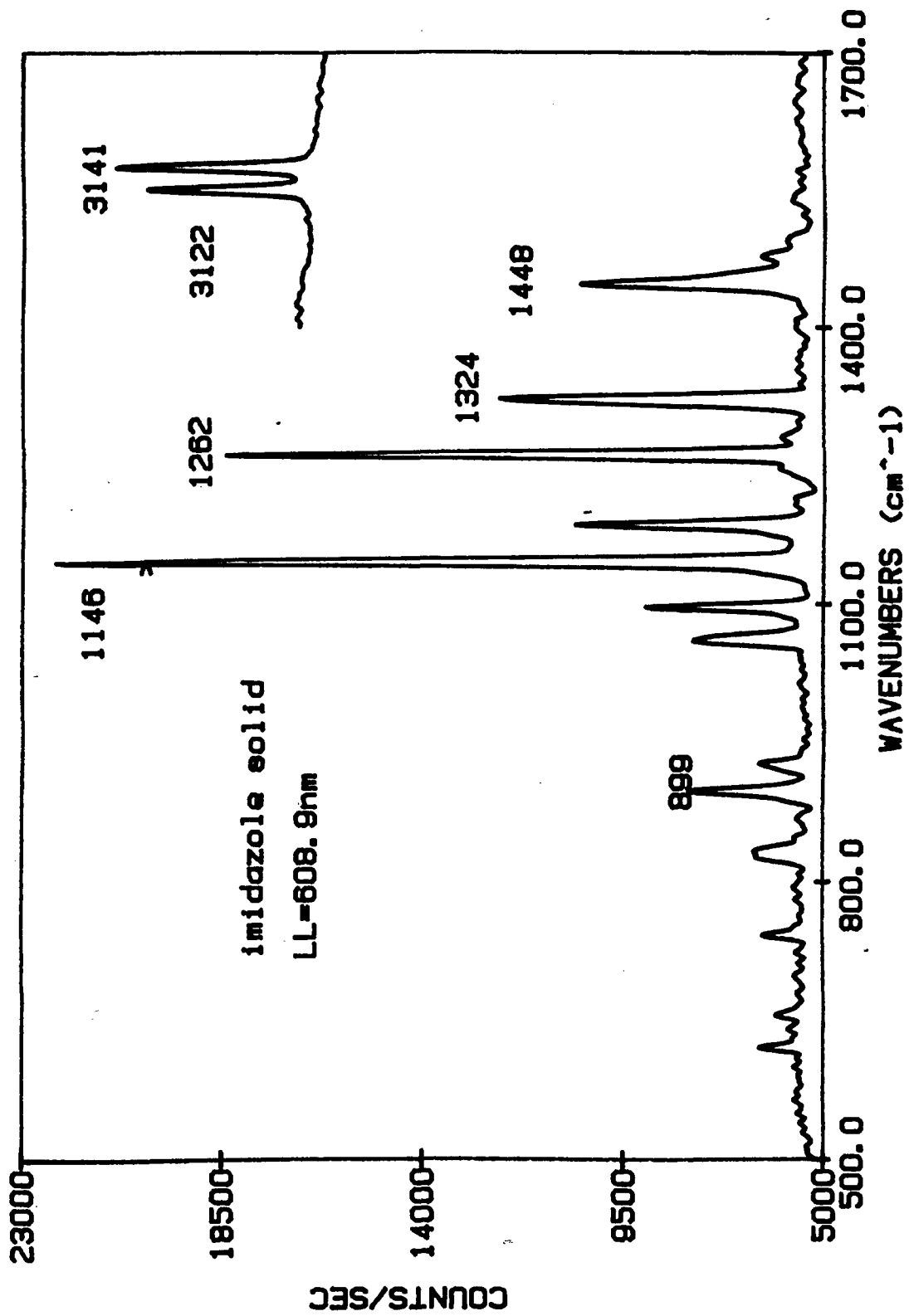
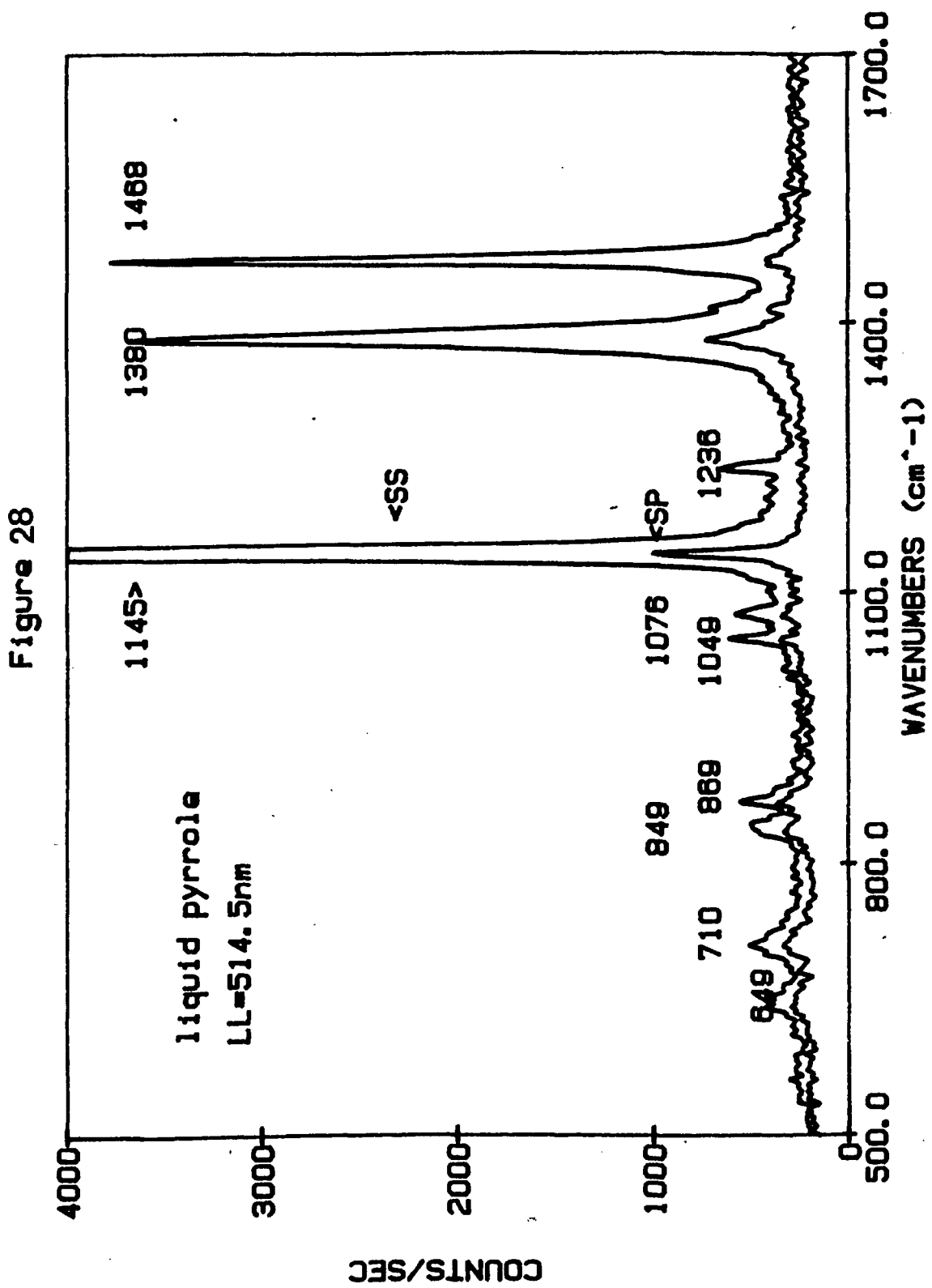


Figure 28. SS & SP polarized Raman spectra of liquid pyrrole.



649 cm^{-1} and 615 cm^{-1} . The remaining vibrations are carbon-hydrogen bending and out of plane deformations.

Resonance Raman (RR) spectra have been reported with normal coordinate analysis for metalloctaethylporphyrins M(OEPs)¹²⁻¹⁴.

These porphyrins are useful for assigning phthalocyanine bands because they lack benzene rings. The phthalocyanines have four bridging aza groups (-N=) while M(OEPs) have bridging methine groups (-CH=). A large number of Raman studies have been done on metalloporphyrins including chlorophylls and heme proteins¹⁵⁻¹⁹.

Tables have been prepared from our Raman data²⁰⁻²⁵ and that of others²⁶⁻²⁸ summarizing frequencies of phthalocyanine vibrations. Table 8.1 compares Raman frequencies for macrocycle breathing and stretching vibrations. Recall the macrocycle is the inner ring of sixteen alternating carbon and nitrogen atoms. Analogous porphyrin frequencies are also listed in the table. The breathing vibration at approximately 680 cm^{-1} in phthalocyanines is a totally symmetric A_g vibration. The 720 cm^{-1} band is a B_{1g} mode which increases in intensity as the laser line approaches resonance.

TABLE 8.1: A COMPARISON OF MACROCYCLE RAMAN FREQUENCIES FOR VARIOUS PHTHALOCYANINES

	Macrocycle Breathing (cm^{-1})		Macrocycle Stretching (cm^{-1})			Reference
Porphyrin	670	---	751	---	795	14
α - H_2 P c	682	720	---	796	---	20
β - H_2 P c	678	720	---	794	---	20
x- H_2 Pc	678	720	---	794	---	20
VOPc	681	723	747	794	835	21
MgPc	682	---	744	775	827	22
CuPc	678	---	743	778	831	22
ZnPc	678	---	748	780	835	22
SnPc	680	722	749	796	---	24
PbPc	672	---	744	773	---	24
(t-bu) $_4$ H_2 Pc	682	723	745	804	---	23
AlPcCl	678	---	752	782	831	25
GaPcCl	678	719	750	779	847	25
InPcCl	671	---	747	780	834	25
FePc	683	---	755	780	833	26
PtPc	679	---	755	---	---	27
PdPc	679	---	755	782	---	28

Pyrrole rings move in and out of phase. In general, totally symmetric modes prevail in normal Raman (off-resonance) while non-totally symmetric modes can be more noticeable in RR spectra. The Pc band at 796 cm^{-1} is the analog of the 795 cm^{-1} porphyrin band¹⁴.

Table 8.2 compares Pc Raman frequencies for vibrations associated with pyrrole subunits. The ring breathing mode of pyrrole¹¹ itself appears at 1148 cm^{-1} . The frequencies for Pcs are remarkably constant at $1141 \pm 5\text{ cm}^{-1}$. A ring stretching mode of pyrrole occurs at 1384 cm^{-1} . With the exception of $(t\text{-bu})_4\text{H}_2\text{Pc}$, this pyrrole stretching mode is present at $1340 \pm 3\text{ cm}^{-1}$ in phthalocyanines. The 1384 cm^{-1} pyrrole band is due mainly to $\text{C}\alpha\text{-C}\beta$ stretching and is observed in other model compounds, isoindole¹⁰ (1352 cm^{-1}) and Ni(OEP)¹³ (1383 cm^{-1}). The CN stretching mode in pyrrole is observed at 1530 cm^{-1} . The band at 1513 cm^{-1} has been assigned to CN pyrrole stretching in H_2Pc ²⁰. DiLella²⁹ has observed Raman vibrations with a large degree of pyrrole CN stretching character for tetracumylphenoxy phthalocyanine [$\text{Pc}(\text{Cp})_4$] Langmuir-Blodgett derivatives $\text{PbPc}(\text{Cp})_4$ (1530 cm^{-1}), $\text{CuPc}(\text{Cp})_4$ (1530 cm^{-1}) and $\text{NiPc}(\text{Cp})_4$ (1555 cm^{-1}).

TABLE 8.2: A COMPARISON OF PYRROLE RAMAN FREQUENCIES FOR VARIOUS PHTHALOCYANINES

	Ring Breathing (cm^{-1})	Ring Stretching (cm^{-1})	CN Pyrrole Stretching (cm^{-1})	Reference
Pyrrole	1148	1384	1530	11
α - H_2 P c	1140	1337	1513	20
β - H_2 P c	1138	1337	1513	20
x- H_2 Pc	1140	1337	1513	20
VOPc	1140	1340	1527	21
MgPc	1141	1340	1506	22
CuPc	1140	1341	----	22
ZnPc	1143	1341	1512	22
SnPc	1141	1342	1513&1519	24
PbPc	1137	1337	1505	24
(t-bu) $_4$ H $_2$ Pc	---	1330	1520	23
AlPcCl	1147	1343	----	25
GaPcCl	1147	1341	----	25
InPcCl	1142	1340	1497	25
FePc	1147	1343	----	26
PtPc	1145	1343	----	27
PdPc	1146	1338	----	28

Table 8.3 compares Raman frequencies of Pc vibrations associated with isoindole ring stretching. The band at 1534 cm^{-1} arises from C-C stretching of the bond common to pyrrole and benzene rings of isoindole groups. This band is absent in Ni(OEP) because this porphyrin does not have benzene ring. Other isoindole stretching vibrations appear at 1406 cm^{-1} , 1428 cm^{-1} and 1450 cm^{-1} in H_2Pc^{20} . The molecule indole¹⁰ has Raman bands at 1412 cm^{-1} , 1455 cm^{-1} and 1487 cm^{-1} .

Three Raman vibrations associated with benzene subunits of Pcs are summarized in table 8.4. Benzene¹ itself has Raman bands at 606 cm^{-1} , 1585 cm^{-1} and 1606 cm^{-1} . Excitation profiles exhibit a steep side toward higher frequencies for H_2Pc 571 cm^{-1} and 1618 cm^{-1} bands²⁰. The benzene groups are largely responsible for the electronic Soret band.

Carbon-hydrogen deformations occur in the range 1000 cm^{-1} to 1350 cm^{-1} . The Raman bands for Pcs are given in table 8.5. It would be useful to have Raman data for a Pc derivative which has all peripheral hydrogens substituted. One such compound would be metal-free hexadecachlorophthalocyanine. Benzene¹ has C-H deformations at 1038 cm^{-1} , 1150 cm^{-1} , 1178 cm^{-1} and 1326 cm^{-1} . Table 8.6 gives Raman frequencies for isoindole ring deformations.

TABLE 8.3: A COMPARISON OF ISOINDOLE RING STRETCHING RAMAN FREQUENCES FOR VARIOUS PHTHALOCYANINES

	WAVENUMBERS (cm ⁻¹)						Reference
Indole	1412	-----	1455	-----	-----	1534	10
α - H ₂ P c	1406	1428	1450	-----	-----	1534	20
β - H ₂ P c	1408	1428	1450	-----	-----	1536	20
x-H ₂ Pc	1408	1428	1450	-----	-----	1536	20
VOPc	-----	1429	1449	1471	1480	1550	21
MgPc	-----	1423	1448	1479	-----	-----	22
CuPc	-----	1431	1452	1470	1484	1528	22
ZnPc	1408	1425	1450	-----	-----	-----	22
SnPc	1393	1429	1451	-----	-----	1527	24
PbPc	1393	1423	1444	1460	-----	-----	24
(t-bu) ₄ H ₂ Pc	1390	1428	-----	-----	-----	1532	23
AlPcCl	-----	-----	1455	-----	-----	1528	25
GaPcCl	-----	-----	1453	-----	-----	1528	25
InPcCl	-----	1427	1447	-----	-----	-----	25
FePc	1404	-----	1450	-----	-----	1520	26
PtPc	-----	1436	1458	-----	-----	1530	27
PdPc	-----	-----	1452	1457	-----	1537	28
			1464				

TABLE 8.4: A COMPARISON OF BENZENE RING RAMAN FREQUENCIES FOR VARIOUS PHTHALOCYANINES

	(cm ⁻¹)	(cm ⁻¹)	(cm ⁻¹)	Reference
Benzene	606	1585	1606	1
α - H ₂ Pc	570	1584	1618	20
β - H ₂ Pc	564	1584	1618	20
x-H ₂ Pc	564	1584	1618	20
VOPc	590	1588	1614	21
MgPc	588	-----	1597	22
CuPc	588	1590	1612	22
ZnPc	591	1590	1617	22
SnPc	589	1584	1616	24
PbPc	590	1580	1610	24
(t-bu) ₄ H ₂ Pc	588&611	1581	1616	23
AlPcCl	591	-----	1614	25
GaPcCl	592	-----	-----	25
InPcCl	589	1585	1613	25
FePc	596	-----	-----	26
PtPc	607	-----	-----	27
PdPc	600	-----	-----	28

TABLE 8.5: A COMPARISON OF C-H DEFORMATION RAMAN FREQUENCIES FOR VARIOUS PHTHALOCYANINES

	WAVENUMBERS (cm ⁻¹)						Reference	
Benzene	-----	1038	-----	-----	1150 1178	-----	1326	1
α - H ₂ P c	1009	1024	1081	1104	1181	1230	-----	20
β - H ₂ P c	1009	1024	1081	1102	1181	1230	-----	20
x-H ₂ Pc	1009	1024	1081	1102	1181	1230	-----	20
VOPc	1002	1032	-----	1108	1185 1197	-----	1306	21
MgPc	-----	1030	-----	1106	-----	-----	-----	22
CuPc	-----	1037	-----	1106	-----	-----	-----	22
ZnPc	-----	1029	-----	1108	-----	-----	-----	22
SnPc	1007	1026	1082	1107	1184	-----	1311	24
PbPc	-----	-----	-----	1107	1197	1217	1303	24
(t-bu) ₄ H ₂ Pc	1013	-----	1060	1094	1126 1168 1198	-----	1286	23
AlPcCl	-----	-----	1072	1109	1191	1212	1308	25
GaPcCl	-----	1040	1085	1108	1167 1188	1214	1306	25
InPcCl	1008	1030	1087	1107	1161 1196	1212	1303	25
FePc	-----	-----	-----	1110	1200	-----	1310	26
PtPc	-----	-----	-----	1114	1196	1219	1312	27
PdPc	1010	-----	-----	1112	1165 1197	1223	1312	28

TABLE 8.6: A COMPARISON OF ISOINDOLE RING DEFORMATION RAMAN FREQUENCIES FOR VARIOUS PHTHALOCYANINES

	WAVENUMBERS (cm ⁻¹)						Reference
Indole	---	---	224,423	---	---	542	10
α - H ₂ P c	182	205	230	480	517	543	20
β - H ₂ P c	184	204	229	480	517	540	20
x-H ₂ Pc	184	204	229	480	517	540	20
VOPc	187	---	225,256	482	---	---	21
MgPc	173	---	221	481	---	555	22
CuPc	169	---	236	486	---	---	22
ZnPc	160	---	232	---	---	---	22
SnPc	---	---	235,286 356	---	---	566	24
PbPc	---	---	234	479	---	---	24
(t-bu) ₄ H ₂ Pc	171	---	---	---	---	---	23
AlPcCl	178	---	237,251	485	---	---	25
GaPcCl	169	---	245,289 346,427	487	511	---	25
InPcCl	174	219	240,267 312,349	480	516	---	25
PtPc	---	---	225,275	482	---	---	27
PdPc	178	212 219	227,270	487	---	---	28

REFERENCES FOR CHAPTER 1: APPLICATIONS

1. R. Kugel, A. Svirnickas, J.J. Katz and J.C. Hindman, Opt. Comm. 23(2) (1977), 189.
2. G.J. Kovacs and P.S. Vincett, J. Imag. Tech. 12(1) (1986), 17.
3. P. Kivits, R. de Bont and J. van der Veen, Appl. Phys. A26 (1981), 101.
4. M.F. Dautartas, S.Y. Suh, S.R. Forrest, M.L. Kaplan, A.J. Lovinger and P.H. Schmidt, Appl. Phys. A36 (1985), 71.
5. T. Venkatesan, S.R. Forrest, M.L. Kaplan, P.H. Schmidt, C.A. Murray, W.L. Brown, B.J. Wilkens, R.F. Roberts, L. Rupp, Jr. and H. Schonhorn, J. Appl. Phys. 56(10) (1984), 2778.
6. H. Wohltjen, W.R. Barger, A.W. Snow and N.L. Jarvis, IEEE Trans. Electr. Dev. 32(7) (1985), 1170.
7. R.O. Loutfy and J.H. Sharp, J. Chem. Phys. 71(3) (1979), 1211.
8. E.R. Menzel and R.O. Loutfy, J. Chem. Phys. Lett. 72(3) (1980), 522.
9. Y.C. Cheng and R.O. Loutfy, J. Chem. Phys. 73(6) (1980), 2911.
10. R.O. Loutfy and Y.C. Cheng, J. Chem. Phys. 73(6) (1980), 2902.
11. R.O. Loutfy, J.H. Sharp, C.K. Hsiao and R. Ho, J. Appl. Phys. 52(8) (1981), 5218.

12. H.J. Wagner and R.O. Loutfy, J. Vac. Sci. 20(3) (1982), 300.
13. A.M. Hor and R.O. Loutfy, Can. J. Chem. 61(5) (1983), 901.
14. A.M. Hor, R.O. Loutfy, C.K. Hsiao, Appl. Phys.. Lett. 42(2) (1983), 165.
15. R.O. Loutfy, L.F. McIntyre, Can. J. Chem. 61 (1983), 72.
16. M. Shimura, A. Toyoda, H. Bara, Mem. Fac. Technol. 33 (1983), 3357-62.
17. R.O. Loutfy, A.H. Hor, Photochem. Photobiol. Proc. Int. Conf. 2 (1983), 759.
18. B.L. Wheeler, G. Nagasubramanian, A.J. Bard, L.A. Schechtman, M.E. Kenney, J. Am. Chem. Soc. 106(24) (1984), 7404.
19. C.A. Linkous, N.R. Armstrong, Prog. Batteries Sol. Cells 5 (1984), 384.
20. H. Homborg, K.S. Murray, Z. Anorg. Allg. Chem. 517 (1984), 149.
21. T. Mezza, N.R. Armstrong, M. Keeney, J. Electroanal. Chem. Interfacial Electrochem. 176(1-2) (1984), 259.
22. Y.I. Verzhimacha, A.V. Koval'chuk, M.V. Kurik, C. Hamann, A. Mrwa, Phys. Status Solidi A 82(1) (1984), K111.
23. P.C. Rieke, N.R. Armstrong, J. Am. Chem. Soc. 106(1) (1984) 47.
24. R. Adzic, B. Simic-Glavaski, E. Yeager, J. Electroanal. Chem. Interfacial Electrochem. 194(1) (1985), 155.

25. R.O. Loutfy, C.K. Hsiao, A.M. Hor, G. DiPaola-Baranyi, J. Imaging Sci. 29(4) (1985), 148.
26. D. Djurado, A. Hamwi, J.C. Cousseins, H. Bidar, C. Fabre, G. Berthet, Synth. Met. 11(3) (1985), 109.
27. M.F. Lawrence, J.P. Dodelet, L.H. Dao, J. Phys. Chem. 89(8) (1985), 1395.
28. C.W. Tang, Phys. Lett. 48(2) (1986), 183.
29. Alan L. Fahrenbruch and Richard H. Bub, in Fundamentals Of Solar Cells, (Academic Press, Toronto, 1983).
30. T.J. Klofta, P.C. Rieke, C.A. Linkous, W.J. Buttner, A. Nanthakumar, T.D. Mewborn, and N.R. Armstrong, J. Electrochem. Soc.: Electrochem. Sci. and Tech. 132(9) (1985), 2134.
31. P.C. Rieke, C.L. Linkous, and N.R. Armstrong, J. Phys. Chem. 88 (1984), 1351.
32. B. Simic-Glavaski, S. Zecevic, and E. Yeager, J. Am. Chem. Soc. 107(20) (1985), 5625.
33. B. Simic-Glavaski, S. Zecevic, and E. Yeager, J. Phys. Chem. 87(23) (1983), 4555.
34. S. Zecevic, B. Simic-Glavaski, E. Yeager, A.B.P. Lever, P.C. Minor, J. Electroanal. Chem. Interfacial Electrochem. 196(2) (1985), 339.
35. B. Simic-Glavaski, S. Zecevic, E. Yeager, J. Raman Spectrosc. 14(5) (1983), 338.

REFERENCES FOR CHAPTER 2: STRUCTURE

1. J.A. Salthouse and M.J. Ware in Point Group Character Tables and Related Data, (Cambridge University Press, London, 1972), p.65.
2. M. Gouterman, in the Porphyrins, vol. III, (Academic Press, New York, 1978).
3. J.M. Robertson, J. Chem. Soc. (1935), 615.
4. J.M. Robertson, J. Chem. Soc. (1936), 1195.
5. R.P. Linstead and J.M. Robertson, J. Chem. Soc. (1936), 1736.
6. J.M. Robertson and I. Woodward, J. Chem. Soc. (1937), 219.
7. J.M. Robertson and I. Woodward, J. CHEM. SOC. (1940), 36.
8. H.F. Shurvell and L. Pinzuti, Can. J. Chem. 44 (1966), 125.
9. J.H. Sharp and M. Lardon, J. Phys. Chem. 72 (1968), 3230.
10. K.Z. Ogorodnik, Opt. Spectrosc. 39(2) (1975), 223.
11. C.J. Brown, J. Chem. Soc. A (1968), 2488.
12. C.H. Griffiths, M.S. Walker, P. Goldstein, Mol. Cryst. Liq. Cryst. 33 (1976), 149.
13. P.T. Cardew, R.J. Davey, Proc. R. Soc. Lond. A(398) (1985), 414.
14. R.O. Loutfy, R. Ho, C.K. Hsaio and J.H. Sharp, J. Appl. Phys. 52 (1981), 5218.
15. J.F. Byrne and P.F. Kurz, U.S. Patent 3,357,989 (1967).
16. G.J. Kovacs and J.H. Sharp, Can. J. Phys. 63(3) (1985), 346.
17. C.J. Brown, J. Am. Chem. Soc. A (1968), 2488-2493.
18. W.R. Scheidt and W. Dow, J. Am. Chem. Soc. 99(4) (1977), 1101.

19. C.J. Brown, *J. Chem. Soc. A* (1968), 2494.
20. K. Ukei, *Acta Cryst.* B29 (1973), 2290.
21. Y. Iyechika, K. Yakushi, I. Ikemoto and H. Kurada, *Acta Cryst.* B38 (1982), 766.
22. M.K. Friedel, B.F. Hoskins, R.L. Martin and S.A. Mason, *Chem. Commun.* (1970), 400.
23. K.J. Wynne, *Inorg. Chem.* 23 (1984), 4658.

**CHAPTER 3:
NORMAL RAMAN, RESONANCE RAMAN AND SURFACE ENHANCED RAMAN REFERENCES**

1. J.R. Durig and W.C. Harris, in *Physical Methods of Chemistry*, Part IIIB, Chapter 2, ed. A. Weissberger and B.W. Rossiter, (Wiley-Interscience, New York, 1972).
2. J.R. Ferraro and J.S. Ziomek, in *Introductory Group Theory*, (Plenum Press, New York, 1969).
3. J. Tang and A.C. Albrecht, in *Raman Spectroscopy Theory and Practice*, ed. H.A. Szymanski, (Plenum Press, New York, 1970).
4. A.C. Albrecht, *J. Chem. Phys.* 34 (1961), 1476.
5. T.G. Spiro, *Biochim. Biophys. Acta* 16 (1975) 169.
6. A. Wokaun, in *Solid State Physics*, ed. H. Ehrenreich and D. Turnbull, (Academic Press, Toronto, 1984), p.224.
7. M. Moskovits, *Rev. Mod. Phys.* 57(3) (1985), 783.
8. *Surface Enhanced Raman Scattering*, edited by R.K. Chang and T.E. Furtak, (Plenum Press, New York, 1982).
9. I. Pockrand, in *Surface Enhanced Raman Vibrational Studies of Solid/Gas Interfaces*, (Springer-Verlag, New York, 1984).
10. A. Otto, in *Topics in Applied Physics (Light Scattering in Solids IV)*, ed. M. Cardona and G. Guntherodt, (Springer-Verlag, New York, 1984).

11. H. Metiu and P. Das, *Ann. Rev. Phys. Chem.* 35 (1984), 507.
12. T.E. Furtak and D. Roy, *Surf. Sci.* 158 (1985), 126.
13. M. Fleischmann, P.J. Hendra and A.J. McQuillan, *Chem. Phys. Letts.* 26(2) (1974), 163.
14. C.A. Melendres, C.B. Rios, X. Feng and R. McMasters, *J. Phys. Chem.* 87 (1983), 3526.
15. C. Jennings, R. Aroca, A.M. Hor, R.O. Loutfy, *Anal. Chem.* 56 (1984), 2033.
16. R. Aroca, C. Jennings, G.J. Kovacs, R.O. Loutfy, P.S. Vincett *J. Phys. Chem.* 89 (1985), 4051.
17. G.J. Kovacs, R.O. Loutfy, P.S. Vincett, C. Jennings, R. Aroca *Langmuir* 2 (1986), 689.
18. R. Aroca and R.O. Loutfy, *J. of Raman Spectrosc.* 12(3) (1982), 262.
19. H. Seki and M.R. Philpott, *J. Chem. Phys.* 73(10) (1980), 5376.
20. Y. Gao, T. Lopez-Rios, *Solid State Commun.* 60(1) (1986), 55.
21. S. Hayashi and M. Samejima, *Surf. Sci.* 137 (1984), 442.
22. R.A. Uphaus and T.M. Cotton, *Thin Sol. Films* 132 (1985), 173.
23. E.V. Albano, S. Daiser, G. Ertl, R. Miranda, K. Wandelt and N. Garcia, *Phys. Rev. Letts.* 51(25) (1983), 2314.
24. C.J. Sandroff and D.R. Herschbach, *Langmuir* 1 (1985), 131.

25. C.A. Murray, D.L. Allara and M. Rhinewine, Phys. Rev. Letts. 46(1), 57.
26. S. Hayashi, Surf. Sci. 158 (1985), 229.
27. C.A. Murray, D.L. Allara, A.F. Hebrand and F.J. Padden Jr., Surf. Sci. 119 (1982), 449.
28. C.A. Murray and D.L. Allara, J. Chem. Phys. 76(3) (1982), 1290.
29. W.L. Parker, R.M. Hexter, A.R. Siedle, Chem. Phys. Letts. 107(1) (1984), 96.
30. P.D. Enlow, M. Buncick, R.J. Warmack and T. Vo-Dinh, Anal. Chem. 58 (1986), 1119.
31. H. Seki, J. of Electron Spectrosc. and Rel. Phenom. 30 (1983), 287.
32. R. Aroca and F. Martin, J. Raman Spectrosc. 16(3) (1985), 156.
33. X.M. Hua, J.I. Gersten, A. Nitzan, J. Chem. Phys. 83(7) (1985), 3650.
34. J. Gersten and A. Nitzan, J. Chem. Phys. 73(7) (1980), 3023.
35. J.I. Gersten, J. Chem. Phys. 72(10) (1980), 5779.
36. G.C. Schatz, Acc. Chem. Res. 17 (1984), 370.
37. H. Ueba, Surf. Sci. 131 (1983), 347.
38. C.Y. Chen and E. Burstein, Phys. Rev. Letts. 45(15) (1980), 1287.
39. D.A. Weitz, S. Garoff, J.I. Gersten, A. Nitzan, J. Chem. Phys. 78(9) (1983), 5324.

40. S.A. Lyon and J.M. Worlock, Phys. Rev. Letts. 57(7) (1983), 593.
41. K. Arya, R. Zeyher and A.A. Mardudin, Solid State Commun. 42(6) (1982), 461.
42. S.L. McCall and P.M. Platzman, Phys. Lett. 77A(4) (1980), 381.
43. P. Gao, M.L. Patterson, M.A. Tadayyoni and M.J. Weaver, Langmuir 1 (1985), 173.
44. Z. Kotler and A. Nitzan, J. Phys. Chem. 86 (1982), 2011.
45. J. G. Bergman, D.S. Chemla, P.F. Liao, A.M. Glass, A. Pinczuk, Optics Letts. 6(1) (1981), 33.
46. U. Laor and G.C. Schatz, Chem. Phys. Letts. 82(3) (1981), 566.
47. U. Laor and G.C. Schatz, J. Chem. Phys. 76(6) (1982), 2888.
48. J.I. Gersten and A. Nitzan, Surf. Sci. 158 (1985), 165.
49. E. Burstein, Y.J. Chen, C.Y. Chen, S. Lundquist and E. Tosatti, Solid State Commun. 29 (1979), 567.
50. M.R. Philpott, J. Chem. Phys. 62 (1975), 1812.
51. S. Efrima and H. Metiu, J. Chem. Phys. 70 (1979), 1939.
52. S. Efrima and H. Metiu, Surf. Sci. • (1980), 433
53. B. Pettinger, U. Wenning and D.M. Kolb, Ber. Bunsenges. Phys. Chem. 82 (1978), 1326.
54. A. Otto, in Proc. Int. Conf. Vibrations in Adsorbed Layers, (Julich, 1978).

CHAPTER 4 REFERENCES FOR POLARIZATION TECHNIQUES

1. T.C. Damen, S.P.S. Porto and B. Tell, Phys. Rev. 142 (1966), 570.
2. C.J.H. Schutte, in Theory of Molecular Spectroscopy, vol 1, (Elsevier, New York, 1976), p. 384.
3. N.M. Amer, Y.R. Shen and H. Rosen, Phys. Rev. Lett. 24 (1970), 718.
4. B.J. Bulkin and F.T. Prochaska, J. Chem. Phys. 54 (1971), 635.
5. N.M. Amer and Y.R. Shen, J. Chem. Phys. 56 (1972), 2654.
6. C.H. Wang and A.L. Leu, J. Am. Chem. Soc. 94 (1972), 8605.
7. E.I. Kamitsos and W.M. Risen, Jr., J. Chem. Phys. 79(1) (1983), 477
8. T.K. Klofta, P.C. Rieke, C.A. Linkous, W.J. Buttner, A. Nanthakumar, T.D. Mewborn, M.R. Armstrong, J. Electrochem. Soc. 132(9) (1985). 2134.
9. H. Goldstein, in Classical Mechanics, (Addison-Wesley, Toronto, 1950), pp. 107-109.
10. R. Loudon, Adv. Phys. 13 (1964), 423.

REFERENCES FOR CHAPTER 5: LANGMUIR-BLODGETT FILMS

1. K.B. Blodgett, J. Am. Chem. Soc. 57 (1935), 1007.
2. K.B. Blodgett, Phys. Rev. 55 (1939), 391.
3. I. Langmuir, Proc. Roy. Soc. (London) 170A (1939), 15.
4. I. Langmuir, J. Am. Chem. Soc. 39 (1917), 1848.
5. H. Kuhn, D. Mobius and H. Bucher, in Techniques of Chemistry, vol. 1, Pt IIIB, ed. A. Weissberger and B.W. Rossiter, (Wiley, New York, 1972), p.577.
6. O. Inacker, H. Kuhn, D. Mobius and G. Debuch, Zeitschr. Fur Physik. Chemie Neue Folge 101 (1976), 337.
7. H. Kuhn, J. of Photochem. 10 (1979), 111.
8. M. Vandevyver, A. Ruaudel-Teixier, L. Brehamet and M. Lutz, Thin Solid Films 99 (1983), 41.
9. W. Knoll, J. Rabe, M.R. Philpott and J.D. Swalen, Thin Solid Films 99 (1983), 173.
10. A.W. Snow and N.L. Jarvis, J. Am. Chem. Soc. 106 (1984), 4706.
11. G.J. Kovacs, P.S. Vincett and J.H. Sharp, Can. J. Phys. 63(3) (1985) 346.
12. H. Yamamoto, T. Sugiyama, M. Tanaka, Jap. J. Of Appl. Phys. 24(5) (1985), L305.
13. G.G. Roberts, M.C. Petty, S. Baker, M.T. Fowler and N.J. Thomas Thin Sol. Films 132 (1985), 113.
14. W.R. Barger, A.W. Snow, H. Wohltjen and N.L. Jarvis, Thin Sol. Films 133 (1985), 197.
15. R.A. Hann and S.K. Gupta, Thin Sol. Films 134 (1985), 35.

16. D.P. DiLella, W.R. Barger, A.W. Snow and R.R. Smardzewski, *Thin Sol. Films* 133 (1985), 207.
17. H. Wohltjen, W.R. Barger, A.W. Snow and N.L. Jarvis, *IEEE Trans. Electr. Dev.* 32(7) (1985), 1170.
18. R. Aroca, C. Jennings, G.J. Kovacs, R.O. Loutfy, P.S. Vincett *J. Phys. Chem.* 89 (1985), 4051.
19. G.J. Kovacs, R.O. Loutfy, P.S. Vincett, C. Jennings, R. Aroca *Langmuir* (1986), 689.
20. J.D. Swalen, in *Proceedings of the Tenth International Conference on Raman Spectroscopy*, ed. W. Peticolas and B. Hudson, (Eugene, Oregon, 1986), p. 6-1.
21. R. Dupeyrat, M. Harrand, M. Masson, *ibid.*, p. 6-3.
22. N.E. Schlotter, *ibid.*, p. 6-5.
23. S.B. Dierker, *ibid.*, p. 6-8.

REFERENCES FOR CHAPTER 6: EXPERIMENTAL

1. H.J. Wagner, R.O. Loutfy, C.K. Hsaio, J. Mat. Sci. 17 (1982), 2781.
2. G.J. Kovacs, P.S. Vincett, J.H. Sharp, Can. J. Phys. 63(3) (1985), 346.
3. F.H. Moser and A.L. Thomas, in Phthalocyanine Compounds, (Reinhold, London,1963).
4. R.O. Loutfy and L.F. M^CIntyre, Can. J. Chem. 61 (1983), 72.
5. P. Fromherz, Rev. Sci. Instrum. 46 (1975), -1380.
6. R. Aroca and P. Cook, Am. Lab. 16 (1984), 138.

REFERENCES FOR CHAPTER 7: RESULTS

1. F.H. Moser and A.L. Thomas, in Phthalocyanines, (Reinhold, New York, 1963).
2. T.J. Klofta, P.C. Rieke, C.A. Linkous, W.J. Buttner, A. Nanthakumar, T.D. Mewborn and N.R. Armstrong, J. Electrochem. Soc. 132(9) (1985), 2134.
3. C.H. Griffiths, M.S. Walker and P. Goldstein, Mol. Cryst. Liq. Cryst. 33 (1976), 149.
4. W.J. Wynne, Inorg. Chem. 23 (1984), 4658.
5. R.S. Nohr, P.M. Kuznesof, W.J. Wynne, M.E. Kenney and P.G. Siebenman, J. Am. Chem. Soc. 103 (1981), 4371.
6. R.O. Loutfy, A.M. Hor, G. Dipaola-Baranyi and C.K. Hsaio, J. Imaging Sci. 29(3) (1985), 116.
7. A.M. Hor and R.O Loutfy, Thin Solid Films 106 (1983), 291.
8. G.J. Kovacs, P.S. Vincett and J.H. Sharp, Can. J. Phys. 63(3) (1985), 346.
9. T.M. Negundadi, Proc. Indian Acad-Sci. 15 (1942), 376.
10. A.S. Davydov, in Theory of Molecular Excitons, (McGraw Hill, Toronto, 1962).
11. C. Jennings, S. Amer and R. Aroca, Can. J. Spectroscopy 30(3) (1985), 51.
12. J.A. Salthouse and M.J. Ware, in Point Group Character Tables and Related Data, (Cambridge University Press, London,1972).

13. R. Aroca, C. Jennings, *Spectrochimica Acta* in press.
14. Y. Iyechika, K. Yakushi, I. Ikemoto and H. Kurada, *Acta Cryst.* 1338(1982),766.
15. R. Aroca, C. Jennings, G.J. Kovacs, R.O. Loutfy and P.S. Vincett, *J.Phys.Chem.* 89(19) (1985), 4051.
16. G.J. Kovacs, R.O. Loutfy, P.S. Vincett, C. Jennings, and R. Aroca *Langmuir* 2 (1986), 689.
17. G.J. Kovacs, P.S. Vincett and J.H. Sharp, *Can. J. Phys.* 63(3) (1985), 346.

REFERENCES FOR CHAPTER 8: ASSIGNMENT

1. T. Shimanouchi, H. Matura, Y. Ogawa and I. Harada, J. Phys. Chem. Ref. Data 9(4) (1981), 1149.
2. M. Muto and S. Horiguchi, Japanese Kokai 73 (1973), 117.
3. M. Ninomiya, A. Komai and N. Shirane, Japanese Kokai 74 (1974).
4. M. Majobe and G. Vergoten, J. Chem. Phys. 76(6) (1982), 2838.
5. M. Majoube, in Proc. Int. Conf. Raman Spectrosc., 6th ed., E.D. Schmid, R.S. Krishnan and W. Kiefer, (Heyden, London, 1978), pp.10-11.
6. D. Kirin, L. Colombo and G. Baranovic, Chem. Phys. Lett. 43(3) (1976), 512.
7. L. Colombo, P. Bleckmann, B. Schrader, R. Schneider and R. Plessner, J. Chem. Phys. 61(8) (1974), 3270.
8. M. Cordes and J.L. Walker, Spectrochim. Acta. 24A (1968), 252.
9. M. Majoube, J. Molec. Struct. 61 (1980), 129.
10. A. Lautie, M.F. Lautie, A. Gruger and S.A Fakhri, Spectrochim. Acta 36A (1980), 85.
11. A. Lautie, A. Novak, J. Chim. Phys. Physiochim. Biol. 69(9) (1972), 1332.
12. L.D. Spaulding, C.C. Chang, N. Yu and R.H. Felton, J. Am. Chem. Soc. 97(9) (1975), 2517.
13. M. Abe, T. Kitigama, and Y. Kyogoku, Chem. Letts. (1976), 249.

14. T. Kitagawa, M. Abe, Y. Kyogoku, H. Ogoshi, E. Watanabe and Z. Yoshida, *J. Phys. Chem.* 80 (1976), 1181.
15. T.G. Spiro, *Biochim. Biophys. Acta* 416 (1975), 169.
16. F. Adar, M. Gouterman, S. Arnowitz, *J. Phys. Chem.* 80 (1976), 2184.
17. J.M. Friedman, D.L. Rousseau and F. Adar, *Proc. Nat. Acad. Sci U.S.A.* 74(7) (1977), 2607.
18. F. Adar, *J. Phys. Chem.* 82(2) (1978), 230.
19. M. Fujiwara and M. Tasumi, *J. Phys. Chem.* 90 (1986), 250.
20. R. Aroca and D.P. DiLella, R.O. Loutfy, *J. Phys. Chem. Solids* 43(8) (1982), 707.
21. R. Aroca and R.O. Loutfy, *Spectrochim. Acta.* 39A(10) (1983), 847.
22. C. Jennings, R. Aroca, A. Hor and R.O. Loutfy, *J. Raman Spectrosc.* 15(1) (1984), 34.
23. R. Aroca, C. Jennings, G.J. Kovacs, R.O. Loutfy and P.S. Vincett, *J. Phys. Chem.* 89(19) (1985), 4051.
24. C. Jennings, R. Aroca, A. Hor and R.O. Loutfy *Spectrochim. Acta.* 41(9) (1985), 1095.
25. C. Jennings, R. Aroca, A. Hor and R.O. Loutfy, *Spectrochim. Acta* 42(9) (1986), 991.
26. C.A. Melendres and V.A. Maronie, *J. Raman Spectrosc.* 15(5) (1984), 319.
27. T. Huang, K.E. Rieckhoff and E. Voigt, *Can. J. Chem.* 56 (1978), 976.

28. T. Huang, W. Chen, R.E. Rieckhoff and E.M. Voigt, J. Chem. Phys. 80(9) (1984), 4051.
29. D.P. DiLella, W.R. Barger, A.W. Snow and R.R. Smardzewski, Thin Solid Films 133 (1985), 207.

VITA AUCTORIS

CAROL ANN JENNINGS

BIRTHDATE: August 15, 1958

EDUCATION:	1972-1977	Alderwood Collegiate Institute Toronto, Ontario
	1977-1981	University of Toronto Toronto, Ontario
	1985-1986	University of Windsor Windsor, Ontario